

UNIVERSITY OF NOTTINGHAM

Dissecting the molecular mechanism of microtubule depolymerising kinesins

Hannah Belsham

MSci (Hons)

Thesis submitted to the University of Nottingham towards the degree of Doctor of
Philosophy

30th September 2019

Abstract

Mitotic Centromere Associated Kinesin (MCAK) is a microtubule depolymerase from the Kinesin-13 family of molecular motors. In cells it plays an important role in regulating microtubule length and in ensuring replicated chromosomes are accurately divided between the two daughter cells during mitosis. MCAK activity is tightly regulated and here I show how phosphorylation of MCAK, at different sites by two different kinases, acts to regulate MCAK's activity through two distinct mechanisms. Firstly I show how phosphorylation of MCAK at T537 by Cdk1 prevents MCAK from recognising the microtubule end, a key function for its depolymerisation activity. Secondly, while phosphorylation of MCAK at S621 by Plk1 has been shown to lead to a reduction in MCAK's activity in cells, I show that this is not reproduced *in vitro*. In this case phosphorylation affects MCAK's activity in cells by affecting the rate of degradation of MCAK. Finally I introduce three MCAK residues, important in Kinesin-13 for microtubule end recognition, into Kinesin-1, at the core interface between the kinesin motor domain and the microtubule. This induces this translocating kinesin to pause at the microtubule end. Together, these data provide further information on both the depolymerisation mechanism of MCAK and the structural distinctions between microtubule regulating and translocating kinesins.

Declaration

This thesis is the result of my own work, except where included data is explicitly mentioned, which has been undertaken during my period of registration for this degree at The University of Nottingham.

Contents

ABSTRACT	1
DECLARATION	2
CONTENTS.....	3
TABLE OF FIGURES	10
TABLES.....	14
ACKNOWLEDGEMENTS.....	15
PUBLICATIONS	16
ABBREVIATIONS.....	17
CHAPTER 1 INTRODUCTION.....	21
1.1 The cytoskeleton.....	21
1.2 Microtubules.....	23
1.2.1 Microtubule accessory proteins.....	27
1.3 Kinesins	29
1.3.1 Translocating kinesins	30
1.3.2 Kinesins that regulate microtubule dynamics	32
1.4 Kinesin-13s.....	33

1.4.1	Kinesin-13 family members have distinct cellular roles	34
1.5	MCAK in cancer	35
1.6	Structure of MCAK	36
1.7	ATP turnover and its impact on MCAK's microtubule affinity	42
1.8	Phosphorylation of MCAK.....	47
1.8.1	Effect of phosphorylation on MCAK's localisation	49
1.8.2	Effect of phosphorylation on MCAK's conformation.....	50
1.8.3	Effect of phosphorylation on MCAK's depolymerisation activity.....	51
1.9	End recognition in kinesins.....	52
	AIMS.....	54
	CHAPTER 2 METHODS.....	56
2.1	Site-directed mutagenesis	56
2.2	Cell culture and protein expression in insect Sf9 cells	57
2.2.1	Cell culture.....	57
2.2.2	Transformation of DH10Bac	57
2.2.3	Baculovirus production.....	58
2.2.4	Protein expression.....	59
2.3	One step purification of MCAK-His6 proteins	60
2.4	Sodium dodecyl sulphate polyacrylamide gel electrophoresis (SDS- PAGE)	61

2.5	Preparing tubulin	61
2.5.1	Preparing tubulin from porcine brain	61
2.5.2	Cycling tubulin.....	62
2.5.3	Rhodamine labelling of tubulin.....	63
2.6	Assembling microtubules.....	64
2.6.1	Freezable microtubules.....	64
2.6.2	Microtubules for microscopy	65
2.6.3	Double stabilised microtubules.....	65
2.7	ATPase assays	66
2.7.1	Discontinuous assay with ADP production monitored by HPLC.....	66
2.7.2	Discontinuous assay with inorganic phosphate production monitored using malachite green.....	69
2.7.3	Continuous assay with ADP production monitored by fluorescence by linking it to the conversion of NADH to NAD ⁺	70
2.8	MantADP dissociation.....	73
2.9	Measuring microtubule depolymerisation using light scattering.....	74
2.10	Silanisation of coverslips.....	75
2.11	Measuring microtubule depolymerisation using microscopy	76
2.12	Pelleting kinesin with microtubules.....	78
2.13	Expression of Kinesin-1	79
2.14	Purification of Kinesin-1.....	79
2.15	TIRF microscopy	80

2.16	Measuring depolymerisation using a single time-point.....	83
------	---	----

2.17	Statistical tests.....	84
------	------------------------	----

**CHAPTER 3 THE MCAK PHOSPHOMIMIC T537E IS UNABLE TO
RECOGNISE MICROTUBULE ENDS.....85**

3.1	Background.....	85
-----	-----------------	----

3.2	Expression and purification of MCAK mutants.....	87
-----	--	----

3.3	Introduction of a Cdk1 phosphomimic mutation impairs MCAK's depolymerisation activity	90
-----	--	----

3.4	Cdk1 phosphomimic and phosphonull mutants have slower ATPase rates than wild type in the presence of microtubules	94
-----	--	----

3.5	Cdk1 phosphomimic and phosphonull mutants can still bind microtubules.....	99
-----	---	----

3.6	Microtubule end residence times are reduced with Cdk1 phosphomimic and phosphonull mutants.....	101
-----	--	-----

3.7	The mADP dissociation rate is not accelerated by the microtubule end in a Cdk1 phosphomimic of MCAK	106
-----	--	-----

3.8	Summary.....	112
-----	--------------	-----

**CHAPTER 4 THE PLK1 PHOSPHOMIMIC MUTANT S621D DOES NOT
ALTER MCAK'S DEPOLYMERISATION ACTIVITY 115**

4.1	Background	115
4.2	Plk1 phosphomimetic and phosphonull mutants of MCAK were expressed and purified	118
4.3	Plk1 phosphomimetic and phosphonull mutants have similar basal ATPase rates to wild type MCAK.....	119
4.4	Plk1 phosphomimetic and phosphonull mutants can depolymerise microtubules at a similar rate to wild type MCAK.....	121
4.5	Summary	123
4.6	The role of phosphorylation by Plk1 at other residues	124
4.7	The use of phosphomimic residues	125

CHAPTER 5 THE EFFECT OF SUBSTITUTING KINESIN-13 RESIDUES, CRUCIAL TO MICROTUBULE END RECOGNITION, IN THE KINESIN-1 MOTOR DOMAIN 128

5.1	Microtubule end recognition is an important feature of microtubule regulating kinesins	128
5.2	Identifying end binding residues	130
5.3	Expression and purification of Kinesin-1	131
5.4	Kinesin-1 has a shorter end residence time than Kinesin-13	133
5.5	Expression and purification of Kinesin-1 mutants	134

5.6	Introducing residues into Kinesin-1 that are important for Kinesin-13s end recognition ability, leads to increased end residence times.....	136
5.7	The increase in residence time is specific to the microtubule end	140
5.8	Amino acid substitutions affect translocation activity, but these changes do not correlate with the effect on end residence time.....	142
5.9	An alanine mutant displays an increased end residence time compared to wild type Kinesin-1, but not as long as substitution to the equivalent Kinesin-13 residue	143
5.10	Differences in mutant kinesin behaviour are not due to deficiencies in protein function	146
5.11	An increase in end residence time is not sufficient to promote microtubule depolymerisation	148
5.12	Summary.....	150
CHAPTER 6 DISCUSSION		155
6.1	Phosphorylation of MCAK regulates its activity through multiple distinct pathways.....	155
6.2	The microtubule residence time of Kinesin-1 and Kinesin-13 can be modified through altering residues in the α 4 helix.....	157
6.3	Further areas for exploration	160

6.4	Implications for cancer	161
6.5	Manipulating kinesin function for nanotechnology	162
6.6	Closing remarks.....	163
BIBLIOGRAPHY		164
APPENDICES.....		181
Appendix 1		181
A1.1	Alignment of the motor domains of Kinesin-1 and Kinesin-13	181
Appendix 2		182
A2.1	T537A and T537E microtubule end and lattice residence fits	182
A2.2	T537A and T537E deviation and fits of mADP dissociation data	183
Appendix 3		184
A3.1	End and lattice residence fits wild type Kinesin-1, G262K, N263E, S266R, Triple and S266A	184

Table of Figures

Figure 1.1. Cells contain three types of cytoskeletal filaments – actin filaments, intermediate filaments and microtubules..	21
Figure 1.2. The structure of the α-β tubulin heterodimer.....	24
Figure 1.3. A schematic to show the structure of the microtubule.	24
Figure 1.4. A GTP-cap stabilises microtubules.....	27
Figure 1.5. The structure of Kinesin-1.	31
Figure 1.6. Domain structure of MCAK.	37
Figure 1.7. Overlay of Kinesin-1 and Kinesin-13 motor domains.....	38
Figure 1.8 MCAK binding induces tubulin curvature.	40
Figure 1.9. The structure of the MCAK motor domain in complex with tubulin.	44
Figure 1.10. The ATP turnover cycle.....	46
Figure 1.11. The coupling of ATP turnover and microtubule depolymerisation by MCAK.....	46
Figure 1.12. The phosphorylation sites of MCAK.	49
Figure 2.1. ADP and ATP were separated by HPLC and produced peaks with concentration dependent integrals.....	69
Figure 2.2. Light absorbed at 650nm by malachite green increases with increasing concentration of phosphate.	70
Figure 2.3. The initial change in fluorescence was converted to change in ADP concentration by making a standard curve of final/ initial fluorescence.	72
Figure 2.4. Construction of channels for a depolymerisation assay.	76

Figure 2.5. The lower surface of a flow channel..	77
Figure 2.6. The length of a microtubule over time with the addition of MCAK.	78
Figure 2.7. Kymographs can show depolymerisation or track kinesin movement.	81
Figure 2.8. Schematic showing the pixel requirements for intensity to be counted as an event.	83
Figure 3.1. Location of T537 residue in MCAK.	87
Figure 3.2. Purification of wild type MCAK, T537A and T537E by nickel affinity.	89
Figure 3.3. A light scattering assay shows wild type MCAK depolymerises microtubules more rapidly than the mutants T537A and T537E.	91
Figure 3.4. The rate of microtubule depolymerisation by wild type MCAK is faster than by the mutants T537A and T537E.	92
Figure 3.5. The rate of depolymerisation by wild type MCAK and T537A is comparable and faster than T537E in the presence of an excess of MCAK.	93
Figure 3.6. The MCAK mutants T537A and T537E have comparable ATPase rates to wild type in solution.	94
Figure 3.7. The ATPase rate of wild type MCAK and the mutants T537A and T537E is comparable in the presence of free tubulin.	96
Figure 3.8. The ATPase rate of wild type MCAK is faster than the mutants T537A and T537E in the presence of microtubules.	97
Figure 3.9. An overview of the ATPase rates of wild type MCAK, T537A and T537E in solution, with unpolymerised tubulin and with microtubules.	99

Figure 3.10. MCAK and the mutants T537A and T537E co-sediment with microtubules.	100
Figure 3.11. T537A and T537E show fewer long end residence events than wild type MCAK.....	102
Figure 3.12. WT MCAK and T537E show comparable lattice residence times, but T537A has a longer lattice residence time.	105
Figure 3.13. The rate of mantADP dissociation from wild type MCAK is comparable for the mutants T537A and T537E.....	107
Figure 3.14. The rate of mantADP dissociation from wild type MCAK is comparable for mutants T537A and T537E in the presence of unpolymerised tubulin.	108
Figure 3.15. The rate of mantADP dissociation from wild type MCAK is faster than from T537A and T537E in the presence of microtubules.....	110
Figure 3.16. Overview of the rate constants of mADP dissociation from wild type MCAK, T537A and T537E in solution, in the presence of unpolymerised tubulin and in the presence of microtubules.....	111
Figure 4.1. Purification of S621A and S621D by Nickel affinity chromatography.....	119
Figure 4.2. The ATPase rate of S621A and S621D is not significantly different from wild type.....	120
Figure 4.3. Wild type MCAK and the mutants S621A and S621D show similar rates of depolymerisation when measured using a light scattering assay.	121

Figure 4.4. The rate of depolymerisation by wild type MCAK and the mutants S621A and S621D are not significantly different.	122
Figure 4.5. Structure of phosphoserine compared with aspartic and glutamic acids.	127
Figure 5.1. Sequence and structural alignment of Kinesin-13 and Kinesin-1.	131
Figure 5.2. Purification of Kinesin-1.	132
Figure 5.3. Kinesin-1 has a shorter end residence time than Kinesin-13... 	134
Figure 5.4 The mutant proteins G262K, N263E, S266R and a triple mutant were expressed and purified.	135
Figure 5.5. Mutant kinesin-1 proteins have a longer end residence time than wild type Kinesin-1.....	137
Figure 5.6. S266R stays at the microtubule end much longer than wild type Kinesin-1.	139
Figure 5.7. The lattice residence time for the mutant proteins is decreased compared to wild type Kinesin-1.....	141
Figure 5.8. Translocation velocity does not correlate with end residence.	142
Figure 5.9. The purification of S266A.	144
Figure 5.10. S266A has a longer end residence time than wild type Kinesin-1, but shorter than S266R.	145
Figure 5.11. Kinesin-1 mutants show no significant difference in ATPase rate from wild type.	147
Figure 5.12 Kinesin-1 mutants cannot depolymerise microtubules.	148

Figure 5.13. Light scattering assay shows no depolymerisation by Kinesin-1 mutants.149

Figure 5.14. The structure of Kinesin-1 in complex with tubulin.151

Tables

Table 1. T537A and T537E have shorter end residence times than WT MCAK and T537A has a longer lattice residence time.106

Table 2. Summary table of depolymerisation, ATPase, mADP dissociation and end residence data.111

Table 3. The ATPase and depolymerisation rates of S621A and S621D are not significantly different from wild type.123

Table 4. The end residence time, microtubule interaction rate constants, velocities and run lengths of wild type Kinesin-1 and the mutants.138

Table 5. The end residence time, microtubule interaction rate constants, velocities and run lengths of S266A.146

Acknowledgements

I am so grateful to everyone who has helped me through this PhD journey.

Thank you to my supervisor Claire Friel and the other members of the Friel, Wickstead, Gadelha and Huett labs for their support and encouragement and consistent drive to help me make this thesis the best it could be. Thank you also to the School of Life Sciences Imaging Facility and Chris Gell in particular for technical assistance and advice. Thank you to the University of Nottingham, BBSRC, and Royal Society for providing me and the lab with the funding to undertake this research.

Thank you to the friends who knew only that there were red lines and green dots and sometimes they were happy and sometimes they were driving me up the wall, but who asked about it anyway.

Thank you to the health professionals who have managed to keep me well enough to complete my PhD.

Thank you to my family. Grandpa I know you would have thought it “tremendous” and I wish you and Granny had been able to see it to the end.

Thank you to God, without who I can do nothing. “Yet the making of things is in my heart from my own making by thee; and the child of little understanding that makes a play of the deeds of his father may do so without thought of mockery, but because he is the son of his father.” J. R. R. Tolkien.

Lastly thanks to ‘my people’ without whom I would never have made it this far.

Publications

Sanhaji M., Ritter A., Belsham H. R., Friel C. T., Roth S., Louwen F. and Yuan J.

Polo-like kinase 1 regulates the stability of the mitotic centromere-associated kinesin in mitosis. Oncotarget, 2014. **5**(10): 3130-3144.

Patel J. T., Belsham H. R., Rathbone A. J., Friel C.T. *Use of stopped-flow fluorescence and labelled nucleotides to analyse the ATP turnover cycle of kinesins.* J Vis Exp., 2014. **17**(92): e52142.

Patel J. T., Belsham H. R., Rathbone A. J., Wickstead B., Gell C., Friel C. T. *The family-specific α 4-helix of the kinesin-13, MCAK, is critical to microtubule end recognition.* Open Biol, 2016. **6**: 160223

Belsham H.R. and Friel C. T. *A Cdk1 phosphomimic mutant of MCAK impairs microtubule end recognition.* PeerJ, 2017. **5**: e4034.

Belsham H.R. and Friel C. T. *Identification of key residues that regulate the interaction of kinesins with microtubule ends.* Cytoskeleton, 2019. **76**: 440-446.

Copies of these publications are attached to the end of the thesis for reference.

Abbreviations

A_x – Absorbance at x nm

AcMNPV – *Autographa californica* multiple nuclear polyhedrosis virus

ADP – Adenosine-5'-diphosphate

APC – Anaphase Promoting Complex

APS – Ammonium Persulfate

ATP – Adenosine-5'-triphosphate

BIIC – Baculovirus Infected Insect Cell

BME – β-mercaptoethanol

BSA – Bovine Serum Albumin

C- – carboxy-

Cdc25 – Cell division cycle 25

Cdk1 – Cyclin dependant kinase 1

ddH₂O – Double distilled water

DMSO – Dimethyl Sulfoxide

DNA – 2-Deoxyribose Nucleic Acid

dNTP – 2-deoxynucleoside-5'-triphosphate

DOL – Degree of labelling

DTT – Dithiothreitol

EDTA – Ethylene Diamine Tetraacetic Acid

EGTA – Ethylene Glycol Tetraacetic Acid

FCS – Foetal Calf Serum

FT – Flow through

GDP – Guanosine-5'-diphosphate

GFP – Green Fluorescent Protein

GMPCPP – Guanylyl α , β -methylene diphosphate

GTP – Guanosine-5'-triphosphate

HEPES – 4-(2-hydroxyethyl)-1-piperazineethanesulfonic acid

H6/His6 – Hexahistidine tag

HPLC – High Performance Liquid Chromatography

ICIS – Inner Centromere KinI Stimulator

kDa - Kilodaltons

KIF – Kinesin family member

LB – Luria Broth

LDH – Lactate Dehydrogenase

MAP – Microtubule Associated Protein

MCAK – Mitotic Centromere Associated Kinesin/ KIF2C

MES – 2-(N-Morpholino)ethanesulphonic acid

N- – amino-

NADH/NAD⁺ - nicotinamide adenine dinucleotide (reduced/oxidised)

OD – Optical density

PAK1 – p21 activated kinase 1

PCR – Polymerase Chain Reaction

PEP – Phosphoenol pyruvate

Pi – Inorganic Phosphate

PIPES – 1, 4-Piperazinediethanesulphonic acid

PK – Pyruvate Kinase

Plk1 – Polo-like kinase 1

PMSF – Phenylmethanesulphonyl Fluoride

SDS – Sodium Dodecyl Sulphate

SDS-PAGE – Sodium dodecyl sulphate polyacrylamide gel electrophoresis

Sf9 cells – *Spodoptera frugiperda* cells

Sgo2 – Shugoshin 2

TAMRA – 5-carboxytetramethylrhodamine

TBS – Tris-buffered saline

TEMED – N, N, N', N'-tetramethylethylenediamine

TIRF – Total Internal Reflection Fluorescence

WT – wild type

Chapter 1 Introduction

1.1 The cytoskeleton

The cytoskeleton has two major roles – to give cells shape and to produce force, which can generate movement. There are three major components of the cytoskeleton: actin, intermediate filaments and microtubules (**Figure 1.1.**) These three types of polymeric protein filaments are dynamic and so can rapidly restructure. Differences in the size and mechanical properties of these filaments allows them to function differently – actin filaments are ~7 nm thick, intermediate filaments ~10 nm thick and microtubules ~25 nm in diameter.

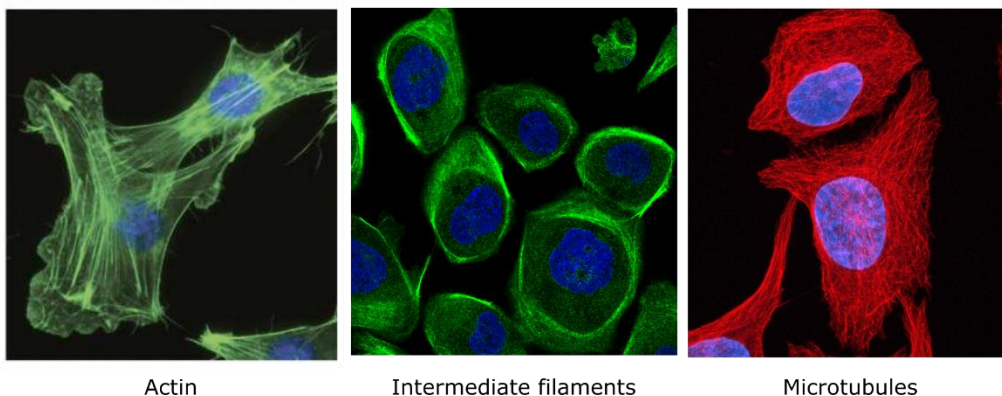


Figure 1.1. Cells contain three types of cytoskeletal filaments – actin filaments, intermediate filaments and microtubules. Actin and intermediate filaments are stained green in their respective images, microtubules are stained red and DNA is stained blue with DAPI in all three images. Image sources (Feldman, Apsel et al. 2009, Uhlen, Oksvold et al. 2010, Appleton 2011).

With the assistance of an array of accessory proteins, the cytoskeleton is involved in diverse cellular processes. These accessory proteins can be grouped into three different types: transporters, regulators of cytoskeletal dynamics and regulators of the structure of the cytoskeleton. Some examples of the functions of transporter accessory proteins include the transport of organelles and vesicles along microtubules by Kinesin-1 (Vale, Reese et al. 1985), bending in cilia and flagella produced by axonemal dynein, creating the characteristic beating motion (Summers and Gibbons 1971), and myosin VI playing a role in endocytosis of glutamate receptors (Osterweil, Wells et al. 2005). Regulators of cytoskeletal dynamics include the Kinesin-13 family of microtubule depolymerisers which are involved in chromosome segregation and correcting kinetochore-microtubule attachments during mitosis (Bakhom, Thompson et al. 2009, Hood, Kettenbach et al. 2012). Profilin acts as a polymeriser for actin filaments (Carlsson, Nystrom et al. 1977), which occurs at the leading edge of a cell as it migrates. Structural regulators can cause branching or severing of cytoskeletal filaments. The actin severing protein gelsolin increases turnover of actin filaments leading to the breakdown of actin networks (Yin, Hartwig et al. 1981). This is important for cell movement and cytokinesis. Conversely proteins such as filamin, which stabilise actin crosslinks, help to stabilise a meshwork of actin and anchors the cell membrane (Wang and Singer 1977).

1.2 Microtubules

Microtubules have several key functions in cells. Firstly, they allow rapid, directional transport across long distances. Secondly, they are important for cellular structures especially protrusions such as cilia and flagella. Thirdly, microtubules are key for forming the mitotic spindle in eukaryotes during cell division. Microtubules are polymers of tubulin, typically formed of 13 protofilaments (although 12-17 have been observed (Chretien and Wade 1991)). Tubulin is a heterodimer formed from an α -subunit and a β -subunit (**Figure 1.2**). Within a protofilament the tubulin heterodimers are arranged in the same orientation, giving the protofilaments polarity with an α -tubulin capped (–) end and a β -tubulin capped (+) end (**Figure 1.3**).

In the microtubule lattice (the region of the microtubule between the two ends) the tubulin dimers are arranged so that the lateral contacts are homotypic (i.e. α - α and β - β), except down a single seam (shown in **Figure 1.3**) (Song and Mandelkow 1993). At this seam there is a discontinuity in the lateral interactions.

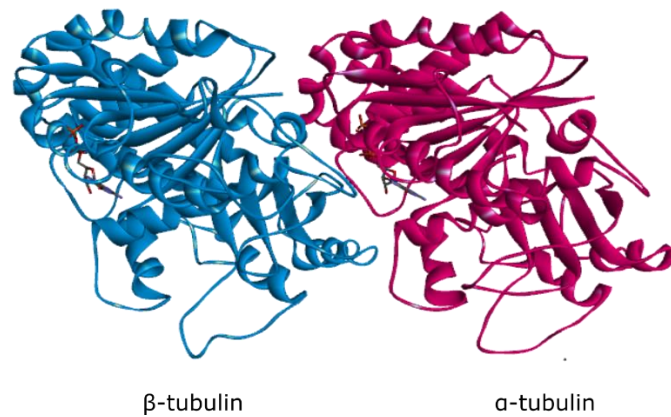


Figure 1.2. The structure of the α - β tubulin heterodimer. α and β tubulin (*Bos taurus*) form a heterodimer, with each subunit binding GTP. The dimers can assemble into protofilaments and then microtubules. PDB ID: 1JFF (Lowe, Li et al. 2001).

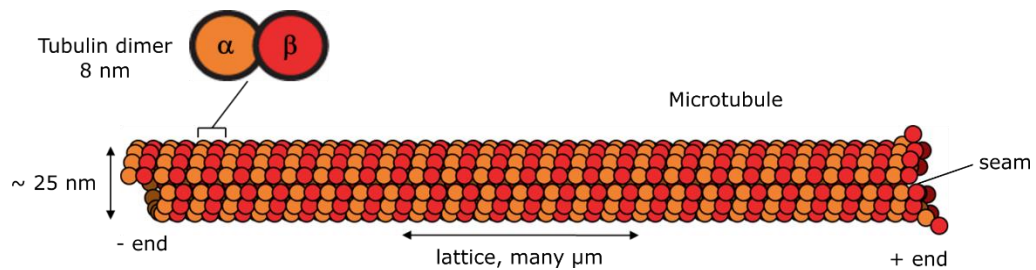


Figure 1.3. A schematic to show the structure of the microtubule. Tubulin heterodimers assemble into protofilaments which form a hollow cylinder called a microtubule. The microtubule is approximately 25 nm in diameter and can be many micrometres long. The arrangement of the tubulin dimers gives the microtubule polarity and also leads to the formation of a single seam.

The structures of the α and β subunits are almost identical, with each containing N-terminal nucleotide binding, central and negatively charged C-terminal (E hook) regions. Both tubulin subunits bind GTP (guanosine-5'-

triphosphate) but only the β -subunit-bound nucleotide is accessible for exchange, whereas the GTP in the binding site of α -tubulin is non-exchangeable (Nogales, Wolf et al. 1998). Upon polymerisation, the catalytic site in the β -subunit is completed by residue E254 from the α -subunit allowing hydrolysis of GTP to GDP (Nogales, Downing et al. 1998, Lowe, Li et al. 2001). However, protofilament formation prevents the GDP from being exchanged back to GTP. In the GDP-bound form, the protofilament is prone to depolymerisation as the tubulin dimer's affinity for other tubulin molecules is reduced to the point where the lateral contacts are not strong enough to constrain the tubulin dimer to a straight position (Manka and Moores 2018). While new, GTP-bound tubulin subunits are added to the end of the microtubule more rapidly than GTP hydrolysis occurs, a stable GTP-bound cap is formed at the growing microtubule end preventing depolymerisation (**Figure 1.4A**). It was thought that if the rate of hydrolysis exceeded the rate of polymerisation then GDP-bound tubulin would be exposed, leading to curvature of the protofilament and a switch to rapid depolymerisation, termed catastrophe (**Figure 1.4B**) (Mitchison and Kirschner 1984). However, the discovery that catastrophe is a multi-step process (Gardner, Zanich et al. 2011), shows that this is an oversimplification. The frequency of microtubule catastrophe is not consistent with it being a first order process, but shows an age dependence. While some studies suggest that this is caused by an accumulation of defects in the microtubule, this would require these defects to be somehow communicated to the microtubule end. Another possibility is that a number of protofilaments have to lose their GTP cap for all the

protofilaments to simultaneously catastrophe. The continual transition between growth and shrinkage is called dynamic instability, and is critical to microtubule function. Tubulin dimers have now been observed binding to growing microtubules, using iSCAT. This has allowed studies of the kinetics of tubulin binding on individual protofilaments (Mickolajczyk, Geyer et al. 2019).

The use of the slowly hydrolysable GTP analogue guanylyl α,β -methylene diphosphate (GMPCPP) for *in vitro* studies produces microtubules which mimic the GTP cap (Hyman, Chretien et al. 1995, Nogales, Wolf et al. 1998). Microtubules containing GMPCPP depolymerise at a rate 5000 times slower than GDP microtubules so are sufficiently stable for analysis (Hyman, Salser et al. 1992). Microtubules assemble spontaneously *in vitro* from tubulin dimers in the presence of GTP (or a GTP analogue such as GMPCPP) and magnesium ions at 37 °C. Taxol (also known as paclitaxel – a β -tubulin binding drug which helps prevent microtubule disassembly) can also be used to stabilise microtubules but, unlike GMPCPP, is added after the microtubules have grown. The length of the microtubules that are produced is dependent on the concentration of tubulin, and DMSO or glycerol can be added to help promote microtubule nucleation.

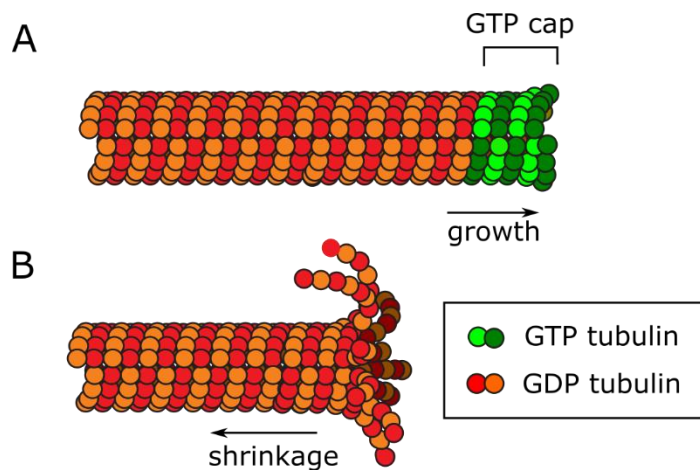


Figure 1.4. A GTP-cap stabilises microtubules. A) When GTP-bound tubulin is added to the microtubule end more rapidly than the GTP is hydrolysed a stable GTP-bound cap is formed. B) Loss of the GTP cap through GTP hydrolysis and a reduced polymerisation rate, or depolymerisation by proteins such as Kinesin-13s leads to microtubule shrinkage (catastrophe).

1.2.1 Microtubule accessory proteins

Microtubule associated proteins (MAPs) can be divided into three main categories: translocators, regulators of dynamics and regulators of structure, although some have functions from more than one category. Kinesins and dyneins are the major types of translocators along microtubules. The first kinesin was discovered in 1985, and was identified as a microtubule associated protein that could transport organelles in an ATP dependent manner (Vale, Reese et al. 1985). It was shown to consist of several different subunits which were later determined to be two heavy chains and two light chains (Bloom, Wagner et al. 1988). This kinesin is now classified as a member of the Kinesin-1 family, and is known to walk towards the plus-end of microtubules (Paschal and Vallee 1987). Kinesins will be discussed in more

detail in section 1.3. Axonemal dynein was isolated from cilia in 1965 as an ATPase (Gibbons and Rowe 1965). A second, cytoplasmic form of mammalian dynein, dynein-1, was isolated in 1987 (Paschal, Shpetner et al. 1987) and has multiple roles in cells. Processes involving cytoplasmic dynein include organelle transport along microtubules, including of endosomes, lysosomes, phagosomes, peroxisomes and mitochondria (Schnapp and Reese 1989, Blocker, Severin et al. 1997, Jordens, Fernandez-Borja et al. 2001, Kural, Kim et al. 2005, Pilling, Horiuchi et al. 2006, Driskell, Mironov et al. 2007), spindle orientation (Busson, Dujardin et al. 1998, Faulkner, Dujardin et al. 2000), the spindle assembly checkpoint (Howell, McEwen et al. 2001) and cell migration (Dujardin, Barnhart et al. 2003). Dynein has now been identified as a large protein complex containing four types of chains: heavy, intermediate, light intermediate and light chains (Vallee, Wall et al. 1988). The motor domain is located within the heavy chain and is very large (350kDa), containing a hexameric ring of AAA ATPase domains (Samso, Radermacher et al. 1998, King 2000, Burgess, Walker et al. 2003).

Dynamic regulators of microtubules include microtubule polymerisers such as XMAP215 (Gard and Kirschner 1987, Shirasu-Hiza, Coughlin et al. 2003, Brouhard, Stear et al. 2008) and the orphan kinesin Nod (Cui, Sproul et al. 2005). Kinesin-1, tau and doublecortin have been shown to stabilise microtubules (Noetzel, Drechsel et al. 2005, Moores, Perderiset et al. 2006, Peet, Burroughs et al. 2018), while EB proteins make them more dynamic (Tirnauer, O'Toole et al. 1999, Rogers, Rogers et al. 2002). CLIP proteins have

the ability to transform shrinking microtubules to growing ones (Komarova, Akhmanova et al. 2002). Microtubule depolymerisers include Kinesin-13s, some Kinesin-8s and also the Kinesin-14 Kar-3 (Hunter, Caplow et al. 2003, Sproul, Anderson et al. 2005, Varga, Helenius et al. 2006). The wide variety of proteins that can have differing effects on microtubule dynamics orchestrate rapid changes in microtubule length according to the needs of the cell but must themselves be tightly regulated and co-ordinated.

Still other accessory proteins are involved in regulating microtubule structure, for example spastin and katanin which are microtubule severing proteins (Hartman, Mahr et al. 1998, Evans, Gomes et al. 2005).

1.3 Kinesins

Kinesins constitute a large protein super-family, characterised by a highly conserved motor domain (Vale and Goldstein 1990). The motor domain is the site of nucleotide binding and the principal microtubule interaction site. It contains sequence motifs typical of ATP binding proteins: a phosphate binding p-loop, switch I (the terminal γ -phosphate sensor) and switch II (magnesium ion binding, through a bridging water molecule). The kinesin motor domain shows structural similarity to the myosin motor domain, despite showing little sequence similarity, and also to a lesser degree to G proteins. In particular, the direction and position of the α helices and β sheets are well conserved as is the γ -phosphate binding region (Kull, Sablin et al. 1996).

Kinesins have been classified into 17 families based on phylogenetic analysis of their sequences, 14 of which are found in humans (Lawrence, Dawe et al. 2004, Wickstead and Gull 2006). ATP cleavage reduces the affinity of kinesin for the microtubule, while nucleotide exchange leads to tight binding (Ma and Taylor 1997). Additionally microtubule binding accelerates ADP dissociation and ATP cleavage. The ATP turnover cycle and microtubule binding of kinesins are tightly coupled. These fundamental mechanisms of nucleotide turnover and microtubule binding and release have been tuned to different cellular functions.

1.3.1 Translocating kinesins

Some kinesins act as translocators. This includes the Kinesin-1 family which transports vesicles, signalling molecules, RNA and organelles including lysosomes and mitochondria (Tanaka, Kanai et al. 1998, Bowman, Kamal et al. 2000, Byrd, Kawasaki et al. 2001, Verhey, Meyer et al. 2001, Kanai, Dohmae et al. 2004). Kinesin-1 has been shown to take 8 nm steps (Svoboda, Schmidt et al. 1993) and walk using a hand-over-hand mechanism (Asbury, Fehr et al. 2003), rotating unidirectionally (Ramaiya, Roy et al. 2017). This requires coordination of the attachment and release of the two motor domains, which in turn are dependent on their nucleotide binding state (Hackney 1994, Hancock and Howard 1999). Translocating kinesins often have the same basic structure. The kinesin motor domains, which can be known as “heads” and are joined to a “neck” region. This is often linked to a coiled-coil “stalk”, which is commonly involved in dimerisation. The kinesin “tail” allows for

cargo specificity as it is highly divergent. As an example of this, the structure of Kinesin-1 is shown in **Figure 1.5**. In humans, the Kinesin-1 KIF5B is expressed ubiquitously while KIF5A and KIF5C are neuron specific (Niclas, Navone et al. 1994, Kanai, Okada et al. 2000).

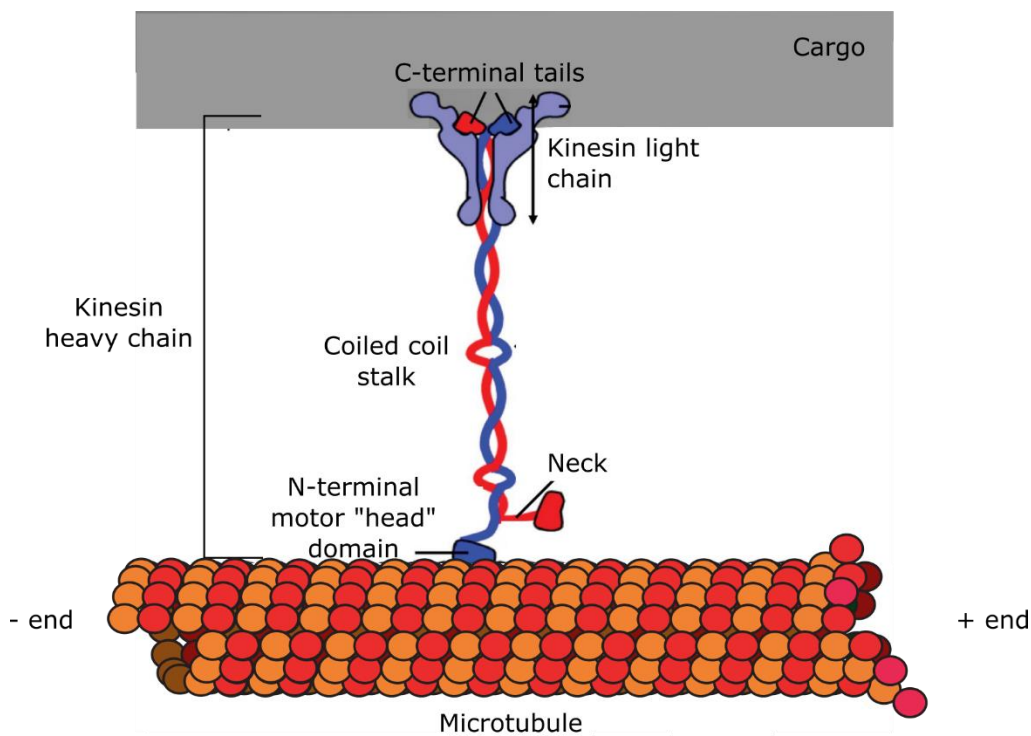


Figure 1.5. The structure of Kinesin-1. Kinesin-1 can translocate along microtubules carrying cargo. It consists of two heavy chains and two light chains. The heavy chains each have an N-terminal motor or “head” domain, a “neck” linker region, a coiled coil “stalk” and a C-terminal “tail”. Figure modified from (Jeppesen and Hoerber 2012).

Another family of translocators is the Kinesin-14 family. Unlike the Kinesin-1 family, which moves towards to the microtubule plus-end and has an N-terminal motor domain, the Kinesin-14 family, uniquely among kinesins, has a C-terminal motor domain and moves towards the microtubule minus-end.

Within this family different members use their minus-end directed translocating activity for different functions. KIFC3 is involved in the positioning of the Golgi apparatus (Xu, Takeda et al. 2002), while KIFC1 (HSET) has been shown to provide inward sliding forces on the spindle, opposing those of Eg5, a Kinesin-5. A balance of inward and outward sliding forces is necessary for bipolar spindle assembly and centrosome separation (Mountain, Simerly et al. 1999). KIF25, another Kinesin-14, is involved in suppressing premature centrosome separation (Decarreau, Wagenbach et al. 2017).

1.3.2 Kinesins that regulate microtubule dynamics

Kinesins can also function as microtubule regulators, by affecting microtubule dynamics, for example the Kinesin-8 family. Although the *S. cerevisiae* Kinesin-8 Kip3 has depolymerase activity (Varga, Helenius et al. 2006), the human equivalent KIF18A has been shown to reduce the dynamicity of the microtubule plus end, rather than being an active depolymerase (Du, English et al. 2010). KIF18A is thought to affect microtubule dynamics in a length dependent manner, confining centromere movement to the spindle midzone and contributing to chromosome oscillations, all of which help align chromosomes at the spindle equator (Stumpff, von Dassow et al. 2008, Jaqaman, King et al. 2010, Stumpff, Wagenbach et al. 2012). KIF19A, another member of the Kinesin-8 family, is a microtubule depolymerase which regulates the length of cilia (Niwa, Nakajima et al. 2012). Other microtubule depolymerising kinesins include Xklp1, a Kinesin-4, which inhibits microtubule

dynamics and slowly depolymerises them (Bringmann, Skiniotis et al. 2004) and the Kinesin-13 family. As MCAK, the subject of this thesis, is a member of the Kinesin-13 family these kinesins will be discussed in more detail in section 1.4. In contrast to microtubule depolymerising kinesins, the Kinesin-5 Eg5 (Chen and Hancock 2015), Nod (Cui, Sproul et al. 2005) and Kip2 (Hibbel, Bogdanova et al. 2015) promote microtubule polymerisation.

Kinesins which act as regulators of microtubule dynamics require different abilities to translocating kinesins. A translocator must be able to co-ordinate the movement of both 'heads' of the motor and recognise the microtubule lattice and its polarity. A microtubule regulator must be able to recognise the microtubule end and promote either removal or addition of tubulin dimers.

To date no kinesins have been found that have microtubule severing or branching functions *in vivo*, although Kinesin-1 has been shown to introduce splitting of the microtubule in *in vitro* assays, similar to microtubule branching (VanDelinder, Adams et al. 2016).

1.4 *Kinesin-13s*

The Kinesin-13 family is a group of microtubule depolymerising kinesins which remove tubulin dimers from both ends of microtubules (Desai, Verma et al. 1999). In humans, there are four members of the Kinesin-13 family, KIF2A, KIF2B, KIF2C (or Mitotic Centromere Associated Kinesin - MCAK) and KIF24. KIF2A, 2B and 2C are all members of the Kinesin-13B animal-specific

subfamily, while KIF24 is a member of the Kinesin-13A subfamily, which is a larger subfamily that is more widely distributed throughout eukaryotes (Wickstead, Gull et al. 2010).

1.4.1 Kinesin-13 family members have distinct cellular roles

The depolymerisation activity of KIF2A leads to microtubule flux, which aids in the transport of chromosomes towards the cell poles. KIF2A is also necessary for spindle assembly and is localised to centrosomes (Ganem and Compton 2004, Ganem, Upton et al. 2005, Ems-McClung and Walczak 2010, Uehara, Tsukada et al. 2013). KIF2B makes a much more significant contribution to the movement of chromosomes to the poles and is also involved in cytokinesis and spindle assembly. It is localised to centrosomes, kinetochores and the midbody (Manning, Ganem et al. 2007). KIF24 is involved in assembly and disassembly of the cilium and maturation of the centriole (Kobayashi, Tsang et al. 2011, Kim, Lee et al. 2015).

MCAK is localised to the centrosomes, centromeres, spindle midzone, outer kinetochore and plus-ends of microtubules during mitosis (Wordeman and Mitchison 1995, Maney, Hunter et al. 1998). During interphase, MCAK is found both in the nucleus and the cytosol, where it tracks growing microtubule plus-ends (Moore, Rankin et al. 2005). MCAK has key roles in regulating spindle formation, kinetochore alignment, microtubule dynamics, chromosome segregation and correcting kinetochore-microtubule attachments (Maney, Hunter et al. 1998, Kline-Smith, Khodjakov et al. 2004,

Wordeman, Wagenbach et al. 2007, Jaqaman, King et al. 2010). MCAK tracks growing microtubule ends, due to its association with the tip-tracking protein EB1 (Moore, Rankin et al. 2005). MCAK's tip-tracking has been shown to be enhanced by association with KIF18B (Tanenbaum, Macurek et al. 2011). MCAK has also been shown to be important in meiosis – it is involved in assembling the meiotic spindle (Ohi, Sapra et al. 2004, Connolly, Sugioka et al. 2015) and silencing the spindle assembly checkpoint in oocytes (Vogt, Sanhaji et al. 2010). Deficiency of MCAK does not significantly impair a cell's ability to form a bipolar spindle (Maney, Hunter et al. 1998, Ganem and Compton 2004). Surprisingly, knockdown of MCAK in cells, using siRNA, leads to a decrease in the rate of microtubule assembly (Wordeman, Decarreau et al. 2016). In contrast, it has been found that when MCAK is rapidly sequestered to the cell membrane then the rate of microtubule assembly is increased (Wordeman, Decarreau et al. 2016). The authors suggest that when MCAK levels are slowly reduced by siRNA treatment the cell is able to compensate through lowering the rate of microtubule nucleation.

1.5 MCAK in cancer

As a result of MCAK's importance in mitosis, disruption of its activity leads to mitotic chromosomal instability, a causative hallmark of solid tumours that correlates with poor prognosis (Carter, Eklund et al. 2006, Bakhoun, Genovese et al. 2009). In contrast, increased MCAK expression has been observed in tongue (Wang, Xiang et al. 2014), colorectal (Ishikawa, Kamohara

et al. 2008), gastric (Nakamura, Tanaka et al. 2007) and breast cancer tissues (Shimo, Tanikawa et al. 2008, Lu, Wang et al. 2019). It has also been linked to increased progression, invasiveness and metastasis of tumours, resulting in a poor prognosis for the patient (Gnjatic, Cao et al. 2010). It is now thought that this increase in MCAK expression may be due to mutations in p53, as p53 has been shown to act on the *MCAK* promoter through Sp1, to repress MCAK expression (Jun, Lee et al. 2017). Additionally, MCAK may regulate cellular senescence through a p53 dependent pathway (Gwon, Cho et al. 2012).

The MCAK substitution E403K has been suggested as a possible causative factor for colorectal cancer (Kumar, Rajendran et al. 2013). MCAK has been shown to be involved in invasiveness of tumour cells and in cell migration (Braun, Dang et al. 2014, Ritter, Sanhaji et al. 2015). Additionally, MCAK has been shown to cause resistance to the chemotherapeutic agents paclitaxel and epothilone A, which act by stabilising microtubules (Ganguly, Yang et al. 2011).

1.6 Structure of MCAK

MCAK is dimeric, with each 82kDa monomer containing four distinct domains, these are the: N-terminal, neck, motor and C-terminal domains (**Figure 1.6**).

The motor domain is highly conserved among kinesins and MCAK's motor domain contains 35% sequence identity with the kinesin-1 heavy chain. The high percentage of sequence and structural conservation (see **Figure 1.7**) is

primarily because the motor domain mediates two functions that are critical to kinesins – nucleotide and microtubule binding. Uniquely among the kinesin superfamily, in kinesin-13s the motor domain is central in the kinesin domain structure (Wordeman and Mitchison 1995). They were previously known as KinI for Kinesin with Internal motor domain, or M-type kinesins – having a motor domain in the Middle of the sequence.



Figure 1.6. Domain structure of MCAK. MCAK has four distinct domains; the N-terminal, neck, motor and C-terminal domains. The neck and motor domains are required for depolymerase activity, while the N- and C-terminal domains allow dimerization.

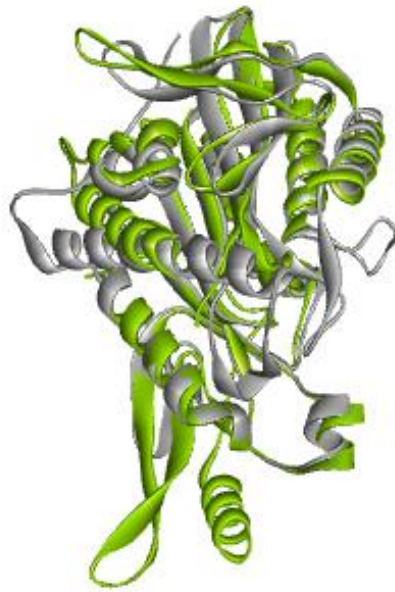


Figure 1.7. Overlay of Kinesin-1 and Kinesin-13 motor domains. Kinesin-13 (Human MCAK, PDB ID: 2HEH) is shown in green and Kinesin-1 (Mouse KIF5C, PDB ID: 3X2T) is shown in grey.

While the motor domain is responsible for destabilizing the microtubule end, depolymerisation activity is not achieved under physiological conditions without the positively charged neck domain, which is responsible for the association of MCAK with the microtubule (Maney, Wagenbach et al. 2001, Ovechkina, Wagenbach et al. 2002, Cooper, Wagenbach et al. 2010). Full-length MCAK can bind adjacent protofilaments at alternate binding sites along a single protofilament. The neck domain of MCAK interacts with the tubulin dimer adjacent to the dimer where the motor domain is bound, precluding another motor domain from binding there (Mulder, Glavis-Bloom et al. 2009, Benoit, Asenjo et al. 2018, Trofimova, Paydar et al. 2018). MCAK is

particularly adapted for binding curved protofilaments, interacting with both ends of the helix H12 in the α and β tubulin subunits (Ogawa, Nitta et al. 2004, Shipley, Hekmat-Nejad et al. 2004, Asenjo, Chatterjee et al. 2013, Wang, Cantos-Fernandes et al. 2017, Benoit, Asenjo et al. 2018). In the α tubulin subunit H12 interacts with the MCAK α 4 helix at one end and the Loop 2 KVD motif at the other end. In the β subunit H12 interacts with the α 5 helix at one end and the β 5a- β 5b hairpin at the other (**Figure 1.8**). In this way the β 5a- β 5b hairpin and Loop 2 act as levers, while α 5, Loop 12 and α 4 act as a wedge, bending the tubulin conformation. The angle at the tubulin intradimer interface is 14.7° when bound to MCAK, compared to 11.7° when bound to Kinesin-1 (Wang, Cantos-Fernandes et al. 2017). The respective contributions of the 'wedge' and 'levers' is unclear.

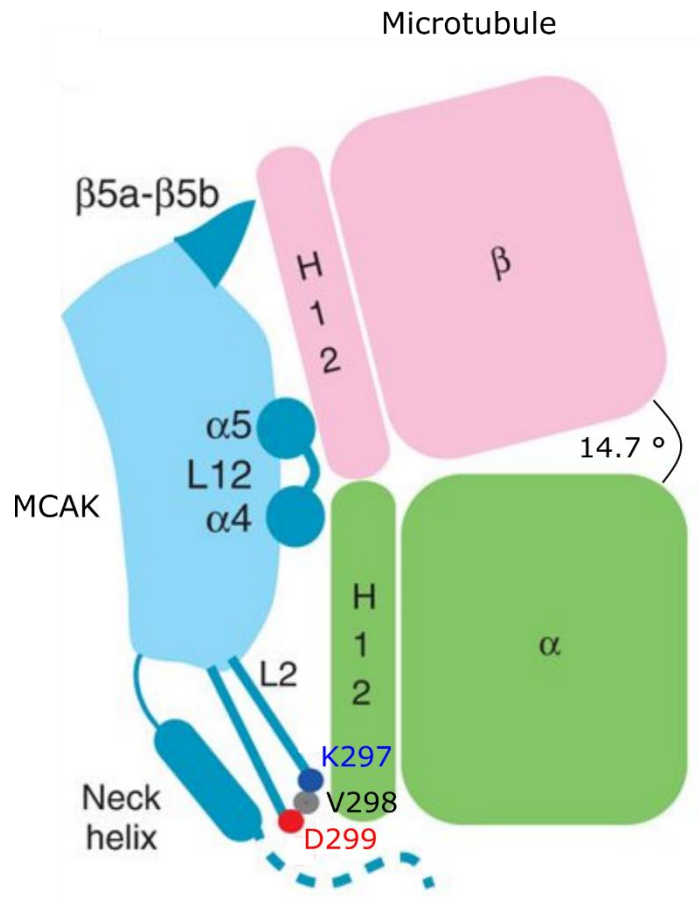


Figure 1.8 MCAK binding induces tubulin curvature. MCAK binds to both ends of H12 in both tubulin subunits, inducing tubulin curvature. Modified from (Wang, Cantos-Fernandes et al. 2017).

The structures of the N- and C-terminal domains have yet to be determined but both domains are believed to be involved in MCAK dimerisation (Maney, Wagenbach et al. 2001, Talapatra, Harker et al. 2015). Dimeric MCAK has a reduced association rate with the microtubule lattice compared to the monomer, leading to a lower concentration at the microtubule end. However, dimerisation enhances MCAK's ability to interact with the microtubule end, increases its ATPase rate and leads to improved processivity of

depolymerisation (Hertzer, Ems-McClung et al. 2006, Cooper, Wagenbach et al. 2010).

The N-terminus of MCAK is important for its localisation (Welburn and Cheeseman 2012). It contains the SxIP motif through which MCAK binds to EB1, allowing it to track growing microtubule ends (Moore, Rankin et al. 2005, Honnappa, Gouveia et al. 2009). At the microtubule end this region of the N-terminus interacts with the microtubule (McHugh, Zou et al. 2019). The N-terminus of MCAK is also required for centromeric localisation (Maney, Hunter et al. 1998, Walczak, Gan et al. 2002). It has now been shown that this is because phosphorylation of Sgo2 by Aurora B recruits MCAK to centromeres through the N-terminus (Tanno, Kitajima et al. 2010). The N-terminal domain is also important for spindle assembly (Ems-McClung, Hertzer et al. 2007).

The C-terminus is necessary for maximal depolymerisation activity of MCAK (Ems-McClung, Hertzer et al. 2007). It also affects MCAK's ATPase activity – the C-terminus can prevent unproductive ATP turnover on the microtubule lattice. MCAK's microtubule lattice-stimulated ATPase activity is increased when the last eight amino acids of the C-terminus of MCAK are deleted (Moore and Wordeman 2004) and the same deletion also abolishes its tip-tracking ability, which is dependent on EB1 binding to the SxIP motif in the N-terminus. This is evidence of the role of the C-terminus in regulating MCAK's activity through interaction with the N-terminus (McHugh, Zou et al. 2019).

The terminal 25 residues of MCAK have been shown to be important for

inducing and stabilising dimerization (Talapatra, Harker et al. 2015). The C-terminus can bind directly to the motor domain in solution and induce it to dimerise and this dimeric structure is stabilised by the binding of the C-terminus to the second motor domain (Ems-McClung, Hainline et al. 2013, McHugh, Zou et al. 2019). In solution the C-terminus interacts with the motor domain interfering with the motor domain's interaction with a microtubule, i.e. it is adopting a closed conformation. The microtubule lattice triggers a change in MCAK's conformation and the interaction between the C-terminus and motor domain alters – switching from a closed state to an open one. When MCAK reaches the microtubule end it reverts back to the closed conformation for microtubule depolymerisation. (Ems-McClung, Hainline et al. 2013, Talapatra, Harker et al. 2015).

1.7 ATP turnover and its impact on MCAK's microtubule affinity

Unlike conventional kinesins, MCAK and other members of the kinesin-13 family do not “walk” along microtubules. Instead, MCAK diffuses one-dimensionally along the lattice (Helenius, Brouhard et al. 2006). The electrostatic interactions between the positively charged neck of MCAK and the negatively charged E hook of the tubulin dimer (a flexible region at the C-terminus of tubulin containing a large number of glutamate residues) increases the association rate of MCAK onto the microtubule, while steric hindrance from adjacent protofilaments impedes tight binding. Once MCAK is interacting with the microtubule it is thought that the restructuring of the

hydration shell around the microtubule lattice and MCAK is sufficient to provide a barrier to dissociation, leading to the 1D diffusive behaviour that has been observed (Cooper, Wagenbach et al. 2010). It is proposed that when MCAK reaches the microtubule end it is able to interact more tightly and stabilise a curved conformation of the protofilament at both the intradimer (through the $\alpha 4$ helix, highlighted in **Figure 1.9**) and interdimer (through the KVD finger, also highlighted) interfaces (Hunter, Caplow et al. 2003, Ogawa, Nitta et al. 2004). This was also shown in the recently solved structure of human MCAK bound to tubulin (Wang, Cantos-Fernandes et al. 2017). The structure of the *D. melanogaster* Kinesin-13 KLP10AHD bound to tubulin shows the shear and curvature induced in the tubulin structure (Benoit, Asenjo et al. 2018). This change in the tubulin conformation is thought to contribute to depolymerisation. Microtubule binding alters the orientation and length of the $\alpha 4$ helix, acting as a relay to the switch II region, which closes around the nucleotide binding site. The switch I and II regions of the motor domain are joined by a salt bridge which forms a tunnel for the ATP molecule. Based on the ATP turnover mechanism defined in Eg5, a water molecule acts as a catalytic base, extracting a proton from between the β and γ phosphates, leaving ADP and the inorganic phosphate Pi (Parke, Wojcik et al. 2010). This reduces MCAK's affinity for the microtubule.

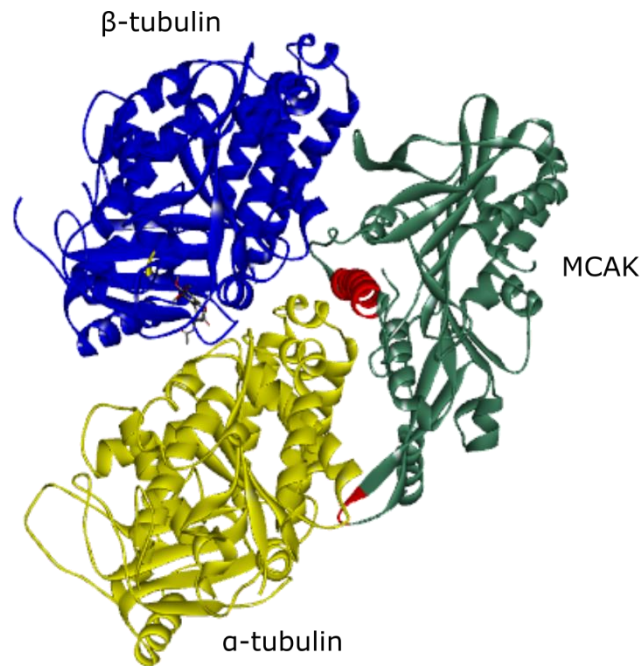


Figure 1.9. The structure of the MCAK motor domain in complex with tubulin. MCAK is thought to stabilise the curved conformation of protofilaments through its $\alpha 4$ helix and KVD finger (highlighted in red). MCAK – *Homo sapien*, Tubulin – *Bos taurus*. Modified from (Wang, Cantos-Fernandes et al. 2017), PDB ID: 5MIO.

The basal rate of ATP turnover (completion of the entire ATP turnover cycle – shown in **Figure 1.10**) by MCAK is low but it is substantially increased by the presence of tubulin or microtubules (Friel and Howard 2011). In contrast to conventional kinesin, where the dissociation of ADP is the rate limiting step in its ATP turnover cycle (Hackney 1988), for MCAK in solution the slowest step of ATP turnover is ATP cleavage (Friel and Howard 2011). As a consequence of this, MCAK in solution is ATP bound (**Figure 1.11 (1)**) and in a closed conformation but, after encountering a microtubule, (**Figure 1.11 (2)**) ATP cleavage occurs and the resulting open, ADP-bound form diffuses along the

microtubule (**Figure 1.11 (3)**) until it dissociates from the microtubule or reaches the microtubule end. Here, the exchange of ADP for ATP is catalysed and then MCAK closes and binds tightly to the microtubule (**Figure 1.11 (4)**). Structures of KLP10AHD show that the nucleotide binding pocket only closes around the nucleotide when the kinesin interacts with curved tubulin (Benoit, Asenjo et al. 2018). When MCAK binds tightly to the microtubule it induces further microtubule curvature and separation of the protofilaments leading to dissociation of the terminal tubulin dimer (**Figure 1.11 (5)**) (Burns, Wagenbach et al. 2014, Trofimova, Paydar et al. 2018). ATP is then cleaved, opening MCAK's conformation again which, if MCAK has left with the tubulin dimer, allows the dimer to be released (**Figure 1.11 (6)**). Exchange of ADP for ATP causes MCAK to return to the closed state, ready to encounter a microtubule for further rounds of depolymerisation (Friel and Howard 2011, Ems-McClung, Hainline et al. 2013). MCAK shows limited processivity *in vitro* with the turnover of one molecule of ATP leading to the dissociation of up to 20 tubulin dimers. Overall, MCAK accelerates the rate of tubulin dimer removal from the microtubule end by 100-fold (Hunter, Caplow et al. 2003). It is unknown whether MCAK can process GTP.

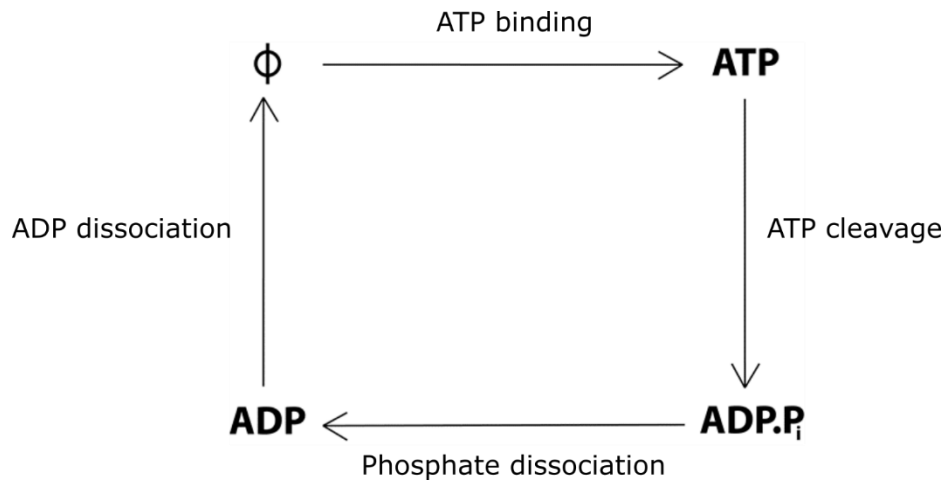


Figure 1.10. The ATP turnover cycle. ATP turnover consists of ATP binding to the nucleotide-free site (ϕ), ATP cleavage to ADP-P_i, dissociation of the free phosphate and release of ADP. Modified from (Friel and Howard 2011).

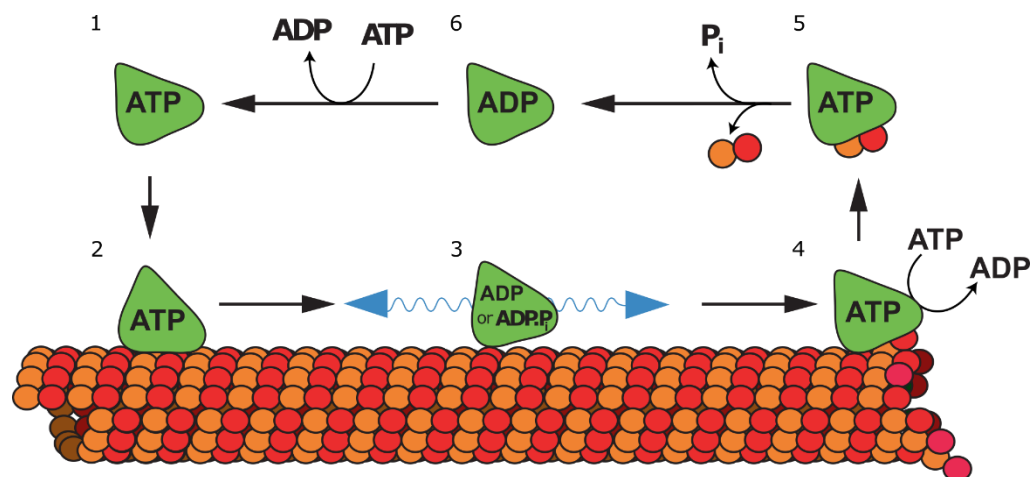


Figure 1.11. The coupling of ATP turnover and microtubule depolymerisation by MCAK. MCAK encounters the microtubule in its ATP bound state, which accelerates ATP cleavage to produce ADP. This converts MCAK from a tightly bound state to a weakly bound state to allow diffusion along the microtubule. When MCAK reaches the microtubule end this accelerates the exchange of ADP for ATP, and MCAK binds more tightly, causing a change in conformation which leads to loss of the terminal tubulin dimer from the microtubule end. When ATP is cleaved the tubulin dimer is

released and ADP is exchanged for ATP in solution. Modified from (Friel and Howard 2011).

1.8 Phosphorylation of MCAK

MCAK's activity is primarily regulated by phosphorylation, although MCAK activity is also stimulated by association with ICIS (Inner Centromere KinI Stimulator) (Ohi, Coughlin et al. 2003). Phosphorylation is achieved by several mitotic kinases including: cyclin dependent kinase 1 (Cdk1) (Sanhaji, Friel et al. 2010), Polo-like kinase 1 (Plk1) (Zhang, Shao et al. 2011), Aurora A (Zhang, Ems-McClung et al. 2008), Aurora B (Andrews, Ovechkina et al. 2004), and also by p21 activated kinase 1 (PAK1) (Pakala, Nair et al. 2012). All five of these kinases have critical roles in mitosis. Cdk1 is an essential protein kinase with over 70 known substrates. Cyclin B-cdk1 targets are involved in separating the centrosomes (e.g. kinesin related motors such as Eg5), chromosome condensation (e.g. condensins and histones), fragmentation of the Golgi network (e.g. Golgi matrix components), breakdown of the nuclear lamina (e.g. nuclear lamins) and spindle assembly (e.g. microtubule binding proteins such as stathmin) (Peter, Nakagawa et al. 1990, Blangy, Lane et al. 1995, Kimura, Hirano et al. 1998, Lowe, Rabouille et al. 1998, Andersen 1999).

Plk1 is involved in centrosome maturation, during which the replicated centrosomes separate and recruit γ -tubulin ring complexes, leading to increased microtubule nucleation. It is also thought to have a role in regulating cytokinesis and in controlling Cdk1 activity through activation of

cdc25 phosphatase promoting entry into mitosis and then by activating the anaphase promoting complex (APC) leading to mitotic exit (Kumagai and Dunphy 1996, Lane and Nigg 1996, Carmena, Riparbelli et al. 1998, Kotani, Tugendreich et al. 1998).

Aurora A has been implicated in centrosome maturation and separation, mitotic entry, bipolar spindle assembly, chromosome alignment on the metaphase plate and cytokinesis (Hannak, Kirkham et al. 2001, Hirota, Kunitoku et al. 2003, Kunitoku, Sasayama et al. 2003, Marumoto, Honda et al. 2003, Cowley, Rivera-Perez et al. 2009).

Aurora B is a key member of the chromosomal passenger complex (Kaitna, Mendoza et al. 2000) which regulates mitotic chromosome structure and microtubule-kinetochore attachments, activates the spindle assembly checkpoint, stabilises the spindle midzone and regulates contractile ring formation and chromosomal abscission (Hauf, Cole et al. 2003, Lipp, Hirota et al. 2007).

The p21-activated kinase 1 (PAK1) is a serine/threonine kinase that interacts with the small Ras-related GTPases (p21 proteins) Cdc42 and Rac1 (Manser, Leung et al. 1994). PAK1 regulates the actin cytoskeleton, activates growth factor signalling, protects cells from apoptosis and regulates gene transcription (Galisteo, Chernoff et al. 1996, Sells, Knaus et al. 1997, Schurmann, Mooney et al. 2000, Barnes, Vadlamudi et al. 2003).

The known phosphorylation sites of MCAK and the associated kinases are shown in **Figure 1.12**. Phosphorylation by Aurora B has been shown to be both spatially and temporally regulated, with different sites being phosphorylated in different locations and at different stages in the cell cycle (Zhang, Lan et al. 2007). It seems possible that this is also the case with phosphorylation by other kinases and this makes it useful to study the effect of phosphorylation sites individually.

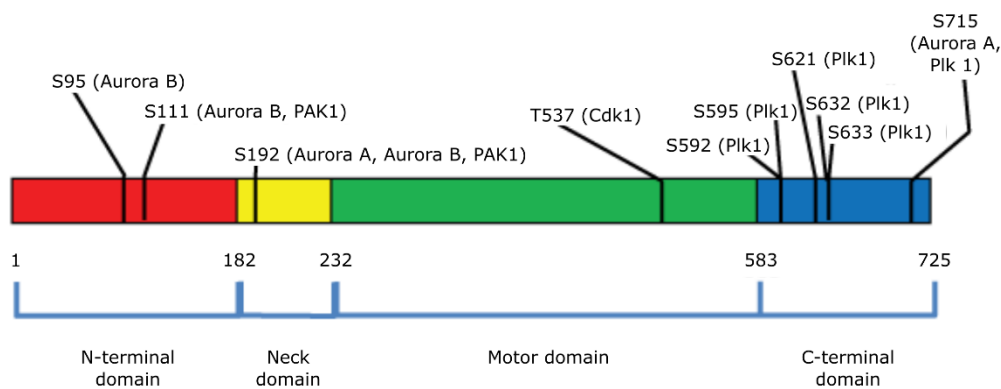


Figure 1.12. The phosphorylation sites of MCAK. The known phosphorylation sites of MCAK and their associated kinases are shown.

Phosphorylation of MCAK has been shown to have three major effects on MCAK's function – it can affect MCAK's cellular localisation, its conformation and its depolymerisation activity.

1.8.1 Effect of phosphorylation on MCAK's localisation

Each kinase involved in phosphorylating MCAK has sites of phosphorylation which are thought to affect the localisation of MCAK rather than its activity: S715 by Aurora A (S719 *X. laevis*), S95 and S111 by Aurora B (S92 and S186 in

C. griseus, T95 and S110 in *X. laevis*) and S111 by PAK1. In early mitosis, MCAK localises to the centre of Ran asters to help promote aster formation and pole focussing. Phosphorylation of MCAK by Aurora A at S715 helps maintain MCAK at the spindle poles (Zhang, Ems-McClung et al. 2008). Phosphorylation by Cdk1 at T537 then promotes both the migration of MCAK away from the spindle poles and correct spindle formation (Sanhaji, Friel et al. 2010). Aurora B mediated phosphorylation at S95 and S111 promotes MCAK's movement from the chromosome arms and on towards the centromeres (Andrews, Ovechkina et al. 2004, Lan, Zhang et al. 2004, Ohi, Sapra et al. 2004) where MCAK can correct improper kinetochore-microtubule attachments. Phosphorylation by Plk1 has also been proposed to contribute to this function, stimulating MCAK's activity to antagonise its inhibition by Aurora B induced phosphorylation (Zhang, Shao et al. 2011). MCAK's ability to track growing microtubule ends has also been shown to be regulated by phosphorylation (Moore, Rankin et al. 2005). Aurora kinase phosphorylation of MCAK reduces its ability to interact with KIF18B, leading to a reduced association with the microtubule end (Tanenbaum, Macurek et al. 2011).

1.8.2 Effect of phosphorylation on MCAK's conformation

Phosphorylation at S192 has been linked to a change in conformation of MCAK leading to a reduction in microtubule association and consequently a reduced depolymerisation activity. An interaction between the C-terminal and neck domains is disrupted by the addition of the phosphate, preventing

formation of the closed conformation in which MCAK depolymerises microtubules (Ems-McClung, Hainline et al. 2013, McHugh, Zou et al. 2019). Moreover phosphorylation at S192 has been shown to affect the migration and invasion of tumour cells (Ritter, Sanhaji et al. 2015).

Additionally phosphorylation at S715 by Aurora A or Plk1 is thought to affect MCAK's conformation. The phosphomimic S715E substitution prevents the C-terminus of MCAK from interacting with the motor domain (Talapatra, Harker et al. 2015). This interaction is thought to stabilise MCAK dimerisation as the C-terminal tail binds along the interface between the two motor domains. Zhang et al. observed that interaction of the C-terminus and N-terminal and neck-motor domains were affected by phosphorylation by Plk1 (Zhang, Shao et al. 2011).

1.8.3 Effect of phosphorylation on MCAK's depolymerisation activity

Phosphorylation by Cdk1 occurs at T537 in the motor domain of MCAK, the only phosphorylation site identified to date in this highly conserved domain (Sanhaji, Friel et al. 2010). T537 is adjacent to the α 4 helix, which, as mentioned in chapter 1.7, is thought to stabilise the curved conformation of protofilament ends, leading to depolymerisation (Ogawa, Nitta et al. 2004). The phosphomimetic MCAK mutant T537E depolymerises microtubules at a decreased rate, suggesting phosphorylation at this site inhibits MCAK's depolymerising activity.

Aurora A, Aurora B and PAK1 are all thought to inhibit MCAK's depolymerisation of microtubules, by phosphorylating S192 (S196 in *Xenopus*

laevis) (Lan, Zhang et al. 2004, Zhang, Ems-McClung et al. 2008, Pakala, Nair et al. 2012). Phosphorylation of MCAK by Aurora B switches the conformation from closed to open, resulting in reduced microtubule affinity, which reduces MCAK's ability to depolymerise microtubules (Ems-McClung, Hainline et al. 2013). The reduction in microtubule affinity is graded dependent on the degree of phosphorylation (McHugh, Zou et al. 2019).

Plk1 is the only kinase that has been shown to be associated with stimulating MCAK's depolymerisation activity (Zhang, Shao et al. 2011). Six phosphorylation sites at the C-terminus of MCAK have been identified for Plk1: S592, S595, S621, S632, S633 and S715 (Zhang, Shao et al. 2011).

Although phosphorylation is known to affect MCAK's conformation and depolymerisation activity, fairly little is understood about how phosphorylation achieves these effects.

1.9 End recognition in kinesins

Microtubule regulating kinesins such as MCAK need to be able to recognise the microtubule end as being distinct from the microtubule lattice. Several different microtubule regulating kinesins have been shown to exhibit microtubule end residence times that are longer than the residence time at any one position on the microtubule lattice. The Kinesin-5, Eg5, is a microtubule polymerase. It is able to slide microtubule bundles against each other and is involved in spindle assembly and axon branching. Eg5 resides at

microtubule ends for 7 seconds where it promotes polymerisation and helps prevent catastrophe (Chen and Hancock 2015). Kip3 is a microtubule depolymerase in the Kinesin-8 family. It translocates along the microtubule lattice and then resides at the microtubule end for tens of seconds, before removing a single tubulin dimer (Varga, Leduc et al. 2009). CENP-E is a slow plus end directed motor, but also shows localisation at the plus end where it promotes microtubule elongation (Sardar, Luczak et al. 2010). KIF4, a Kinesin-4 has also been shown to be localised to the plus end of microtubules (Subramanian, Ti et al. 2013), where it blocks microtubule polymerisation (Hu, Coughlin et al. 2011) and Nod, an orphan kinesin, binds to plus ends and promotes polymerisation (Cui, Sproul et al. 2005). KIF15 suppresses microtubule catastrophe by binding to growing microtubule plus-ends (Drechsler and McAinsh 2016). Similarly in *S. pombe*, the Kinesin-7 Tea2 stabilises microtubule plus end dynamics, antagonising the activity and restricting the access of the destabilising Kinesin-8s, Klp5 and Klp6, to the microtubule end.

MCAK has also been shown to have a long microtubule end residence time and this has been shown to be important for its microtubule depolymerising activity (Helenius, Brouhard et al. 2006, Patel, Belsham et al. 2016).

Aims

In my introduction I have given a broad overview of what is currently known about the roles of kinesins in cells and in particular the activities of MCAK and how they are regulated. To extend this knowledge I first wanted to find out more about the mechanisms by which phosphorylation affects MCAK's activity. I did this by investigating phosphorylation at T537, the only known phosphorylation site in MCAK's motor domain, to understand how phosphorylation at this site led to a decrease in MCAK's depolymerisation activity. This work is discussed in Chapter 3.

As the motor domain contains the major interaction sites between MCAK and the microtubule, phosphorylation events which occur outside of this domain cannot directly affect that interaction. I was curious about how phosphorylation events outside of the motor domain could affect MCAK's activity and so Chapter 4 shows my work looking at Plk1 phosphorylation, which occurs in the C-terminal domain of MCAK and had been shown previously to lead to an increase in MCAK's depolymerisation activity.

Having looked at the molecular mechanisms by which MCAK is regulated, I wanted to investigate more about the features of MCAK that underlie the molecular mechanism of its depolymerisation activity. A key requirement for MCAK to be able to depolymerise microtubules is the ability to recognise the microtubule end. In Chapter 5 I describe work investigating the possibility of introducing end recognition and/or depolymerisation ability in Kinesin-1 by

introducing residues that have been shown to be important for MCAK's recognition of the microtubule end.

Chapter 2 Methods

2.1 Site-directed mutagenesis

Mutagenesis to create single amino acid substitutions was achieved using mismatched primers, minimally altered to encode the new amino acid required (Integrated DNA Technologies). Mutagenic primers were incorporated into the pFastBac plasmid by polymerase chain reactions (PCRs) using pFastBac containing the wild-type gene of interest as the template. PCRs were carried out using Phusion High Fidelity DNA polymerase (Thermo Scientific) in Phusion reaction buffer containing a final concentration of 1 ng/ μ l double stranded pFastBac containing the cDNA of interest, 2.5 ng/ μ l forward primer, 2.5 ng/ μ l reverse primer, 800 μ M dNTP mix, 1 % (v/v) DMSO. Control reactions without primers and without polymerase were also set up. The reactions were started at 95 °C for 30 seconds and then went through 18 cycles of 95 °C for 30 seconds, 55 °C for 1 minute and 9 minutes at 68 °C. At the end of the temperature cycles the reaction was held at 4 °C. *Dpn I* (New England Biolabs) was added to each reaction to a final concentration of 2 U/ μ l to digest the original plasmid DNA template. After gentle mixing, the mixture was incubated at 37 °C overnight. 2 μ l of the reaction mix was added to 45 μ l XL1 Blue competent cells (made using the Inoue method (Inoue, Nojima et al. 1990)), which were then incubated on ice for 30 minutes before heat-shocking at 42 °C for 40 seconds. After 2 minutes on ice, 0.5 ml pre-warmed (42 °C) NZY+ broth (10 g/l NZ amine, 5 g/l yeast extract, 85 mM NaCl) containing 12.5 mM MgCl₂, 12.5 mM MgSO₄ and 20 mM glucose was added to

each reaction, and the mixture was incubated at 37 °C for 1 hour with shaking at 225 rpm. After spinning down the cells at 269 x g for 3 minutes, 250 µl media was removed and the cells were resuspended in the remaining media and spread onto LB-ampicillin agar plates. The plates were incubated at 37 °C overnight. A single colony from each plate was then grown up overnight, in 5 ml LB broth containing ampicillin (0.1 mg/ml), at 37 °C with shaking at 225 rpm. The cells were pelleted by centrifugation at 8228 x g for 5 minutes and the supernatant was removed. The DNA was extracted from the pellet using the QIAPREP SPIN Miniprep kit (Qiagen) and sequenced. DNA sequencing was carried out by Source-BioSciences.

2.2 *Cell culture and protein expression in insect Sf9 cells*

2.2.1 Cell culture

Spodoptera frugiperza (Sf9) cells were propagated in Insect-XPRESS™ protein-free insect cell medium (Lonza), with 200 units/ml penicillin, 0.2 mg/ml streptomycin and 10 % (v/v) foetal bovine serum (FBS, Gibco). They were incubated, in suspension, at 27 °C with shaking at 150 rpm.

2.2.2 Transformation of DH10Bac

The mutated pFastBac vectors were transformed into DH10Bac cells, which transposed the pFastBac vector into the baculovirus genome. Briefly, 50 µl DH10Bac cells (Thermo Fisher Scientific) were mixed with the pFastBac vector (1 µl) and incubated on ice for 30 minutes. The cells were then heat-shocked

for 45 seconds at 42 °C and chilled on ice for 2 minutes. LB media (900 µl) was added and the mixture was then incubated at 37 °C for 4 hours with shaking at 250 rpm. The cells were then spun down at 340 x g for 10 minutes, resuspended in approximately one quarter of the supernatant and spread onto LB agar plates containing 30 µg/ml kanamycin, 7 µg/ml gentamicin, 10 µg/ml tetracycline, 100 µg/ml 5-bromo-4-chloro-3-indolyl-β-D-galactopyranoside (X-gal) and 40 µg/ml isopropyl β-D-1-thiogalactopyranoside (IPTG). After 72 hours at 37 °C, white colonies were picked, restreaked on a fresh agar plate and cultured overnight at 37 °C. The overnight cultures were made into glycerol stocks by adding glycerol to a final concentration of 15 % (v/v), and were stored at -80 °C provided the restreaking showed no blue colonies.

2.2.3 Baculovirus production

A 5 ml culture was grown overnight from the glycerol stock of transformed DH10Bac cells and the bacmid DNA was extracted using the ZR BAC DNA Miniprep kit (Zymo Research) and stored at 4 °C overnight. Sf9 cells (2 ml), at 0.5×10^6 cells/ml, were allowed to adhere for 1 hour to each well of a 6-well plate. Meanwhile, 5 µl bacmid DNA was diluted in 500 µl Xpress media (serum and antibiotic free), and 5 µl Escort IV transfection reagent (Merck) was also diluted in 500 µl Xpress media (serum and antibiotic free). The DNA was mixed with the transfection reagent and incubated at room temperature for approximately 30 minutes. The media was removed from the plated cells, which were washed with 1 ml of fresh Xpress media before incubation with

the transfection mix for 5 hours at 27 °C. After this time, the transfection mix was removed, cells washed with 1 ml of fresh media and 1 ml of media containing 2 % (v/v) penicillin/ streptomycin and 2 % (v/v) FCS was added. 5 days post-transfection the cell suspension was removed and spun down at 340 x g for 5 minutes and 1 ml of the supernatant was used to infect Sf9 cells (50 ml in suspension) at 0.5×10^6 cells/ml. The infected cells were monitored to 'catch' them when they had produced large amounts of virus but had not yet lysed. To achieve this, the cell count and diameter were measured after 24 and 42 hours. When the cell diameter reached 1-2 μm larger in the infected cells compared to uninfected (15-16 μm) the cells were harvested by centrifugation at 453 x g for 5 minutes, resuspended in 2.5 ml Xpress media with 10 % (v/v) DMSO and 2 % (v/v) penicillin/ streptomycin, aliquoted into 500 μl fractions in cryovials and frozen in a -1 °C/minute cooling rate rack in a -80 °C freezer, before being transferred to liquid nitrogen. This is referred to as the BIIC (Baculovirus infected insect cell) stock.

2.2.4 Protein expression

MCAK proteins were expressed in Sf9 cells by adding 100 μl BIIC stock per 300 ml Sf9 cells in suspension (approximately 1×10^6 cells/ml) in media without FCS. After 72 hours incubation at 27 °C with shaking at 150 rpm, the cells were centrifuged at 453 x g for 10 minutes, resuspended in 4 ml lysis buffer (50 mM HEPES pH 7.5, 150 mM NaCl, 5 % (v/v) glycerol, 0.1 % (v/v) Tween 20, 1 mM MgCl_2 , 1 mM EGTA) / g cell wet weight and frozen as drops in liquid nitrogen to form cell pearls, which were stored at -80 °C.

2.3 *One step purification of MCAK-His6 proteins*

MCAK was purified using a nickel affinity chromatography column.

Approximately 5 g of cell pearls were lysed by 30 minutes incubation on rollers at 4 °C in 15 ml lysis buffer (50 mM Tris pH 7.5, 300 mM NaCl, 10 % (v/v) glycerol, 5 mM MgCl₂, 0.1 % (v/v) Tween 20, 10 mM Imidazole, 10 mM Dithiothreitol (DTT), 1 mM ATP, 5 µg/ml Leupeptin, 0.7 µg/ml Pepstatin A, 18 µg/ml PMSF). The lysate was cleared by centrifugation at 48,384 x g for 1 hour. The cleared lysate was incubated with 0.5 ml Ni-NTA beads for 1 hour at 4 °C. The protein-loaded beads were then loaded into an empty gravity flow column (Biorad) and washed with 5 ml of 70 mM imidazole nickel affinity buffer (50 mM Tris pH 7.5, 300 mM NaCl, 10 % (v/v) glycerol, 1 mM MgCl₂). Protein was eluted using 3 ml of 200 mM imidazole nickel affinity buffer, and collected in fractions of approximately 300 µl. The protein content of the fractions was assessed using SDS-PAGE (Section 2.4). If required, fractions were then buffer exchanged using a desalting column (Thermo Scientific). The buffer used was dependent on the assay in which the protein was to be used. BRB20 (20 mM PIPES/KOH pH 6.9, 1 mM MgCl₂, 1 mM EGTA) with 75 mM KCl, 10 % (v/v) glycerol and 0.1 % (v/v) Tween 20 was used for measuring depolymerisation using microscopy, while 75 mM KCl, 10 % (v/v) glycerol, 0.1 % (v/v) Tween 20 in BRB80 (80 mM PIPES/KOH pH 6.9, 1 mM MgCl₂, 1 mM EGTA) was used for the light scattering assay. The concentration of each

MCAK protein was determined using the Bradford assay with BSA as a standard.

2.4 Sodium dodecyl sulphate polyacrylamide gel electrophoresis (SDS-PAGE)

Samples for SDS-PAGE analysis were mixed with an equal volume of sample buffer (100 mM Tris HCl pH 8, 4 % (w/v) SDS, 0.2 % (w/v) bromophenol blue, 20 % (v/v) glycerol, 25 mM DTT) and separated by electrophoresis using a 10 % acrylamide resolving gel and 3 % acrylamide stacking gel at 120 V for approximately 1.5 hours. Gels were stained with Instant Blue (Expedeon).

2.5 Preparing tubulin

2.5.1 Preparing tubulin from porcine brain

Porcine brains have a high tubulin content and so were used as a tubulin source (as described previously (Castoldi and Popov 2003)). The tubulin was isolated using successive rounds of polymerisation and depolymerisation in high molarity PIPES (to remove tubulin binding proteins). Briefly, 1 L depolymerisation buffer (50 mM 2-(N-morpholino) ethanesulphonic acid (MES) pH 6.6, 1 mM CaCl₂) at 4 °C was added per kilogram of halved porcine brain. The brains were then homogenised and centrifuged for 1 hour at 20,000 x g at 4 °C. To the supernatant an equal volume of 37 °C high molarity PIPES buffer (1 M PIPES pH 6.9, 10 mM MgCl₂, 20 mM EGTA) and an equal

volume of glycerol were added. ATP and GTP were added to final concentrations of 1.5 mM and 1 mM respectively. The mixture was incubated for 1 hour at 37 °C with stirring and centrifuged at 33,000 x g for 2 hours at 37 °C. The pellets were then snap frozen and stored at -80 °C. The pellets were resuspended in a minimum volume of cold depolymerisation buffer, dounced and incubated on ice for 30 minutes. The mixture was then centrifuged at 180,000 x g for 30 minutes at 4 °C. The supernatant was mixed with an equal volume of warm (37 °C) high molarity PIPES buffer and glycerol and ATP and GTP to final concentrations of 1.5 mM and 1 mM respectively. It was then incubated at 37 °C for 45 minutes before centrifugation at 200,000 x g for 30 minutes at 37 °C. The pellets were then resuspended in a minimum volume of ice cold BRB80 and incubated on ice for 10 minutes. The mixture was then centrifuged at 200,000 x g for 30 minutes at 4 °C and the supernatant was snap frozen and stored at -80 °C.

2.5.2 Cycling tubulin

Tubulin was polymerised and centrifuged and then depolymerised and centrifuged to prepare a sample of tubulin that was both polymerisation and depolymerisation competent. 4 ml purified tubulin (from 2.5.1) was polymerised for 60 minutes at 37 °C in a final volume of 10 ml, containing 4 mM MgCl₂, 1 mM GTP and 30 % (v/v) glycerol in BRB80. The microtubules were then spun through a cushion of 60 % glycerol at 105,370 x g for 1 hour at 37 °C. The pellet was rinsed in BRB80 and incubated on ice for 20 minutes in the minimum volume of 0.1 % (v/v) β-mercaptoethanol in BRB80 for

resuspension. The pellet was then resuspended and the mixture was spun at 105,370 x g for 15 minutes at 4 °C. The supernatant was collected and the concentration was measured on a nanodrop spectrophotometer, using $\epsilon=115,000 \text{ M}^{-1} \text{ cm}^{-1}$ (Desai and Mitchison 1998).

2.5.3 Rhodamine labelling of tubulin

Tubulin was polymerised, labelled, depolymerised and then polymerised and depolymerised again to ensure that only polymerisation and depolymerisation competent tubulin, after the labelling process, was retained. In brief, 5x BRB80 was diluted 10-times with purified tubulin, and MgCl_2 and GTP were added to final concentrations of 3.5 mM and 1 mM respectively. The mixture was then stored on ice for 5 minutes and glycerol was then added to a concentration of 33 % (v/v). The mixture was then incubated at 37 °C for 30 minutes. The polymerised tubulin was then centrifuged at 80,674 x g for 35 minutes at 37 °C in a pre-warmed rotor on a cushion of 0.1 M NaHEPES pH 8.6, 4 mM MgCl_2 , 1 mM EGTA, 60 % (v/v) glycerol. The pellets were then washed with warm labelling buffer (0.1 M NaHEPES pH 8.6, 4 mM MgCl_2 , 1 mM EGTA, 40 % (v/v) glycerol) and resuspended in a total volume of approximately 600 μl . 5(6)-carboxytetramethylrhodamine N-succinimidyl ester (TAMRA) dye (Invitrogen) in DMSO was added in a 10-fold molar excess to tubulin (assuming a tubulin recovery of 70 %), and incubated at 37 °C for 40 minutes. An equal volume of quench buffer (2 x BRB80, 100 mM potassium glutamate, 40% (v/v) glycerol) was added and the mixture was spun at 197,120 x g for 20 minutes at 37 °C in

a pre-warmed rotor on a cushion of 60 % (v/v) glycerol in BRB80. The pellet was washed with warm BRB80 and then resuspended in a minimal volume of cold BRB80 before incubation at 4 °C for 30 minutes with repeated mixing. The depolymerised tubulin was then spun at 126,157 x g for 10 minutes at 4 °C in a pre-cooled rotor. BRB80, MgCl₂ and GTP were added to the supernatant to final concentrations of 1 x, 4 mM and 1 mM respectively, which was then incubated on ice for 3 minutes. It was then warmed to 37 °C for 2 minutes and glycerol was added to a final concentration of 33 % (v/v), and the tubulin was allowed to polymerise at 37 °C for 30 minutes. It was then spun at 197,120 x g for 20 minutes at 37 °C in a pre-warmed rotor on a cushion of 60 % (v/v) glycerol in BRB80. The pellet was washed with warm BRB80 and then resuspended in 500 µl cold BRB80 and left at 4 °C for 30 minutes, and mixed repeatedly. The depolymerised tubulin was spun at 126,157 x g for 10 minutes at 4 °C and the supernatant was snap-frozen and stored at -80 °C. The concentration of tubulin (in mg/ml) was calculated from $A_{280} - (0.3A_{555})/1.15$. The degree of labelling (DOL) was then calculated as $(110,000A_{555}) / (65,000 \times \text{tubulin concentration})$.

2.6 Assembling microtubules

2.6.1 Freezable microtubules

Tubulin (20 µM) was mixed with GMPCPP (1 mM) in BRB80, and incubated on ice for 5 minutes and then at 37 °C for 30 minutes. The microtubules were

then spun down in the airfuge at 12 psi (approximately 61 000 x g) for 5 minutes and resuspended in 720 μ l BRB80. After 20 minutes on ice, the microtubules were spun at 11,500 x g for 2 minutes and 80 μ l GMPCPP (1 mM) was added. The mixture was incubated on ice for 5 minutes, followed by 30 minutes at 37 °C. The microtubules were then spun down at 12 psi (approximately 61 000 x g) for 5 minutes and resuspended in 420 μ l BRB80. They were then snap frozen and stored in liquid nitrogen. Tubulin concentration was calculated by measuring the absorbance at 280 nm using a Nanodrop spectrophotometer and the extinction coefficient $\epsilon=115,000 \text{ M}^{-1} \text{ cm}^{-1}$ (Desai and Mitchison 1998).

2.6.2 Microtubules for microscopy

Fluorescently labelled microtubules were prepared by mixing 2 μ M tubulin (25 % Rhodamine (TAMRA) labelled – prepared by mixing appropriate volumes of labelled and unlabelled tubulin, taking the DOL into account), 1 mM GMPCPP and 1 mM MgCl_2 in BRB80 in a total volume of 50 μ l. They were incubated on ice for 5 minutes, followed by 2 hours at 37 °C. The microtubules were then diluted in 200 μ l BRB80, centrifuged in an airfuge (Beckmann Coulter) at 12 psi (approximately 61 000 x g) on a 200 μ l cushion of 30 % (v/v) glycerol in BRB80 for 10 minutes and the pellet was resuspended in 400 μ l BRB80.

2.6.3 Double stabilised microtubules

To create microtubules that MCAK could not depolymerise they were stabilised with both the slowly hydrolysable GMPCPP and the microtubule

binding agent taxol. Tubulin (70 μM), 5 % (v/v) DMSO, 4 mM MgCl_2 and 1 mM GMPCPP were incubated in BRB80 (100 μl total volume) on ice for 5 minutes and then for 30 minutes at 37 $^\circ\text{C}$. Taxol (400 μl , 10 μM) in BRB80, 75 mM KCl was then added. The microtubules were centrifuged in an airfuge (Beckmann Coulter) at 12 psi (approximately 61 000 x g) for 5 minutes and the pellet resuspended in 600 μl of taxol (10 μM) in BRB80, 75 mM KCl.

2.7 *ATPase assays*

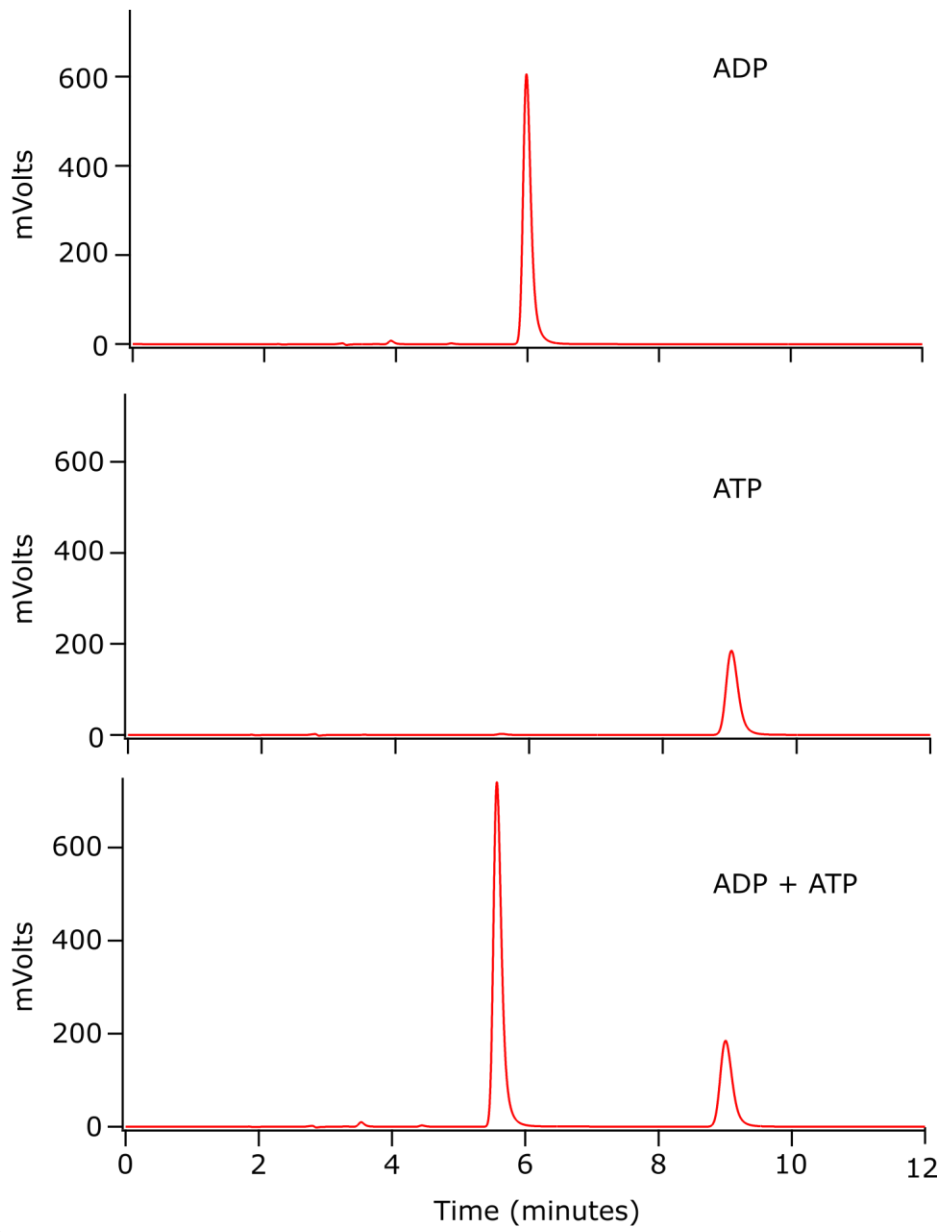
2.7.1 Discontinuous assay with ADP production monitored by HPLC

A reaction mix of 2 mM ATP and 3 μM MCAK in BRB80, 75 mM KCl, 0.05 % (v/v) Tween 20, 1 mM DTT was incubated at 25 $^\circ\text{C}$. Samples were taken every 15 minutes from 0 to 120 minutes, and quenched with 0.6 M perchloric acid before neutralisation with 6 M KOH. The samples were centrifuged at 11,500 x g and the supernatant mixed 1:1 with HPLC running buffer (100 mM potassium phosphate pH 6.5, 10 mM tetrabutylammonium bromide, 12 % acetonitrile). They were then run on a Gilson HPLC through a Luna C18 column (Phenomenex) in HPLC running buffer (as described (Friel and Howard 2011)).

The peaks corresponding to ATP and ADP on the HPLC trace were pre-determined, as shown in **Figure 2.1A** using known standards. The areas under the peaks corresponding to ADP and ATP were integrated, and shown to be concentration dependent **Figure 2.1B**. For traces from experimental samples,

the area under the peak corresponding to ADP was then divided by the area under the ADP and ATP areas combined to find what proportion of the total nucleotides present was ADP. This proportion was then plotted over time and the gradient – the change in proportion of ADP of total nucleotide over time – was calculated for each experiment. This was then converted to a rate per second, multiplied by the total nucleotide concentration (2000 μM) and divided by the concentration of MCAK monomers (3 μM) to give the ATPase rate per MCAK monomer per second.

A



B

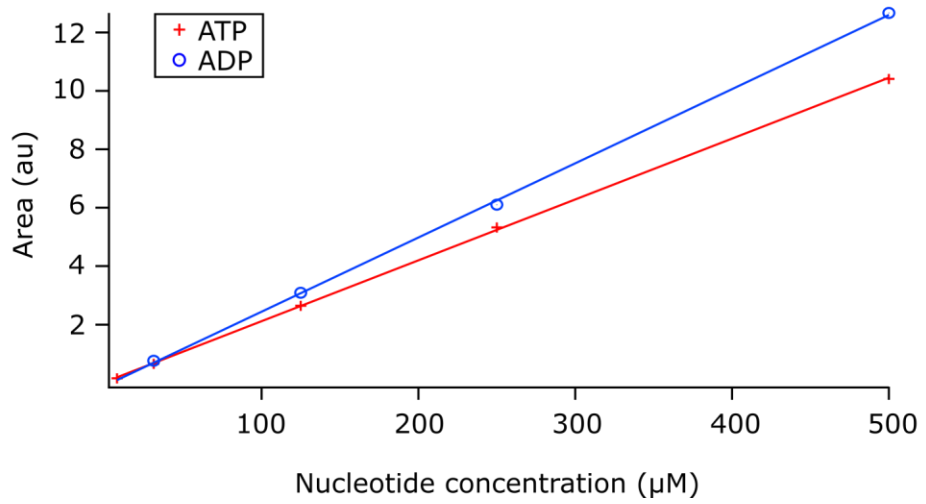


Figure 2.1. ADP and ATP were separated by HPLC and produced peaks with concentration dependent integrals. A) HPLC traces from solutions of ADP, ATP and ADP + ATP. B) Integrals of ATP and ADP peaks correlate with the concentration of nucleotides run on the HPLC.

2.7.2 Discontinuous assay with inorganic phosphate production monitored using malachite green

A reaction mix of 2 mM ATP/MgCl₂ and 3 μM MCAK in BRB80, 75 mM KCl, 0.05 % (v/v) Tween 20, 1 mM DTT was incubated at 25 °C. Samples were taken every 15 minutes from 0 to 120 minutes, and quenched with 2 M HCl before neutralisation with 1 M Tris, 3 M KOH. All samples were then incubated with an equal volume of BIOMOL Green™ phosphate detection reagent (Enzo Life Sciences) for 20 minutes. Absorption at 650 nm was then measured.

The plate reader output was normalised to a blank well and then converted to phosphate concentration using a standard curve, shown in **Figure 2.2**. The gradient of a graph of change in phosphate concentration over time was then divided by the MCAK monomer concentration to give the number of ATP molecules cleaved per MCAK monomer per second.

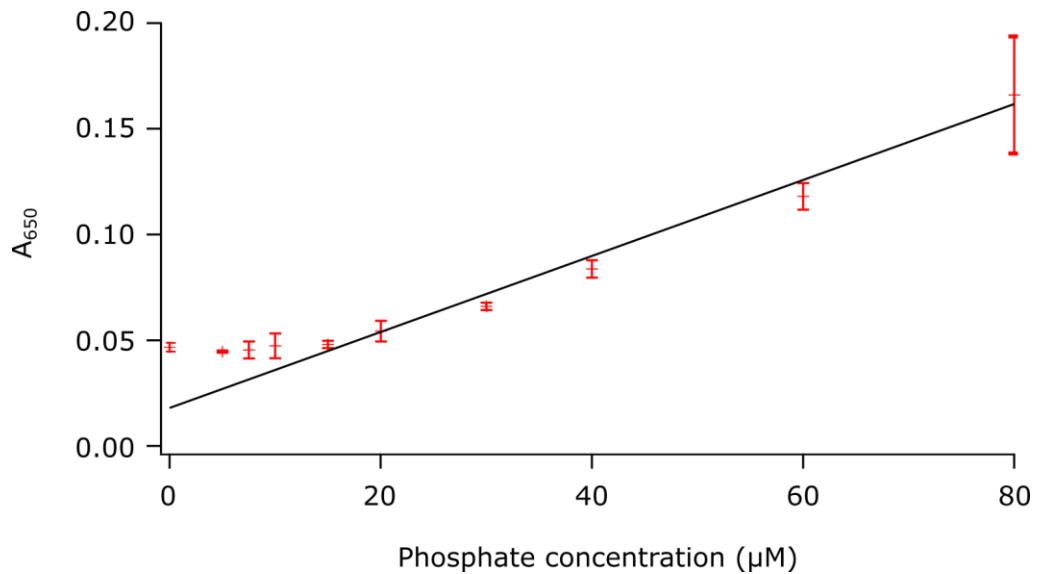
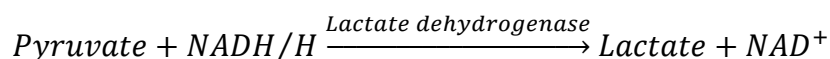
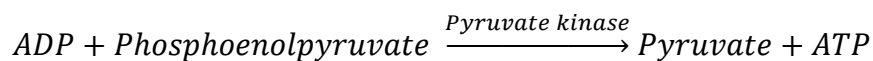


Figure 2.2. Light absorbed at 650nm by malachite green increases with increasing concentration of phosphate. Phosphate standards fit from 15 to 80 µM phosphate, below 15 µM is the limit of detection of the plate reader used for this assay.

2.7.3 Continuous assay with ADP production monitored by fluorescence by linking it to the conversion of NADH to NAD⁺

ATP turnover in the presence of microtubules was measured by linking ATP cleavage to the oxidation of NADH using phosphoenolpyruvate (PEP), pyruvate kinase (PK) and lactate dehydrogenase (LDH).



A reaction mix was set up of 4.3 mM PEP, 1.4 mM ATP, 0.1 mM NADH/H and approximately 21 U/ml PK and 31 U/ml LDH in BRB80, 75 mM KCl, 0.05 % (v/v) Tween 20. Tubulin or microtubules were added to this mix at a final

concentration of 10 μM . Fluorescence was detected using excitation and emission wavelengths of 340 nm and 460 nm respectively. Once a stable baseline had been established MCAK was added to give a concentration of 0.1 μM .

The fluorimeter data were plotted and the initial gradient of the trace after the addition of kinesin was calculated, an example is shown in **Figure 2.3A**.

To convert the change in fluorescence signal over time to the change in ADP concentration over time a standard curve was prepared. This was created by adding known concentrations of ADP to the assay instead of the kinesin

Figure 2.3B. The fluorescence value seen after the addition of ADP was then divided by the fluorescence observed directly before the ADP was added and plotted against the concentration, see **Figure 2.3C**. The change in

fluorescence in each experiment was normalised by dividing the resultant fluorescence value by the fluorescence just before the addition of kinesin and then converted to change in ADP concentration over time using the standard curve. The change in concentration of ADP over time was then divided by the concentration of MCAK monomers to give the rate of ATP turnover per second per motor domain. The rates were averaged and the standard deviation calculated (n=3).

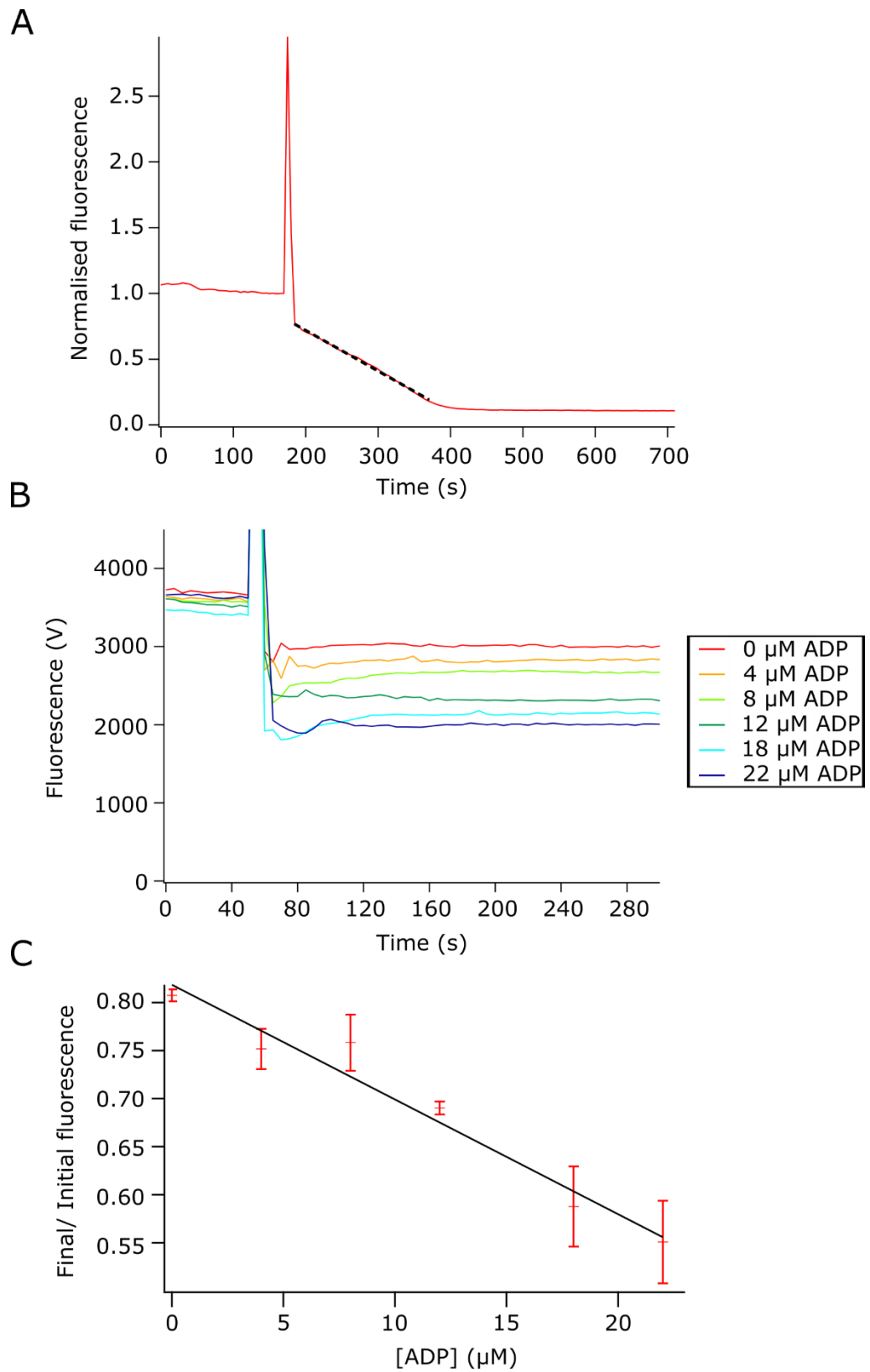


Figure 2.3. The initial change in fluorescence was converted to change in ADP concentration by making a standard curve of final/ initial fluorescence.

A) The initial gradient was identified and used to calculate the change in ADP

concentration. An example of normalised fluorescence trace is shown in red and the initial gradient used is indicated with the dashed black line. The peak at 180 seconds shows when the kinesin was added. B) The change in fluorescence on the addition of ADP at various concentrations. The peak at 55 seconds shows when the ADP was added. C) The change in the ratio of fluorescence after and prior to the addition of increasing concentrations of ADP. Points are mean \pm standard deviation, $n = 3$, with fit in black.

2.8 *MantADP dissociation*

MCAK (2 μ M) was loaded with mantADP (50 μ M, Jena Bioscience) by incubation at 25 °C for 30 minutes. A NAP-5 column (GE Healthcare) was equilibrated with 10 ml reaction buffer (BRB80, 75 mM KCl, 0.05% (v/v) Tween 20, 1 mM DTT) and then loaded with 0.5 ml MCAK-mantADP. The protein was eluted in 1 ml reaction buffer. This 1 μ M MCAK-mantADP complex was mixed 1:1 with 100 μ M ATP (+ where indicated 10 μ M tubulin or 5.7 μ M microtubules – chosen to give a comparable number of ends to 10 μ M microtubules in ATPase assay) in an SX20 stopped-flow fluorimeter (Applied Photophysics). Fluorescence was measured using an excitation wavelength of 365 nm, and emitted fluorescence was collected between 395 nm and 495 nm using a BP445/50 filter (Zeiss) over a period of 100 seconds.

For each independent experiment, 5 measurements were obtained and were fitted to an exponential with the fewest terms required to adequately describe the curve (fitting of mADP dissociation data has been described previously (Patel, Belsham et al. 2014)). In the majority of cases this was a

single exponential with a linear component to account for bleaching of the mant group. Data were fitted to the equation $Fluorescence = A_0e^{-kt} + mt + c$ where A_0 is the amplitude of exponential decay, k is the observed rate constant, t is time and $mt + c$ is a linear function to account for the photobleaching of mant. When a single exponential was not able to adequately describe the curve, a double exponential was used $Fluorescence = A_0e^{-k_{fast}t} + A_1e^{-k_{slow}t} + mt + c$ This gives two k values, which are termed k_{fast} for the larger value and k_{slow} for the smaller value.

The data for each of the five fluorescent traces in each experiment were averaged and then fitted to the relevant exponential equation. Three independent experiments were carried out. Averages and standard deviations were calculated for the k values and the average fluorescence traces from each experiment. The traces were normalised on a scale of 1 to 0 over a time period of 100 seconds.

2.9 Measuring microtubule depolymerisation using light scattering

Frozen microtubules were thawed rapidly at 37 °C, diluted to 1 µM in MCAK turbidity buffer (BRB80 pH 6.9, 75 mM KCl, 1 mM MgATP, 1 mM DTT, 200 µg/ml BSA) and left to stand at room temperature for 15 minutes. After this the light scattering of the sample was measured every 5 seconds using an F-2500 fluorimeter at 350 nm in quartz cuvettes. The signal from microtubules

alone was measured for 2.5 minutes, MCAK was added to a final concentration of 50 nM and the signal was monitored for a further 12.5 minutes.

2.10 Silanisation of coverslips

Coverslips were incubated in acetone with sonication for 20 minutes, followed by 20 minutes incubation in methanol with sonication. They were then washed in double distilled water (ddH₂O) and sonicated for 1 hour in 1 M potassium hydroxide. The slides were rinsed three times in ddH₂O then sonicated in acetone again for 20 minutes followed by 20 minutes sonicating in methanol. They were then rinsed in ddH₂O and sonicated in 5 M potassium hydroxide for 1 hour. Next the slides were rinsed three times in ddH₂O before being dried completely using compressed air. Coverslips were submerged in 250 ml trichloroethanol to which 125 µl dichlorodimethylsilane was applied under the surface of the solvent using a 1 ml syringe and spinal needle. The coverslips were then agitated in the mixture and incubated for 60 minutes. The coverslips were washed three times in methanol with 5, 15 and 30 minutes of sonication respectively and dried using compressed air.

2.11 Measuring microtubule depolymerisation using microscopy

Channels of approximately 0.1 mm x 3 mm x 18 mm were constructed using silanized coverslips of 18 mm x 18 mm and 22 mm x 22 mm separated by double-sided tape (as shown in **Figure 2.4**).

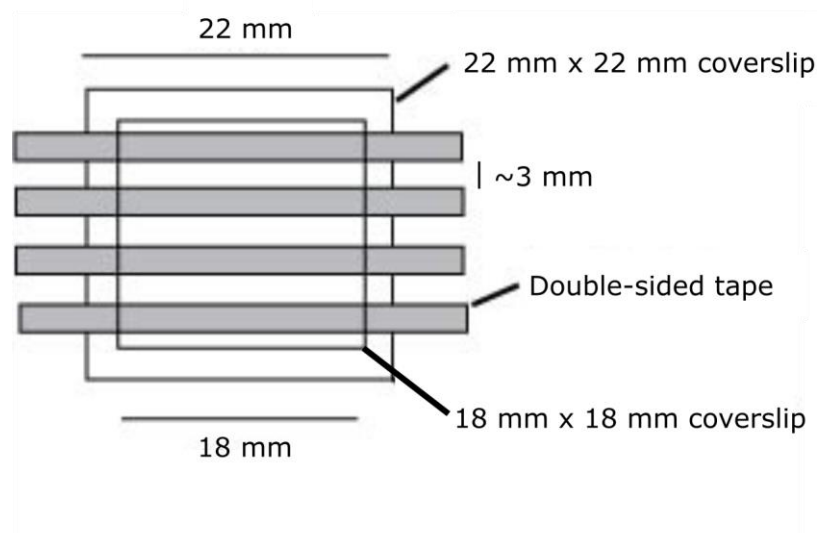


Figure 2.4. Construction of channels for a depolymerisation assay. Strips of double-sided tape were laid across a silanized 22 mm x 22 mm coverslip. A second silanized coverslip of 18 mm x 18 mm was then added on top to create flow channels.

Flow channels were incubated with 20 μ l anti- β -tubulin I antibody (Sigma, mouse, 1:200 in BRB80) for 5 minutes (**Figure 2.5A**), washed with 20 μ l BRB80, incubated for 5 minutes with 20 μ l Pluronic F-127 (Invitrogen, 1 % (v/v) in BRB80, **Figure 2.5B**), washed again with 100 μ l BRB80 and incubated with 20 μ l GMPCPP stabilised, fluorescently labelled microtubules (2.6.2 and **Figure 2.5C**) until they were observed to have been captured on the surface

at a suitable density for analysis. Channels were then incubated with 20 μ l reaction mixture containing anti-fade (BRB20 (20 mM PIPES/ KOH pH 6.9, 1 mM MgCl₂, 1mM EGTA), 75 mM KCl, 1 mM ATP/MgCl₂, 0.1 mg/ml bovine serum albumin, 40 mM α -D-glucose, 40 μ g/ml glucose oxidase, 16 μ g/ml catalase, 1% (v/v) β -mercaptoethanol). Images were taken every 5 seconds for 20 minutes, or until all the microtubules had depolymerised, with 10 μ l of reaction mixture containing 40 nM MCAK added after 1 minute (**Figure 2.5D**). Assays were carried out at 25 °C. Images were acquired using a DeltaVision Elite microscope (Applied Precision/ GE Healthcare), 100x objective lens (Olympus, UPlanSApo/ 1.4 NA oil), TRITC filters and an Evolve 512 EMCCD camera (Photometrics). FIJI software (Schindelin, Arganda-Carreras et al. 2012) was used to measure the lengths of individual microtubules through successive frames. These lengths were then plotted and the initial rate of the change of length over time was measured by fitting using Igor Pro (Wavemetrics) (**Figure 2.6**).

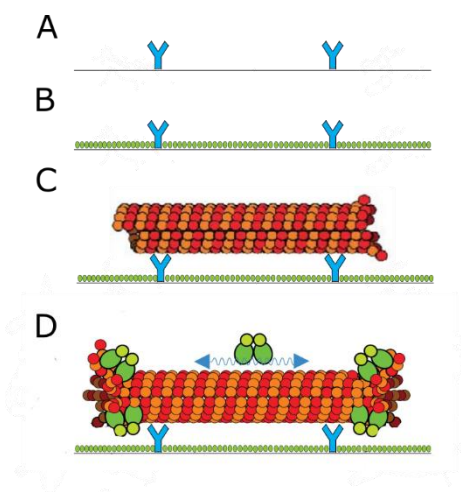


Figure 2.5. The lower surface of a flow channel. Once a flow channel has been constructed anti-tubulin antibodies (a), BRB80, F127 (b), BRB80,

microtubules (c), BRB80, reaction mix and reaction mix containing MCAK (d) were successively passed through the channel.

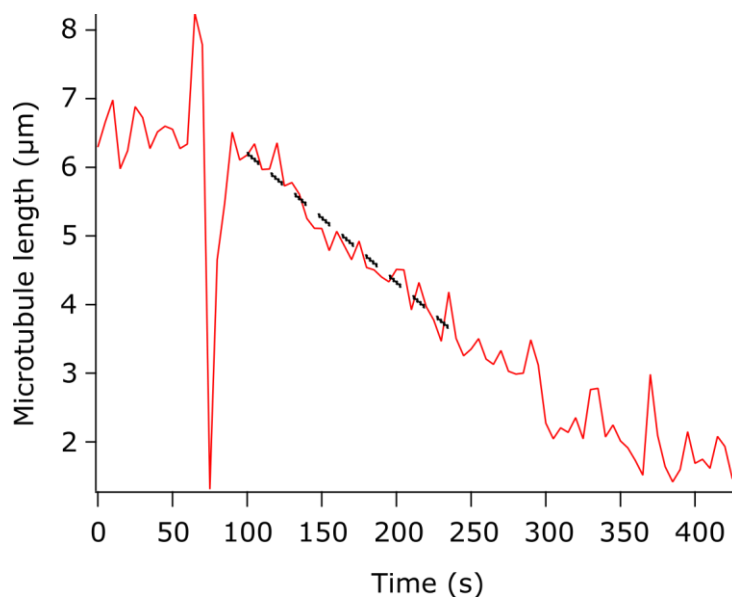


Figure 2.6. The length of a microtubule over time with the addition of MCAK. The initial rate of change in microtubule length over time was calculated. The large peak and trough just after 60 s shows when MCAK was added. The red line shows the microtubule length and the black dotted line shows the fit to the initial rate.

2.12 Pelleting kinesin with microtubules

Double-stabilised microtubules ($2 \mu\text{M}$) and MCAK ($2 \mu\text{M}$) were incubated with 1 mg ml^{-1} casein for 30 minutes at 37°C in BRB80, 75 mM KCl ($400 \mu\text{l}$ total volume). The mixture was then centrifuged in an airfuge (Beckmann Coulter) at 12 psi (approximately $61\,000 \times g$) for 5 minutes and the supernatant was removed. The pellet was resuspended in $400 \mu\text{l}$ sample buffer. Samples of the supernatant and pellet were then run on an SDS-PAGE gel (Section 2.4).

2.13 Expression of Kinesin-1

rKin430GFP in pET17b was supplied by Stefan Diez, Centre for Biomolecular Engineering TU Dresden, Germany. The plasmid was used to transform BL21 cells as follows, 2 μ l plasmid was added to 50 μ l BL21 cells and the mixture was incubated on ice for 30 minutes, heat-shocked for 45 seconds at 42 °C and returned to ice for 2 minutes. LB (900 μ l) was then added and the cells were incubated at 37 °C with shaking at 225 rpm for 1 hour. They were then spun down for 5 minutes at 269 x g and the pellet resuspended in approximately 250 μ l of the supernatant. This was then spread onto LB agar plates containing ampicillin (0.1 mg/ml) and incubated at 37 °C overnight. A single colony was selected and grown in 5 ml LB with 50 μ M ampicillin overnight at 37 °C. This culture was then spun down at 1814 x g and then resuspended in 700 ml of fresh LB with 50 μ M ampicillin and grown at 37 °C with 150 rpm shaking to an OD of 0.6. The cells were then cooled to 18 °C and induced with 1 mM IPTG and grown for an additional 16 hours at 18 °C. They were then spun down at 5000 x g for 10 minutes and the pellets were combined, snap frozen and stored at -80 °C.

2.14 Purification of Kinesin-1

The combined pellet was resuspended in 100 ml lysis buffer (50 mM Sodium phosphate buffer (Na_2HPO_4 and NaH_2PO_4 titrated to pH 7.5), 100 mM NaCl, 1

mM MgCl₂, 5 mM 2-mercaptoethanol (BME), 10 μM ATP, protease inhibitor cocktail tablet (Roche)) and the cells were lysed in a cell disruptor (Constant Systems) at 35 kpsi. The lysate was centrifuged at 75,600 x g for 1 hour and the supernatant was loaded onto a prepacked HisTrap Q column (GE Healthcare) and washed with 10 ml anion exchange buffer (50 mM PIPES pH 6.9, 5 mM MgCl₂, 1 mM DTT, 100 mM NaCl). The protein was then eluted in 10 ml anion exchange buffer with 200 mM NaCl. The elution was loaded onto a HisTrap HP column (GE Healthcare). The column was then washed with 10 ml wash buffer (50 mM sodium phosphate buffer pH 7.5, 300 mM KCl, 75 mM imidazole, 5 % (v/v) glycerol, 1 mM MgCl₂, 10 mM BME, 0.1 mM ATP) and then 4 ml elution buffer (50 mM sodium phosphate buffer pH 7.5, 300 mM KCl, 300 mM imidazole, 5 % (v/v) glycerol, 1 mM MgCl₂, 10 mM BME, 10 mM ATP, 10 % w/v sucrose) was used to elute the protein. Fractions were collected of approximately 300 μl, snap frozen and stored at -80 °C.

2.15 TIRF microscopy

Channels were constructed and treated in the same way as with the depolymerisation assay (see 2.11) up to the addition of reaction mixture. Images were taken using a Zeiss Observer Z1 microscope with a Zeiss TIRF 3 module, QuantEM 512SC EMCCD camera (Photometrics), Zeiss filter sets 20 and 38, and using a 100 x objective lens (Zeiss, alphaPlanApo/ 1.46NA oil). The kinesin was tracked by streaming 100 ms exposure images (1 image every 134 ms) for kinesin-13 and 300 ms exposure images (1 image every 374 ms)

for kinesin-1. From these image stacks kymographs were produced.

Kymographs show an individual microtubule over time, allowing the change over time to be shown in a single 2D image. The microtubule is shown at the top of the image and the same slice from a time series of images is shown underneath. For instance, the microtubule shortening during a depolymerisation assay can be observed or the progress of a kinesin molecule moving along the microtubule followed in TIRF assays (**Figure 2.7**).

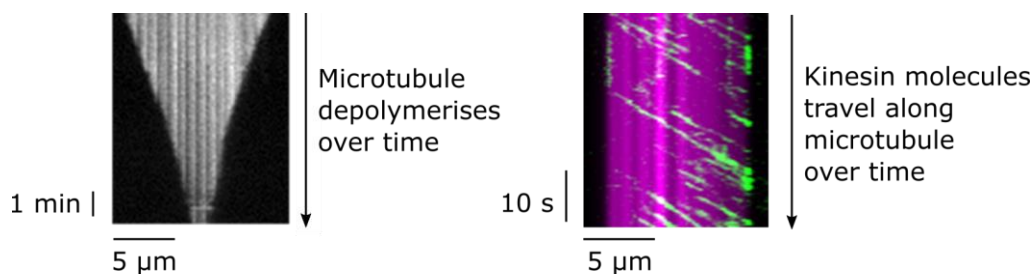


Figure 2.7. Kymographs can show depolymerisation or track kinesin movement. Depolymerisation is shown on a kymograph in black and white, while the kinesin tracking kymograph shows the microtubule in magenta and the kinesin in green.

To quantitate interaction events between a kinesin and a microtubule, thresholds for the kymograph images were set in the GFP channel using the maximum signal of an adjacent region not containing microtubules as the minimum intensity for the kymograph. An event was characterised by any intensity above this threshold of at least 2 pixels in the horizontal and at least 1 pixel in the vertical. Events had to be separated by at least 1 blank pixel in any direction. These requirements are represented schematically in

Figure 2.8. A translocation event was characterised as being when an event moved both horizontally and vertically in successive frames in a unidirectional manner. The number and duration of events was measured and, if applicable, the horizontal distance travelled. Histograms were created showing the number of events lasting a specific duration, either at the microtubule end or on the microtubule lattice. The data were also plotted as cumulative frequency histograms and were fitted to an exponential curve with the formula $y = Ae^{-k_{off}x} + b$. This gives the value of k_{off} . In chapter 3, the end residence times are quoted as mean \pm standard deviation, for consistency, as this was how it was quoted in the related publication (Belsham and Friel 2017). However, in chapter 5, the inverse of k_{off} for the end residence time was used as this is now considered a more accurate measure. This is because it is less skewed by a small number of long events. The value for k_{on} is quoted as events per nM kinesin per μm microtubule per second. The error quoted for k_{on} is a combination of the standard deviation of the k_{on} for different microtubules and the error in concentration calculations.

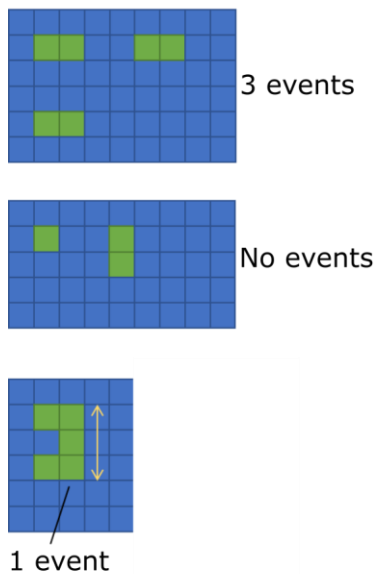


Figure 2.8. Schematic showing the pixel requirements for intensity to be counted as an event. An event was characterised by any intensity above this threshold of at least 2 pixels in the horizontal and at least 1 pixel in the vertical. Events had to be separated by at least 1 blank pixel.

2.16 Measuring depolymerisation using a single time-point

When looking at depolymerisation by Kinesin-1 and the Kinesin-1 mutants it was not possible to use the standard microscopy method (section 2.11) as the microtubules glided. This occurs as a result of kinesin molecules adhering to the coverslips and then as they translocate along the microtubule, the microtubule moves. This makes analysis of the lengths of individual microtubules very difficult as they move and may even move out of the field of view. Instead, microtubules were incubated with the kinesin and then deposited onto coverslips for observation using fluorescence microscopy. Briefly, poly-L-lysine coverslips were prepared by incubating the coverslips in

1 mg/ml poly-L-lysine for 1 hour at room temperature. The coverslips were washed in ddH₂O and then in 95 % (v/v) ethanol and allowed to dry. GMPCPP-stabilised, rhodamine labelled microtubules (made as described in 2.6.2) were incubated with 40 nM kinesin and 1 mM ATP in BRB12 for 20 minutes. The microtubules were then flowed into a channel made from poly-lysine coated coverslips and imaged.

2.17 Statistical tests

Whether a difference between measured parameters was statistically significant was determined using Welch's t-test. Differences between distributions, for example those of end residence time, were assessed using the Kolmogorov-Smirnov test. Values of $p < 0.05$ were considered statistically significant.

Chapter 3 The MCAK phosphomimic T537E is unable to recognise microtubule ends

3.1 Background

As described in the Introduction (Chapter 1.8) MCAK is known to be regulated by phosphorylation. There are five kinases that have been shown to phosphorylate MCAK – Aurora A, Aurora B, Cdk1, PAK1 and Plk1. These kinases phosphorylate MCAK across 10 different sites (**Figure 1.12**), affecting MCAK's activity and localisation through the cell cycle (Andrews, Ovechkina et al. 2004, Zhang, Ems-McClung et al. 2008, Sanhaji, Friel et al. 2010, Zhang, Shao et al. 2011, Pakala, Nair et al. 2012). T537 is the only known phosphorylation site within the motor domain of human MCAK. The T537 residue is not well conserved among Kinesin-13s (see Appendix 1 for sequence alignment). It is phosphorylated by Cdk1 and this has been observed to reduce MCAK's depolymerisation activity (Sanhaji, Friel et al. 2010). In HeLa cells in which endogenous MCAK has been knocked down by siRNA, expression of T537A, a phosphonull mutant, results in the cells unable to form a normal mitotic spindle, with most microtubules at the centrosomes, forming asters that do not reach the chromosomes. This leads to prometaphase arrest. Expression of T537E, a phosphomimetic mutant, in cells with wild type knockdown leads to metaphase arrest - cells are able to form a spindle but fail to align chromosomes correctly at the metaphase plate, producing lagging chromosomes. Both T537A and T537E expressing cells have reduced inter-centromeric distances, in those cells that reach

metaphase, compared to cells expressing wild type MCAK, indicating a lack of tension between the centromeres. This may be because the mutant proteins are unable to correct kinetochore-microtubule attachments (Sanhaji, Friel et al. 2010). Overall, as has been observed with phosphorylation of MCAK at other sites (outside of the motor domain), these data show the importance of being able to regulate the microtubule depolymerising activity of MCAK as the cell cycle progresses, a form of regulation which phosphorylation is well suited to provide.

The T537 site is located close to the $\alpha 4$ helix (**Figure 3.1**), which is part of the core interface between MCAK and the microtubule - sitting in the intra-dimer groove of the α/β -tubulin heterodimer when MCAK is bound to tubulin (Asenjo, Chatterjee et al. 2013, Wang, Cantos-Fernandes et al. 2017, Benoit, Asenjo et al. 2018, Trofimova, Paydar et al. 2018). The $\alpha 4$ helix, together with loop 8 and loop 2 has been proposed to be involved in stabilising the curved conformation of protofilaments found at the end of microtubules, with the loops acts as 'levers' and the $\alpha 4$ helix acting as a 'wedge' (as discussed in chapter 1.6) (Ogawa, Nitta et al. 2004, Asenjo, Chatterjee et al. 2013). Additionally, three residues in the $\alpha 4$ helix have been identified as being important for microtubule end recognition by MCAK (Patel, Belsham et al. 2016). Phosphorylation of T537 has been shown to reduce the depolymerisation activity of MCAK both *in vivo* and *in vitro* (Sanhaji, Friel et al. 2010) and we hypothesise that this might be caused by affecting MCAK's ability to recognise the microtubule end.

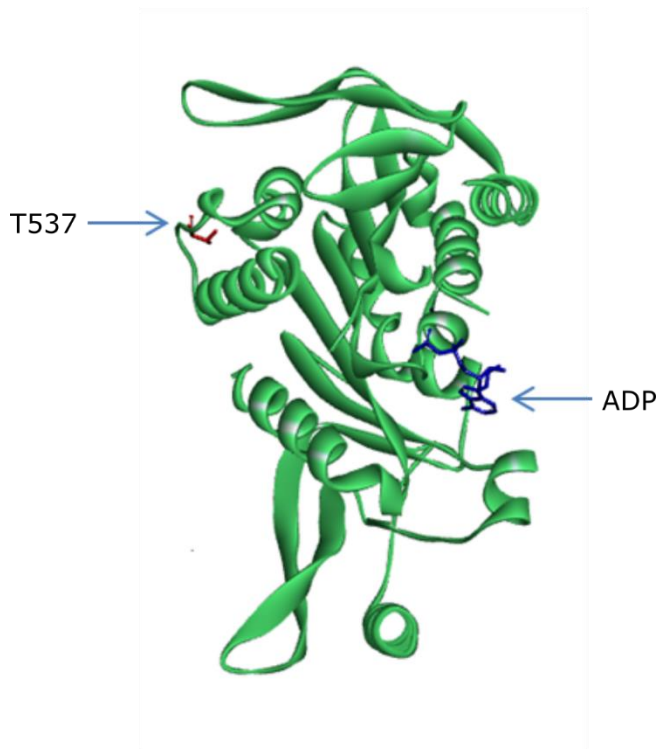


Figure 3.1. Location of T537 residue in MCAK. T537 residue is represented as a ball and stick structure in red. MCAK – *Homo sapien*. PDB ID:2HEH.

3.2 Expression and purification of MCAK mutants

To understand more about the effect of phosphorylation on MCAK's activity, phosphomimic and phosphonull MCAK mutants, T537E and T537A respectively, were created. These proteins could be used in *in vitro* assays to assess MCAK's activity. Site-directed mutagenesis of the MCAK-h6 and MCAK-h6-GFP pFastBac vectors was used to create the MCAK variants T537A and T537E (Chapter 2.1). Mismatched primers, designed to encode the desired substitutions, were used in PCRs in which the entire plasmid is replicated and the mutagenic primers incorporated. The unmutated, methylated template DNA was digested using *DpnI* and the products were

transformed into *E. coli* (DH5 α). Colonies were grown and plasmid DNA was then purified. The introduction of the required mutations was verified by sequencing. The Bac-to-Bac expression system was used to express protein (Chapter 2.2.2-2.2.4). Briefly, DH10Bac cells were transformed with the pFastBac plasmid containing the gene for MCAK or MCAK variants. The pFastBac vector contains an *Autographa californica* multiple nuclear polyhedrosis virus (AcMNPV) promoter which allows high levels of protein expression in insect cells and is flanked by Tn7. The DH10Bac cells contain a bacmid with an *attTn7* target site and a helper plasmid. When the DH10Bac cells are transformed with the pFastBac plasmid transposition occurs between the Tn7 site in the pFastBac vector and the *attTn7* target site on the bacmid, using proteins encoded by the helper plasmid including the transposase. This results in a recombinant bacmid containing the gene of interest, which is then isolated. The bacmid was then transfected into *Spodoptera frugiperda* (Sf9) insect cells. The bacmid contains genes which encode baculovirus proteins, which are translated and transcribed by the host Sf9 cells. This leads to the production of baculovirus particles containing the desired gene under the AcMNPV promoter. The baculovirus was then used to infect 3×10^8 cells which produced the desired MCAK protein. Insect cells contain chaperones that help MCAK to fold correctly and are also capable of modifying the proteins post-translationally. The T537A and T537E proteins and the wild type MCAK were purified by nickel affinity chromatography (2.3), as shown in **Figure 3.2**. In brief, the infected cells were lysed and then centrifuged to remove the cell debris. The supernatant was applied to a column of nickel-

NTA resin to bind the His-tagged protein and then the column was washed with buffer containing 70 mM imidazole to remove non-specifically bound protein. His tagged protein was then eluted from the column using buffer containing 200 mM imidazole.

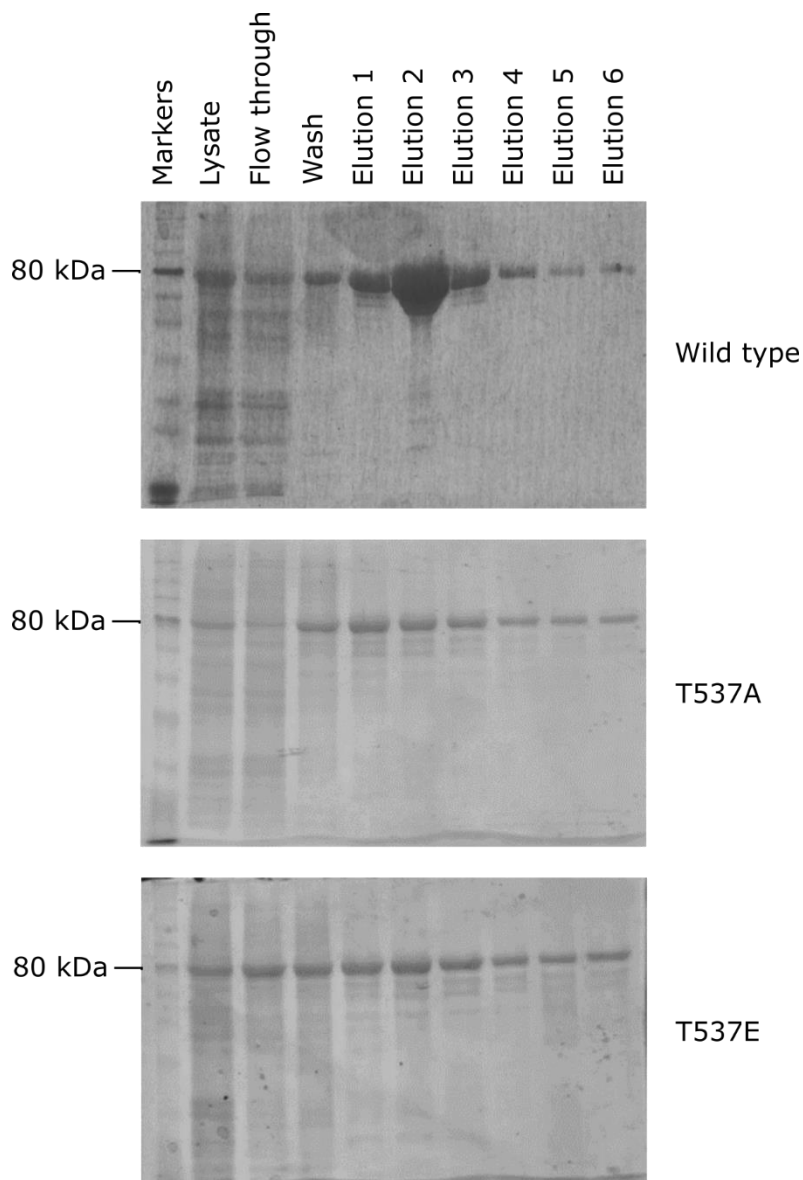


Figure 3.2. Purification of wild type MCAK, T537A and T537E by nickel affinity. SDS-PAGE gel stained with Instant Blue of progression through purification. Lysate: Cleared cell lysate. Flow through: Flow through from Sf9 cell lysate applied to Nickel affinity column. Wash: 75 mM imidazole wash.

Elutions 1-6: Eluate from Nickel affinity column in 200 mM imidazole in 300 μ l fractions. MCAK molecular weight 82 kDa.

3.3 Introduction of a Cdk1 phosphomimic mutation impairs

MCAK's depolymerisation activity

To confirm previous observations that the phosphomimic mutant, T537E, has reduced depolymerisation activity relative to wild type (Sanhaji, Friel et al. 2010), two different methods were used to observe the depolymerisation rate of wild-type MCAK and the phosphomimic and phosphonull variants. First, a light scattering assay was used to exploit the fact that microtubules scatter light at 350 nm whilst unpolymerised tubulin does not. When MCAK is added to microtubules a decrease in light scattering is observed as the microtubules depolymerise and it was possible to monitor this process every 5 seconds using a fluorimeter (2.9). Both the T537A and T537E proteins showed reduced depolymerisation activity compared to the wild type protein (**Figure 3.3**).

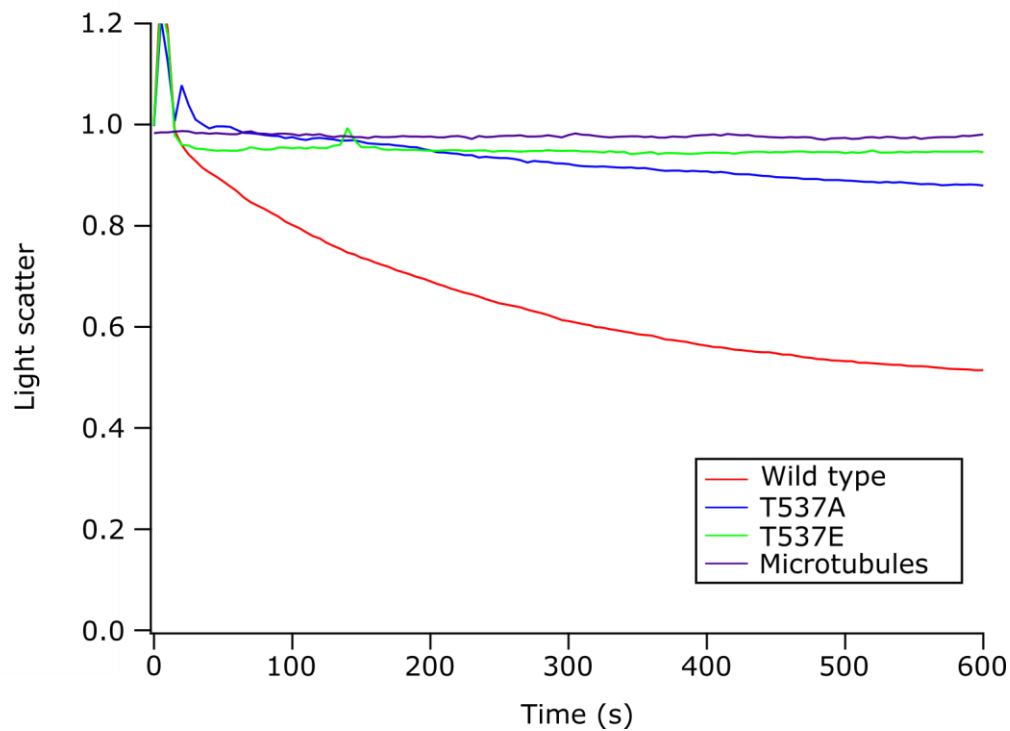


Figure 3.3. A light scattering assay shows wild type MCAK depolymerises microtubules more rapidly than the mutants T537A and T537E. The depolymerisation of microtubules was measured using light scattering and normalised to the average reading of 1 μ M microtubules over 150 seconds prior to the addition of 50 nM MCAK. The curves on the graph represent the average values for 3 experiments for each protein.

Secondly, fluorescence microscopy was used to observe the effect of MCAK and variants on fluorescently labelled microtubules (2.11). This showed that the depolymerisation rate by T537A and T537E is significantly reduced compared to wild type protein (**Figure 3.4**).

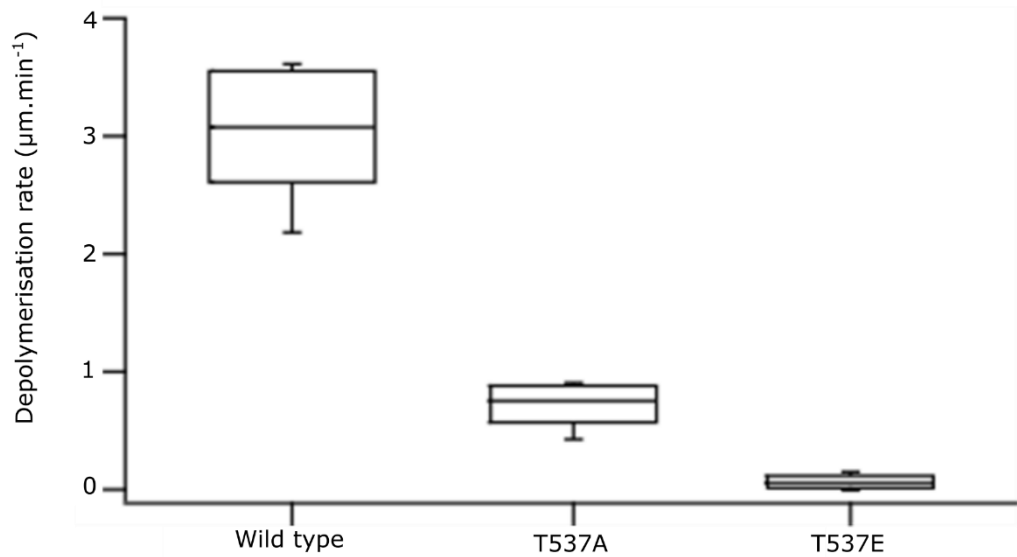


Figure 3.4. The rate of microtubule depolymerisation by wild type MCAK is faster than by the mutants T537A and T537E. The rate of depolymerisation by 40 nM MCAK measured using the depolymerisation assay. For each protein n=20. Data published in (Belsham and Friel 2017).

Previously the rate of depolymerisation by the T537A and wild type proteins had not appeared significantly different but the rate of depolymerisation had been measured with MCAK in excess (400 nM) (Sanhaji, Friel et al. 2010) rather than the 40 nM concentration used here. To confirm these earlier results, the experiment was repeated using 400 nM MCAK. This produced results similar to those published previously where T537E still has a decreased rate of depolymerisation but T537A has a rate similar to the wild type (**Figure 3.5**).

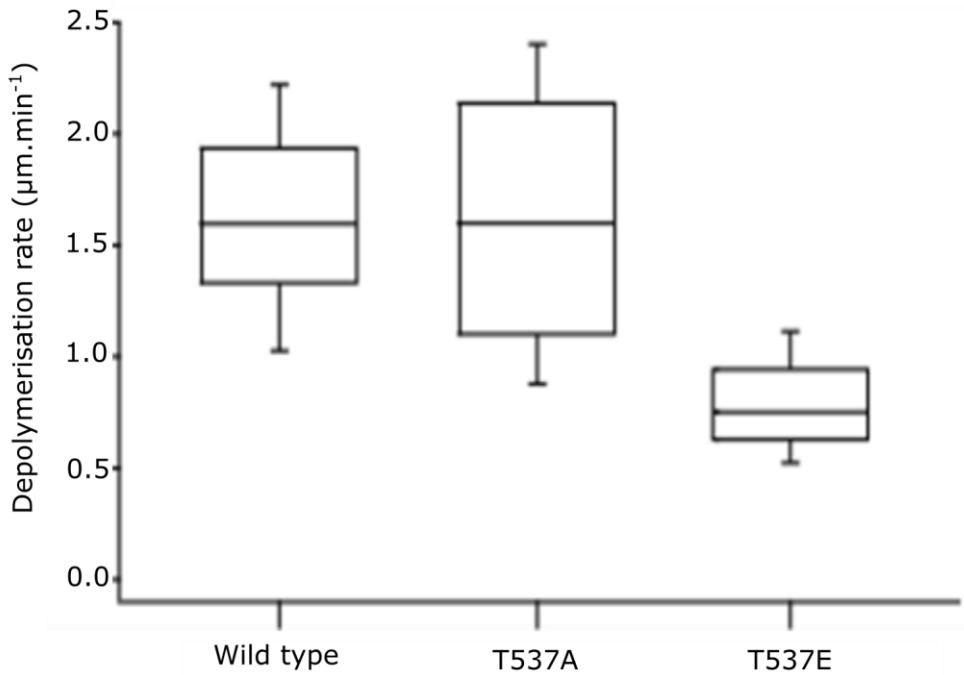


Figure 3.5. The rate of depolymerisation by wild type MCAK and T537A is comparable and faster than T537E in the presence of an excess of MCAK.

The rate of depolymerisation by 400 nM MCAK measured using the depolymerisation assay. For each protein n=20.

T537E has reduced depolymerisation activity compared to wild type in all the conditions measured, although the rate does increase from 0.06 µm/min with 40 nM MCAK to 0.79 µm/min with 400 nM. However, T537A has a reduced depolymerisation activity at 40 nM but can depolymerise microtubules at the same rate as wild type MCAK at higher concentrations.

3.4 *Cdk1 phosphomimic and phosphonull mutants have slower ATPase rates than wild type in the presence of microtubules*

One possible explanation for the reduced depolymerisation activity of these MCAK variants is that the mutation has caused improper folding of the motor domain resulting in a loss of function. To test if this was the case the rate of ATP turnover was measured in solution (basal ATPase rate) (2.7.1). The reaction of MCAK with ATP was quenched at 15 minute intervals with acid and then neutralised. The fraction of ADP out of the total nucleotides present at each time point was measured using HPLC (**Figure 3.6A**) and the change over time was calculated. Each mutant had a basal ATPase rate not significantly different to wild type (**Figure 3.6**) thus indicating that the motor domain is correctly folded and can turn over ATP.

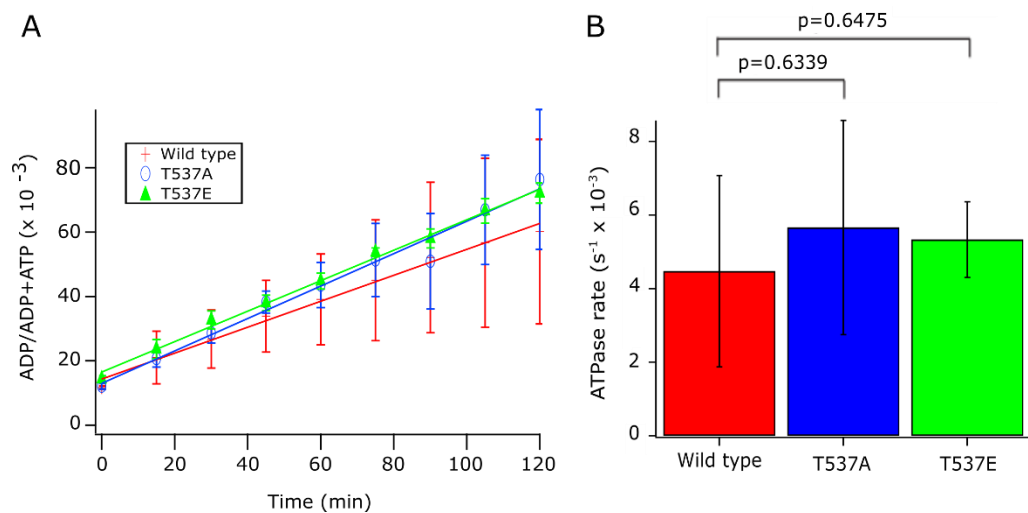


Figure 3.6. The MCAK mutants T537A and T537E have comparable ATPase rates to wild type in solution. A) The change in the fraction of ADP of total nucleotides at fifteen minute intervals was measured using HPLC. Points are mean \pm standard deviation, $n=3$ for each protein, and a line of best fit is

shown. B) The mean ATPase rate, from the gradient of the fit for each experiment \pm standard deviation is shown for each protein.

Next, the rate of ATP turnover by MCAK and the T537 mutants was analysed in the presence of unpolymerised tubulin and microtubules. With wild type protein the ATPase rate is accelerated by unpolymerised tubulin and to a greater extent by microtubules. To see if this was also true for the mutants an enzyme-linked assay was employed which uses the ADP produced from MCAK's cleavage of ATP to convert phosphoenol pyruvate to pyruvate and then, using the oxidation of NADH, to lactate (2.7.3). The conversion of NADH/H⁺ to NAD⁺ led to a decrease in fluorescence which was measured and converted to a concentration of ADP from a standard curve, thus allowing the measurement of the production of ADP with time. In the presence of unpolymerised tubulin, the mutants showed a similar ATPase rate to wild type (**Figure 3.7**), demonstrating that their ability to interact with tubulin has not been affected by the mutation.

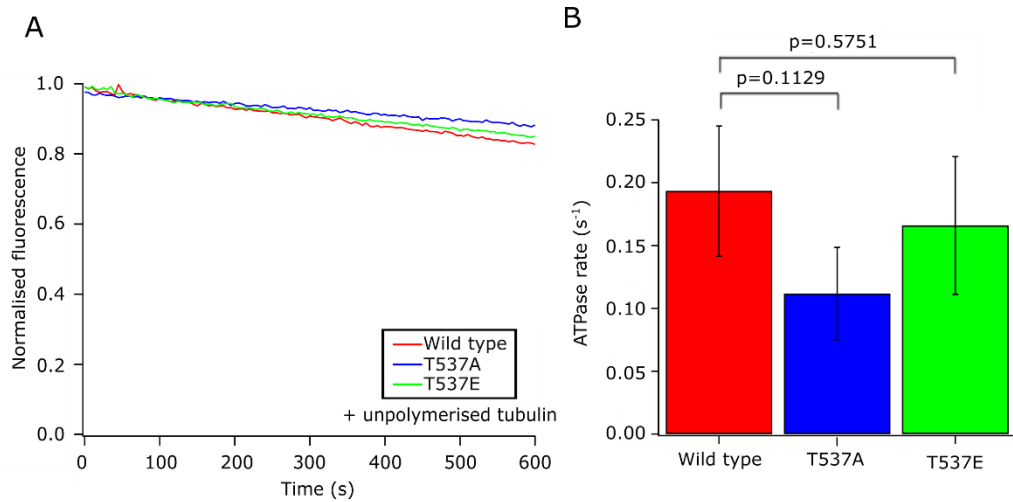


Figure 3.7. The ATPase rate of wild type MCAK and the mutants T537A and T537E is comparable in the presence of free tubulin. A) Average traces for enzyme linked assay, measuring the loss of NADH as ADP is produced. B) The average ATPase rate is shown for wild type MCAK, T537A and T537E \pm standard deviation, $n=3$ for each protein.

In contrast with the ATPase rates in solution and in the presence of unpolymerised tubulin where all three protein have ATPase rates that are not significantly different from each other, both T537A and T537E have a significantly decreased ATPase rate in the presence of microtubules compared to the wild type protein (See **Figure 3.8**).

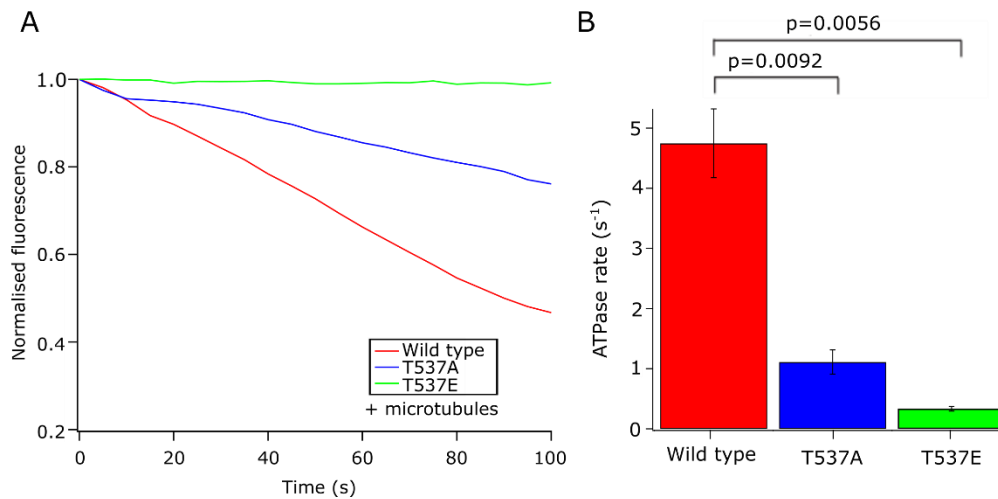


Figure 3.8. The ATPase rate of wild type MCAK is faster than the mutants T537A and T537E in the presence of microtubules. (A) Average traces for enzyme linked assay, measuring the loss of NADH as ADP is produced. (B) The average ATPase rate for wild type MCAK, T537A and T537E \pm standard deviation, $n=3$ for each protein.

The ATPase rate of T537E in the presence of microtubules is not significantly different to its ATPase rate in the presence of unpolymerised tubulin ($p=0.0672$, see **Figure 3.9**). For T537A the MT-stimulated ATPase rate is clearly faster than tubulin-stimulated alone (about 14x), but not as fast as wild type. The simplest explanation for this would be that mutant proteins are not able to interact with microtubules. However, both mutants show a rate of ATP turnover in the presence of microtubules that is much faster than in solution and have a tubulin stimulated ATPase rate that is comparable to wild type. Also, although the mutants have a reduced depolymerisation activity, they are able to depolymerise microtubules to some degree, which requires them to interact with the microtubule. Another possible explanation

for the reduced microtubule-stimulated ATPase rate could be that the mutations have affected MCAK's ability to interact with the microtubule end. The residue T537 is located close to the $\alpha 4$ helix of MCAK, a region which is important for MCAK's interaction with microtubules, and in particular for stabilising the curved protofilament conformation found at microtubule ends (Ogawa, Nitta et al. 2004, Asenjo, Chatterjee et al. 2013). Residues K524, E525 and R528 in the $\alpha 4$ helix have also been shown to be important for MCAK's ability to recognise the microtubule end (Patel, Belsham et al. 2016). Altering MCAK's ability to recognise the microtubule end might not affect its ability to interact with tubulin, and hence the tubulin stimulated ATPase, but would affect the microtubule-stimulated ATPase, as MCAK's ATPase rate is maximally stimulated by microtubule ends (Friel and Howard 2011). The difference between the microtubule stimulated and in solution rates for the mutants could be explained by the ability of the lattice to stimulate ATP cleavage. However unlike microtubule ends, the microtubule lattice does not act to stimulate the ADP dissociation required for the maximum number of further molecules of ATP to bind and be cleaved (Friel and Howard 2011). The fact that T537E has no significant difference between the tubulin and microtubule stimulated ATPase rates would fit with the microtubule rate being a result of only lattice stimulated activity. This would suggest that T537A is more able to interact with the microtubule end than T537E, which would fit with the depolymerisation data, which shows that T537A has a decreased rate of depolymerisation compared with wild type but not as slow as T537E.

To discover whether the difference in ATPase rate observed for the mutants is because the mutations have affected MCAK's ability to interact with the microtubule as a whole, or because they have affected MCAK's ability to interact with the microtubule end, the direct interaction between MCAK and the microtubule was studied.

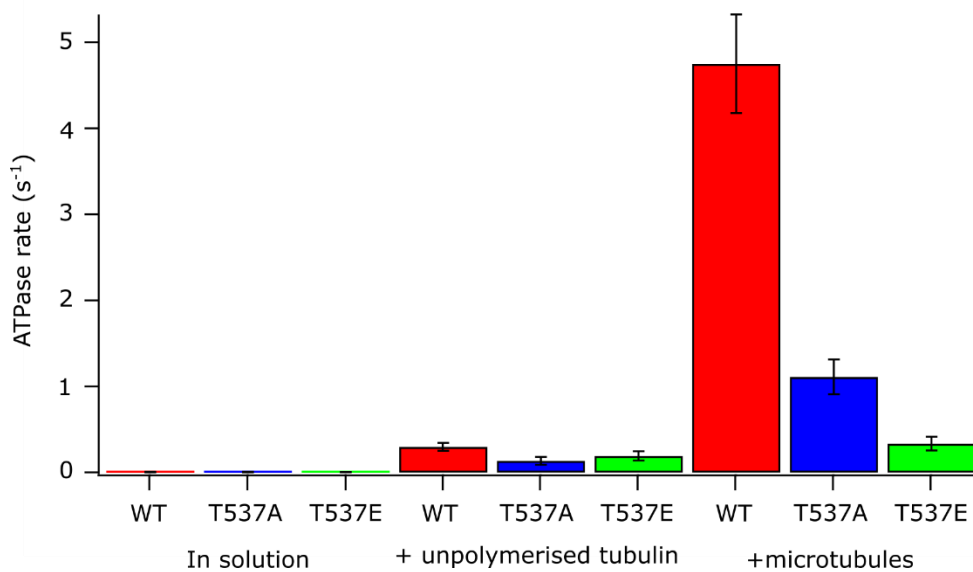


Figure 3.9. An overview of the ATPase rates of wild type MCAK, T537A and T537E in solution, with unpolymerised tubulin and with microtubules.

3.5 Cdk1 phosphomimic and phosphonull mutants can still bind microtubules

To test whether the differences observed in the microtubule stimulated ATPase data for T537A and T537E are because the mutant proteins are unable to bind to microtubules, a microtubule pelleting assay was used. This assay assesses whether the protein and microtubules can interact by observing

whether microtubules can pellet the MCAK protein. The microtubules and MCAK were incubated together and then centrifuged to pellet the microtubules (2.12). In the absence of microtubules, MCAK is found in the supernatant but when incubated with microtubules the interaction between MCAK and the microtubules leads to MCAK being found predominantly in the pellet fraction (**Figure 3.10**). No difference was observed between MCAK and the mutants, suggesting the difference in ATPase is not due to a general inability to interact with microtubules and that the reduction in microtubule-stimulated ATPase is due to impairment of a specific interaction with the microtubule.

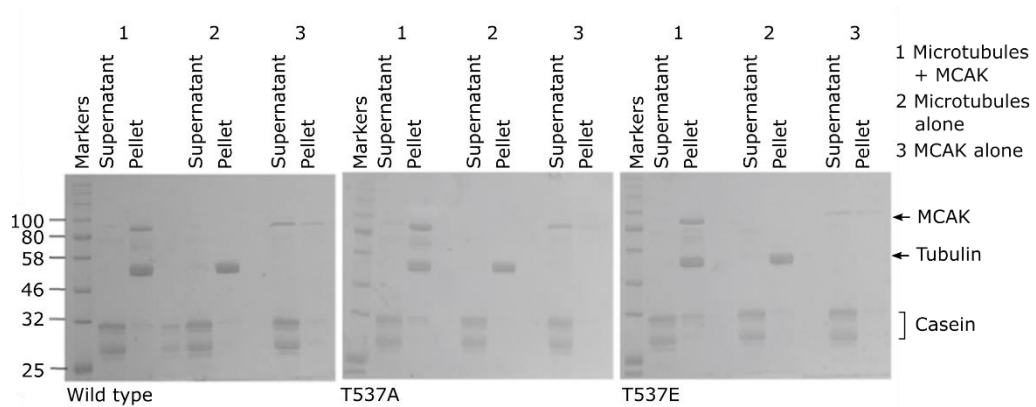


Figure 3.10. MCAK and the mutants T537A and T537E co-sediment with microtubules. MCAK and microtubules, microtubules alone or MCAK alone were incubated together and then centrifuged. The supernatant and resuspended pellet were then run on an SDS-PAGE gel. Representative SDS-PAGE gels from 3 replicates for each protein.

3.6 Microtubule end residence times are reduced with Cdk1 phosphomimic and phosphonull mutants

The differences observed in the ATPase data in the presence of microtubules suggests that their interaction with the microtubule has been affected, while the pelleting assay confirms that they are still able to interact with the microtubule to some degree. To understand more about how their interaction with the microtubule had been affected, TIRF microscopy was used to look at the behaviour of single molecules of MCAK on microtubules (2.15). By taking images of GFP-labelled MCAK proteins with immobilised, GMPCPP-stabilised, rhodamine-labelled microtubules every 0.134 seconds it was possible to observe single MCAK molecules. Using an image of a single microtubule over time a kymograph could be made, which makes it possible to analyse the residence time of MCAK at the microtubule end. Wild type MCAK showed a much larger range of residence times than the mutants. Only 0.4 % of T537E and 11 % of T537A molecules stayed at the microtubule end for longer than 2 s, compared with 32 % of wild type (**Figure 3.11**).

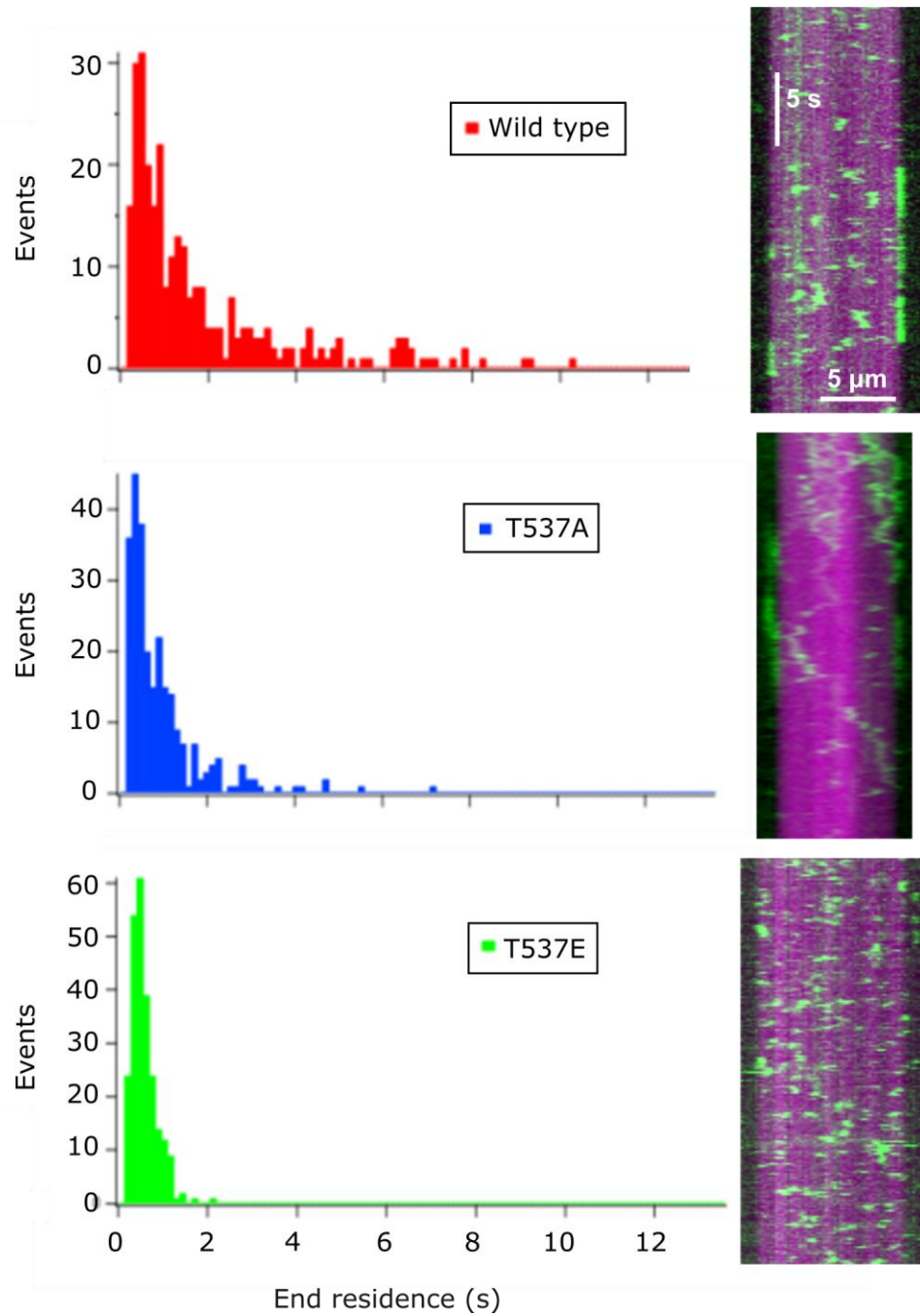


Figure 3.11. T537A and T537E show fewer long end residence events than wild type MCAK. Histograms show the number of events with a specific duration of end residence (WT n=289, T537A n=261, T537E n=242). Representative kymographs show the behaviour of T537A, T537E and wild type MCAK-GFP (green) on GMPCPP-stabilised microtubules (magenta).

The average end residence time was reduced from 2.03 ± 0.13 s (mean \pm s.e.m.) for wild type MCAK to 1.00 ± 0.06 for T537A ($p < 0.0001$) and 0.64 ± 0.02 for T537E ($p < 0.0001$). This offers an explanation for why the mutants display decreased depolymerisation and ATPase activity displayed by the mutants. The reduction and loss of long residence events observed with the mutants could mean that ADP dissociation is not being accelerated in these mutants in the same way as with wild type protein. This would lead to a lack of ATP binding and the consequent tight binding of MCAK to the microtubule that leads to depolymerisation. As ADP dissociation is the rate limiting step for MCAK's ATPase rate in the presence of microtubules (Friel and Howard 2011), if ADP dissociation is not accelerated to the same degree this can be expected to lead to a corresponding decrease in the ATPase activity.

To determine whether the mutations had impaired MCAK's ability to reach the microtubule end or impaired its ability to recognise the microtubule end upon arrival, the number of end events per unit time were measured. It was found that the rates were 0.71 ± 0.29 $\text{nM}^{-1} \text{s}^{-1}$ for wild type ($n = 15$), 0.62 ± 0.16 $\text{nM}^{-1} \text{s}^{-1}$ for T537A ($n = 19$, $p = 0.2933$) and 0.97 ± 0.27 $\text{nM}^{-1} \text{s}^{-1}$ ($n=17$, $p = 0.0142$) for T537E. This shows that the T537A substitution has not had a significant effect on the ability of MCAK to reach the microtubule end and the T537E mutant actually gets to the microtubule end more frequently than the wild type. One possible explanation of this could be if the diffusion distance of T537E on the lattice is increased, increasing the probability of reaching the microtubule end.

It was also possible to measure the lattice residence time for wild type MCAK and the mutants. Histograms are shown in **Figure 3.12**. Wild type MCAK and T537E showed comparable lattice residence times and k_{off} (rate constant of MCAK's dissociation from the microtubule) values which shows that the difference in end residence times is specific to the microtubule end, and not a global loss of affinity. This is consistent with the pelleting assay data (**Figure 3.10**). Interestingly T537A showed an increase in lattice residence time, which actually means that like T537E it has a much smaller difference in the values of k_{off} at the microtubule end and on the lattice than wild type MCAK, as shown in **Figure 3.12** and **Table 1**. The fits used to calculate k_{off} values are shown in Appendix 2 (A2.1).

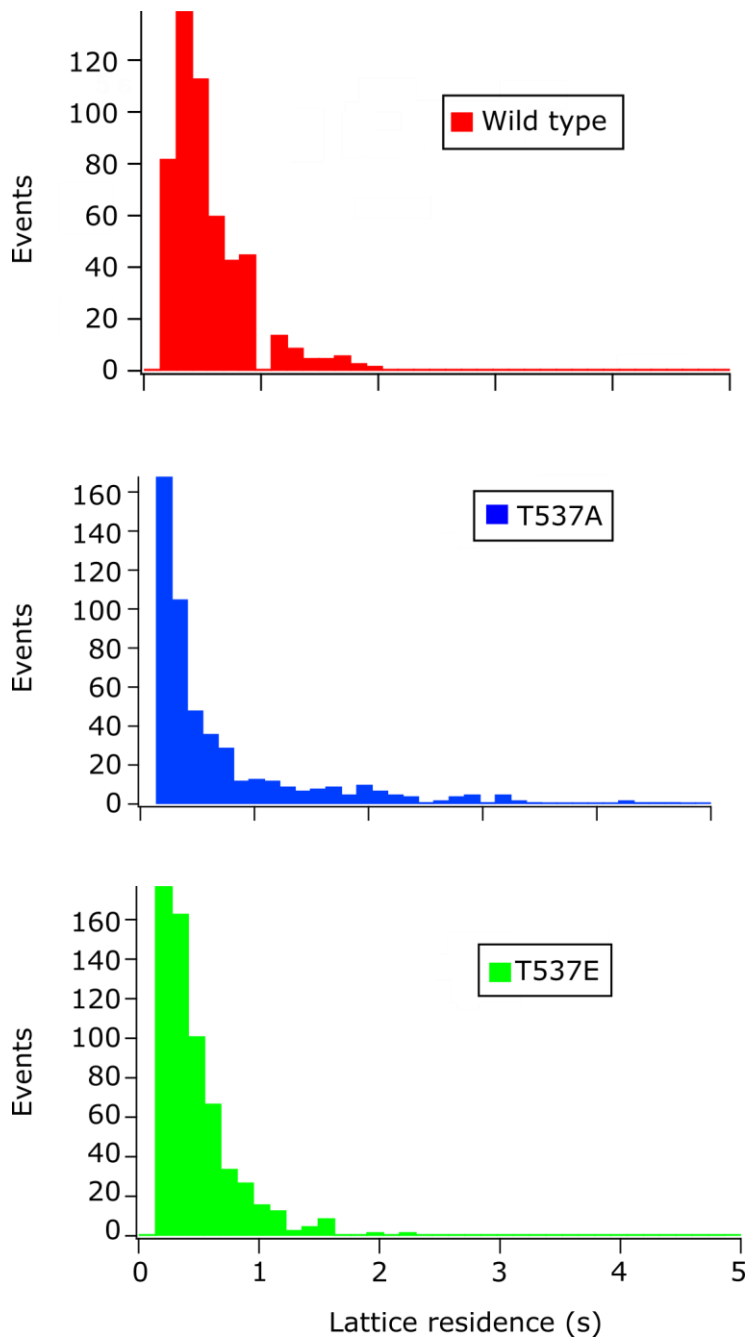


Figure 3.12. WT MCAK and T537E show comparable lattice residence times, but T537A has a longer lattice residence time. Histograms show the number of events with a specific duration of lattice residence (WT n = 526, T537A n = 582, T537E n = 622).

Table 1. T537A and T537E have shorter end residence times than WT MCAK and T537A has a longer lattice residence time.

	WT	T537A	T537E
Lattice residence time (s, mean \pm s.e.m.)	0.48 \pm 0.02 (n = 526)	0.70 \pm 0.04 (n = 582)	0.42 \pm 0.01 (n = 622)
Lattice k_{off} (s^{-1} , mean \pm s.d.)	2.90 \pm 0.16 (n = 526)	1.54 \pm 0.22 (n = 582)	2.64 \pm 0.19 (n = 622)
Microtubule end k_{off} (s^{-1} , mean \pm s.d.)	0.98 \pm 0.06 (n = 289)	1.41 \pm 0.12 (n = 261)	2.30 \pm 0.40 (n = 242)
k_{on} (s^{-1} , mean \pm s.d.)	0.59 \pm 0.28 (n = 3)	0.40 \pm 0.11 (n = 3)	0.48 \pm 0.06 (n = 3)

3.7 *The mADP dissociation rate is not accelerated by the microtubule end in a Cdk1 phosphomimic of MCAK*

To discover whether the lack of long end binding events by the mutants is preventing the microtubule end from accelerating ADP dissociation, stopped flow was used to measure the rate of ADP dissociation (2.8). To do this, MCAK was pre-loaded with ADP attached to a small fluorescent label – mant. MantADP (mADP) has a higher fluorescence intensity when bound to MCAK than in solution, so after rapid mixing of MCAK-mADP with an excess of ATP the rate of decrease in fluorescence was measured as mADP dissociates and ATP binds. Studying the ADP dissociation rate from the mutants in solution showed comparable rate constants to wild type MCAK (**Figure 3.13**). This supports the idea that the ATP turnover cycle itself is not disrupted in these mutant proteins.

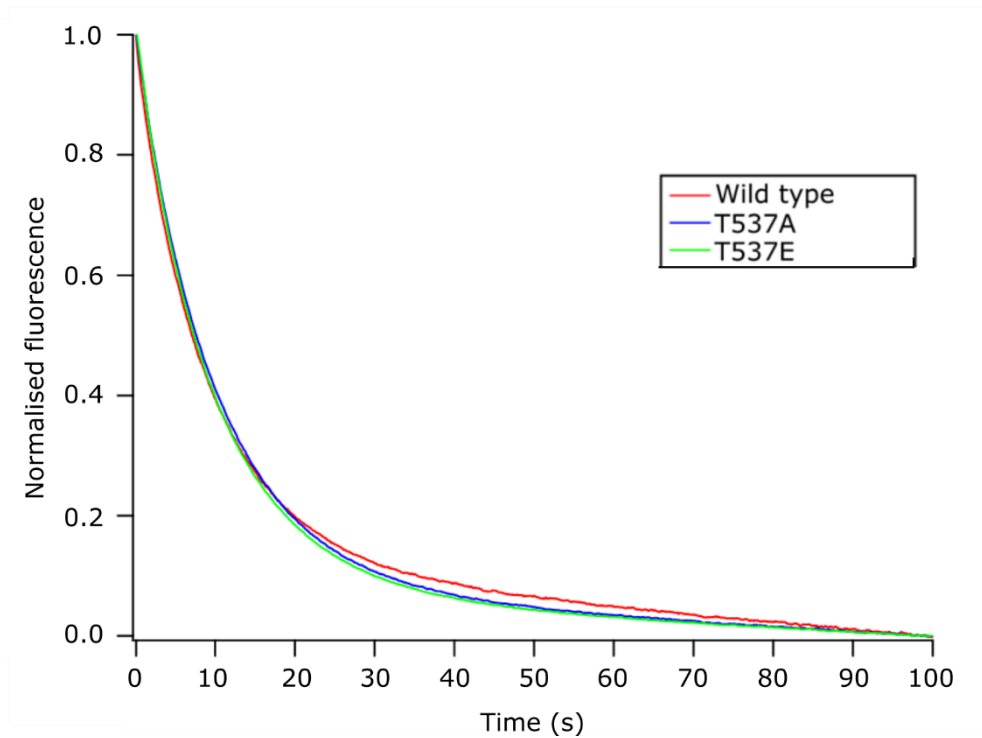


Figure 3.13. The rate of mantADP dissociation from wild type MCAK is comparable for the mutants T537A and T537E. MCAK was pre-loaded with mantADP and then rapidly mixed with ATP. The change in fluorescence of mantADP from being bound to free in solution was measured. For each protein $n = 15$ from 3 independent experiments. For individual graphs showing standard deviations and fits, see Appendix 2 (A2.2).

The addition of free tubulin did not significantly affect the rate constant of ADP dissociation as seen previously with wild type protein (Friel and Howard 2011) and is shown in **Figure 3.14**.

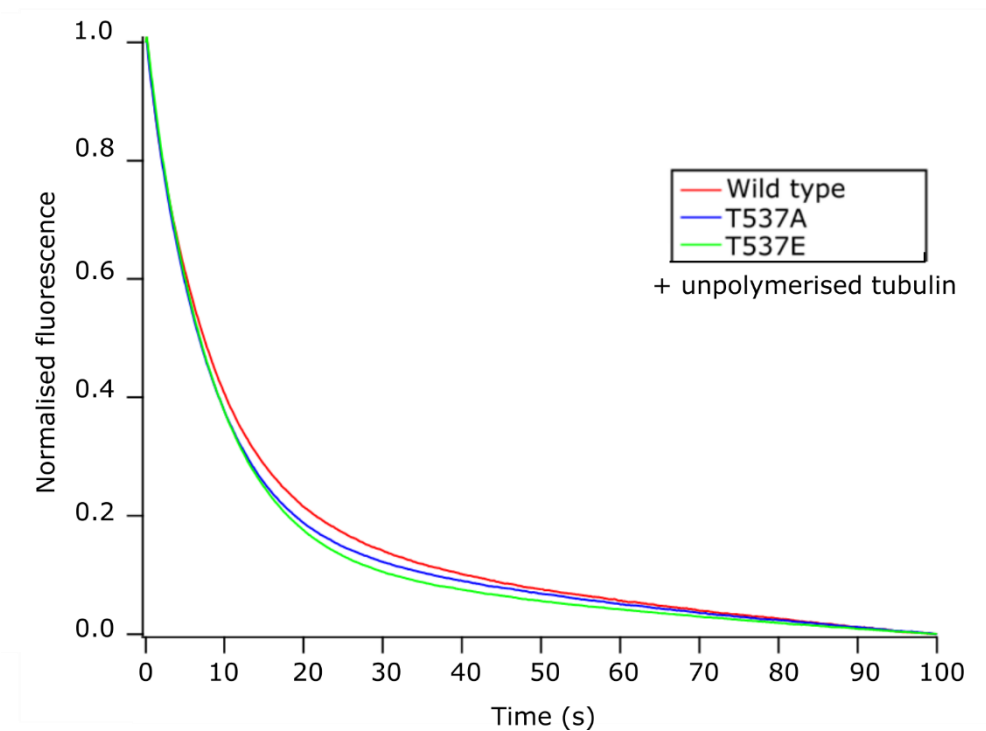


Figure 3.14. The rate of mantADP dissociation from wild type MCAK is comparable for mutants T537A and T537E in the presence of unpolymerised tubulin. MCAK was pre-loaded with mantADP and then rapidly mixed with ATP. The change in fluorescence of mantADP from being bound to free in solution was measured. For each protein n=15 from 3 independent experiments. For individual graphs for each protein showing standard deviations and fits see Appendix 2 (A2.2).

In the presence of microtubules, both T537A and T537E showed a significantly reduced rate of ADP dissociation as shown in **Figure 3.15**. ADP dissociation from wild type MCAK is well described by a double exponential function. The two phases of the exponential are attributed to the microtubule end-stimulated events and those stimulated by lattice, free-tubulin or in solution (which all have the same rate). It is not currently known precisely why free tubulin is unable to accelerate mADP dissociation when the microtubule end

is, as in both these places the tubulin is free to adopt the more curved conformation preferred by MCAK. Recent structural studies have shown the neck domain of Kinesin-13s interacting with the next tubulin dimer towards the (-) end (Benoit, Asenjo et al. 2018). This could be a mechanism by which MCAK can 'sense' whether the tubulin is part of a microtubule or not. The results for T537A are also best described by a double exponential. However, the data for T537E can be fitted to a single exponential equation, as the rapid microtubule end-stimulated phase is not observed (individual graphs for each protein with the fits are shown in Appendix 2, A2.2). These data suggest that T537E has lost the ability to distinguish the microtubule end from the microtubule lattice, resulting in loss of microtubule end stimulated acceleration of ADP dissociation.

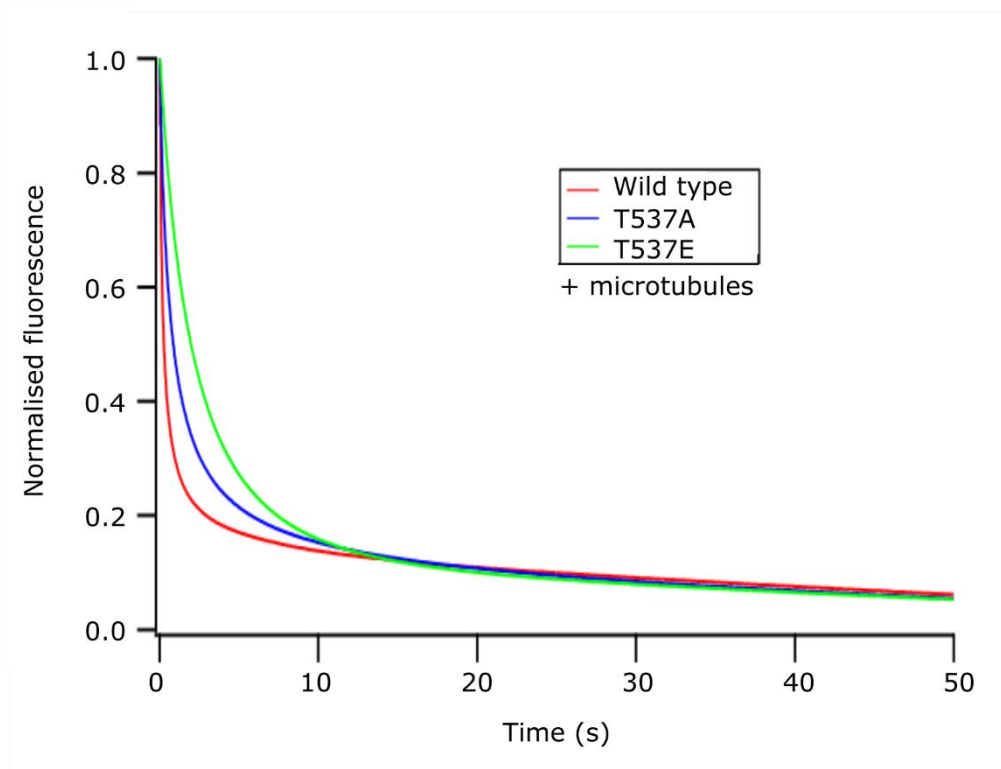


Figure 3.15. The rate of mantADP dissociation from wild type MCAK is faster than from T537A and T537E in the presence of microtubules. MCAK was pre-loaded with mantADP and then rapidly mixed with ATP. The change in fluorescence of mantADP from being bound to free in solution was measured. For each protein n=15 from 3 independent experiments. For individual graphs of each protein with standard deviation and fits see Appendix 2 (A2.2).

Figure 3.16 shows the striking differences in behaviour of the different proteins and with the different substrates. All three proteins behave in a similar manner in solution and in the presence of unpolymerised tubulin. For wild type MCAK, the addition of microtubules accelerated ADP dissociation over 40-fold, compared with 11-fold for T537A and only 3-fold for T537E. In fact the rate constant for T537E is not significantly different from the rate constant of the slow phase for wild type ($p = 0.2477$). The rates of mADP dissociation and ATPase in the presence of tubulin and microtubules for all the mutants correspond well, suggesting that ADP dissociation remains the rate-limiting step in the ATP turnover cycle for these proteins (**Table 2**).

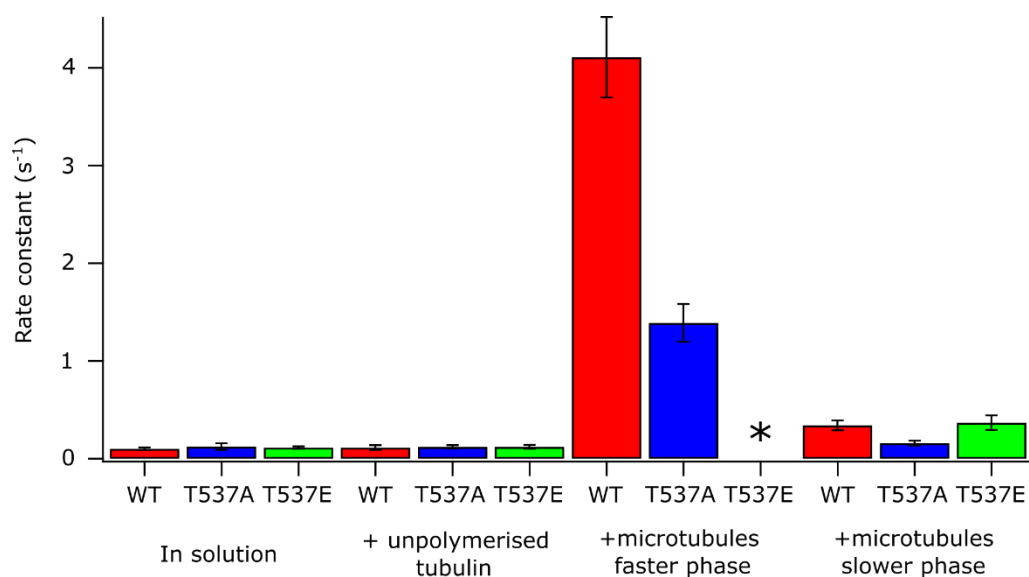


Figure 3.16. Overview of the rate constants of mADP dissociation from wild type MCAK, T537A and T537E in solution, in the presence of unpolymerised tubulin and in the presence of microtubules. The data for T537E, in the presence of microtubules, was fitted to a single exponential and so does not have a faster phase rate constant, shown with an asterisk.

Table 2. Summary table of depolymerisation, ATPase, mADP dissociation and end residence data.

* Indicates where there is a statistically significant difference from wild type.

	WT	T537A	T537E
Depolymerisation rate (40 nM, $\mu\text{m}/\text{min}$, mean \pm s.d., n=20)	3.04 \pm 0.53	0.71 \pm 0.19 *	0.06 \pm 0.06 *
ATPase in solution (s^{-1} , mean \pm s.d., n=3)	0.00447 \pm 0.00260	0.00566 \pm 0.00291	0.00533 \pm 0.00033
ATPase + unpolymerised tubulin (s^{-1} , mean \pm s.d., n=3)	0.299 \pm 0.047	0.136 \pm 0.045	0.194 \pm 0.055
ATPase + microtubules (s^{-1} , mean \pm s.d., n=3)	4.75 \pm 0.572	1.11 \pm 0.202 *	0.335 \pm 0.081 *
mADP dissociation in solution (s^{-1} , mean \pm s.d., n=15)	0.102 \pm 0.013	0.124 \pm 0.035	0.114 \pm 0.013
mADP dissociation + unpolymerised tubulin (s^{-1} , mean \pm s.d., n=15)	0.113 \pm 0.024	0.120 \pm 0.018	0.120 \pm 0.019
mADP dissociation + microtubules (s^{-1} , mean \pm s.d., n=15)	k_{fast} 4.11 \pm 0.411 k_{slow} 0.341 \pm 0.051	k_{fast} 1.39 \pm 0.193 * k_{slow} 0.160 \pm 0.024 *	k 0.369 \pm 0.076
Rate constant amplitudes	A_0 0.653 \pm 0.001 A_1 0.159 \pm 0.001	A_0 0.591 \pm 0.003 A_1 0.237 \pm 0.001	A_0 0.791 \pm 0.002
Microtubule end residence time (s, mean \pm s.e.m.)	2.03 \pm 0.13 (n = 289)	1.00 \pm 0.06 * (n = 261)	0.64 \pm 0.02 * (n = 242)

3.8 Summary

Residue T537 in MCAK is phosphorylated *in vivo* by Cdk1 to regulate MCAK's activity and localisation through mitosis. Phosphorylation leads to a reduced rate of depolymerisation. To investigate the mechanism of this effect phosphomimic and phosphonull mutants T537E and T537A, respectively, were produced. These proteins were expressed in insect cells and purified using nickel affinity chromatography. A summary table of the results from this chapter is given in **Table 2**.

It was found that T537A had a 4-fold reduction and T537E had a 50-fold reduction in the rate of depolymerisation compared to wild type protein at the optimal concentration of MCAK (40 nM). However, when the concentration of protein was increased (to 400 nM), the rate of depolymerisation by wild type and T537A converged to the same rate, while the rate of depolymerisation by T537E remained 2-fold slower.

In solution, and in the presence of unpolymerised tubulin, the ATPase rates of the two mutants were not significantly different from wild type. However in the presence of microtubules the ATPase rate of T537E was 14-fold slower and T537A was 4-fold slower than wild type. Using a pelleting assay and TIRF microscopy, it was shown that this is not because the proteins do not interact with microtubules. Instead, even though the mutants can interact with microtubules, they exhibit fewer events with long residence times at the microtubule end, with only 0.4 % of T537E and 11 % T537A molecules staying

at the microtubule end for longer than 2 seconds, compared to 34 % of wild type molecules.

The rates of ADP dissociation, in solution and in the presence of unpolymerised tubulin, were unaffected by the substitutions but in the presence of microtubules both T537A and T537E have significantly slower ADP dissociation rates and T537E no longer shows a two-phase reaction rate.

Together this data shows that T537A and T537E have an impaired ability to recognise the microtubule end. For T537E, the microtubule lattice and microtubule end are no longer recognised as two different substrates.

Our lab has previously identified 3 other residues that affect MCAK's ability to recognise the microtubule end – K524, E525 and R528 (Patel, Belsham et al. 2016). In a similar way to T537E, alanine substitutions at these 3 residues led to decreased rates of depolymerisation, decreased ATPase and mADP dissociation in the presence of microtubules, and shorter end residence times compared to wild type protein. E525A, like T537E, has a rate of mADP dissociation with microtubules that can be described by a single exponential function, indicating that it too cannot distinguish the microtubule end (Patel, Belsham et al. 2016). T537 is located adjacent to the $\alpha 4$ helix, where K524, E525 and R528 are located. The $\alpha 4$ helix is thought to stabilise the curved conformation of tubulin, which is found at microtubule ends, compared with the straighter conformation found in the microtubule lattice. This stabilisation may then promote further deformation of the tubulin dimers, leading to the breakage of interdimer bonds and depolymerisation. Mutating residues in

this region of MCAK appears to impair its ability to distinguish between the microtubule end and the microtubule lattice.

In cells, phosphorylation at T537 provides the cell with a means to disrupt the interaction between the $\alpha 4$ helix and the microtubule end, without affecting the interaction between MCAK and the microtubule lattice. This allows MCAK to move into position, while its ability to depolymerise can be rapidly activated and deactivated by phosphorylation.

Chapter 4 The Plk1 phosphomimic mutant S621D does not alter MCAK's depolymerisation activity

4.1 Background

One of the kinases that is known to phosphorylate MCAK, other than Cdk1 discussed in Chapter 3, is Plk1. MCAK is phosphorylated at six different residues by Plk1, all in the C-terminal domain (S592, S595, S621, S632, S633 and S715) (Zhang, Shao et al. 2011). Zhang et al generated plasmids that expressed GFP-tagged forms of MCAK that had either phosphomimetic or phosphonull substitutions using glutamate (E) or alanine (A) respectively to substitute all 6 residues simultaneously. When these plasmids were transfected into HeLa cells, relative microtubule intensities (calculated by integrating the pixel intensities of maximum projections of z-stacks as a measure of the amount of microtubules in a cell) were 0.57 for MCAK-6E, 0.8 for MCAK WT and 1.0 for MCAK-6A. Also, spindle density was reduced by 21 % in cells expressing the 6E mutant compared to WT and 6A. It was concluded that phosphorylation of MCAK by Plk1 enhances MCAK's depolymerisation activity. In cells expressing MCAK-6E, microtubule bundling was increased, and after nocodazole treatment (which prevents microtubule polymerisation) the microtubules repolymerised more slowly than in cells that expressed wild type MCAK or MCAK-6A. In contrast to the effect of MCAK-6E, microtubule bundling was decreased in cells with MCAK-6A. Overexpression of wild type MCAK or MCAK-6E caused misaligned chromosomes and multipolar spindles, whereas MCAK-6A expression led to

fewer displaced chromosomes and almost normal spindles but a chromosome instability phenotype (Zhang, Shao et al. 2011).

However, no further work was done at that time to try to understand how MCAK's activity was affected by these phosphorylation events or whether phosphorylation at all sites was required or had the same function. The structure of MCAK, outside of the motor domain, has not been determined, but there are several publications that show an effect of the C-terminus on motor activity. For example, a truncation of just 9 residues from the C-terminus increased depolymerisation activity and microtubule-stimulated ATPase (Moore and Wordeman 2004). In addition, Ems-McClung et al. (2007) showed a small reduction in microtubule and microtubule-end binding by C-terminal truncated mutants, together with a 4-fold increase in the release of MCAK, in the presence of excess tubulin. They suggested that this could be caused by defective release of the tubulin dimer at the end of its catalytic cycle or decreased ability to diffuse along the microtubule lattice (Ems-McClung, Hertzler et al. 2007).

A collaboration with Juping Yuan's lab, in Frankfurt, was established to look particularly at the role of phosphorylation at S621, which this group identified as the primary site of phosphorylation by Plk1 (Sanhaji, Ritter et al. 2014). They also found clear effects on the progress of cell division when the phosphomimetic and phosphonull S621D and S621A mutant forms of MCAK were expressed in HCT116 or HeLa cells. Expression of S621D led to a reduced inter-kinetochore distance, indicative of a lack of tension and expression of

either S621A or S621D led to defects in spindle formation and chromosome congression. Cells expressing S621A had shorter spindles and contained 25 % less polymerised tubulin than those expressing wild type protein, while those expressing S621D contained 8 % more polymerised tubulin. These results suggested that the S621A mutant was more active than wild type, while the S621D mutant was less active. However, the interpretation of the cellular phenotype data was confounded by the discovery that the inhibition of Plk1, or depletion of APC/C cofactors Cdc20 or Cdh1, led to an increased stability of MCAK and wild type and S621D MCAK were stabilised by modification of the D-box, where MCAK is ubiquitinated. Wild type and S621D MCAK are ubiquitinated more than S621A; the latter shows little evidence of ubiquitination. Comparable spindle lengths were observed in cells expressing each of the proteins when the proteasome was inhibited. S621A accumulates in cells, whereas S621D is only present at low levels, as a result of its rapid degradation.

To determine whether the cellular phenotypes of cells expressing S621A and S621D were caused by a change in MCAK's activity or by the altered protein stability, direct measurements of MCAK's ATPase and depolymerisation activity were carried out.

4.2 Plk1 phosphomimetic and phosphonull mutants of MCAK were expressed and purified

DNA constructs of both S621A and S621D mutants of MCAK were provided by the Yuan lab to enable production of phospho-null and phosphomimetic mutant proteins. These mutated sequences were inserted into bacmid vectors using the Bac-to-Bac expression system as described in 2.2.3. Baculoviruses were then amplified from cells transfected with each plasmid and used to infect approximately 3×10^8 *Spodoptera frugiperda* (Sf9) cells to produce the desired proteins. These MCAK mutants were then purified using a nickel affinity column. The protocols used for expression and purification are described in sections 2.2.4 and 2.3 and the results of the purifications are shown in **Figure 4.1**.

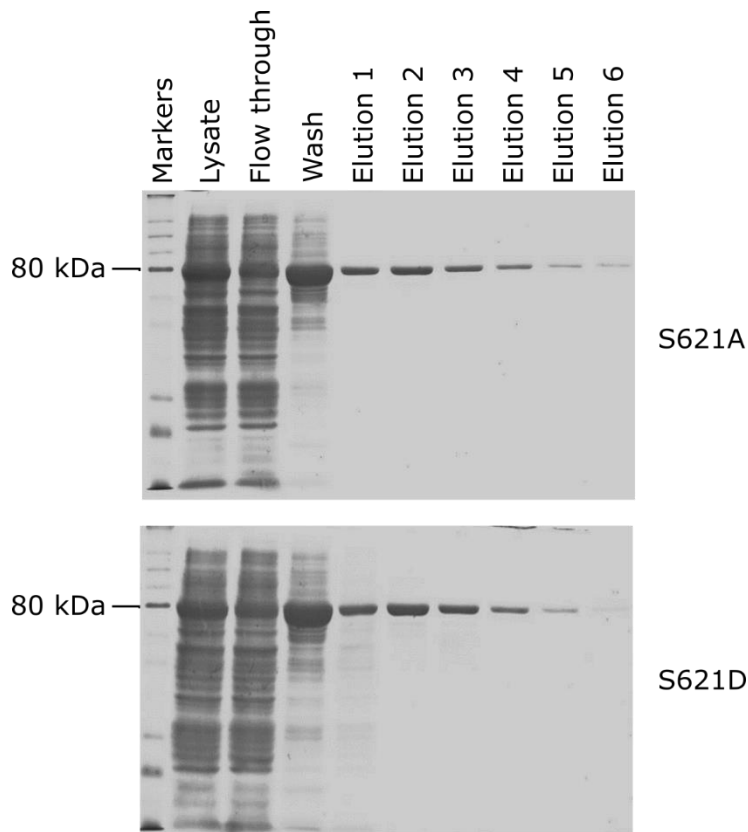


Figure 4.1. Purification of His-tagged S621A and S621D by Nickel affinity chromatography. SDS-PAGE gel stained with Instant Blue of progression through purification. Lysate: Cleared Sf9 cell lysate. Flow through: Flow through from cell lysate applied to Nickel affinity column. Wash: 75 mM imidazole wash. Elutions 1-6: Eluate from Nickel affinity column in 200 mM imidazole in 300 μ l fractions. MCAK molecular weight 82 kDa.

4.3 *Plk1 phosphomimetic and phosphonull mutants have similar basal ATPase rates to wild type MCAK*

The effect of these substitutions on MCAK's enzymatic activity was investigated by measuring the rate of nucleotide turnover in the absence of tubulin and the rate of microtubule depolymerisation. To measure the rate of ATP turnover in solution, the amount of free phosphate produced over time

was measured using a BIOMOL green phosphate detection reagent (2.7.2).

The data was then converted into the amount of phosphate produced per MCAK monomer per second, using a standard curve.

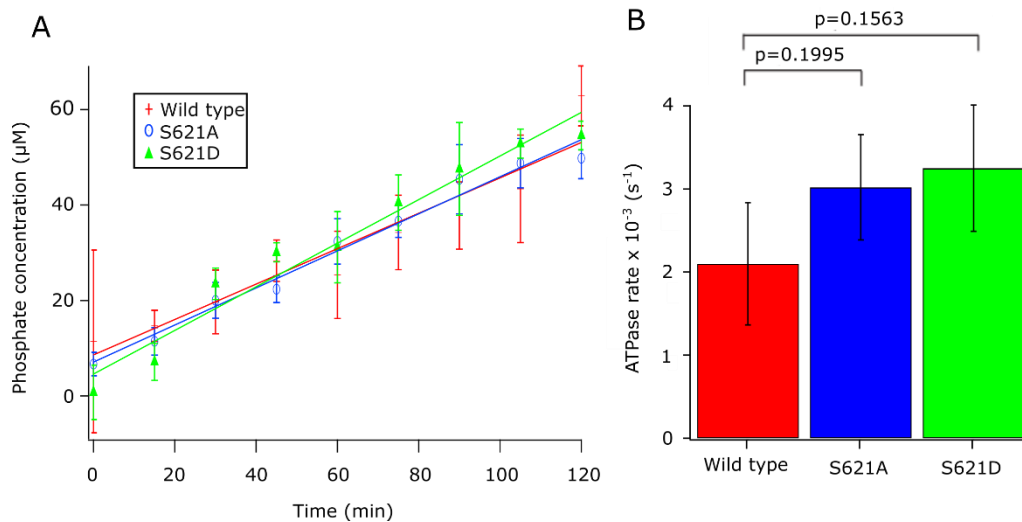


Figure 4.2. The ATPase rate of S621A and S621D is not significantly different from wild type. A) Production of inorganic phosphate from ATP over time by wild type MCAK and the mutants S621A and S621D. Points are mean \pm standard deviation, $n = 3$, and a fit is shown B) Mean ATPase rate \pm standard deviation is shown, $n = 3$.

No statistically significant difference was observed in the rate of ATP turnover

between the wild type protein and S621A ($p=0.1995$) or S621D ($p=0.1563$).

This confirms that the mutant versions of MCAK retain ATPase activity

suggesting that they are correctly folded. As S621 is outside the motor

domain (residues 232-583), it is perhaps unsurprising that phosphorylation at

this site does not affect ATP turnover.

4.4 *Plk1 phosphomimetic and phosphonull mutants can depolymerise microtubules at a similar rate to wild type*

MCAK

The effect of the substitutions on MCAK's ability to depolymerise microtubules was measured. The ability of the MCAK variants S621A and S621D to depolymerise microtubules was compared to the wild type protein using a light scattering assay. As microtubules scatter more light than its constituent subunits, the degree of light scatter over time was measured using a fluorimeter (see Chapter 2.9). The results are shown in **Figure 4.3**.

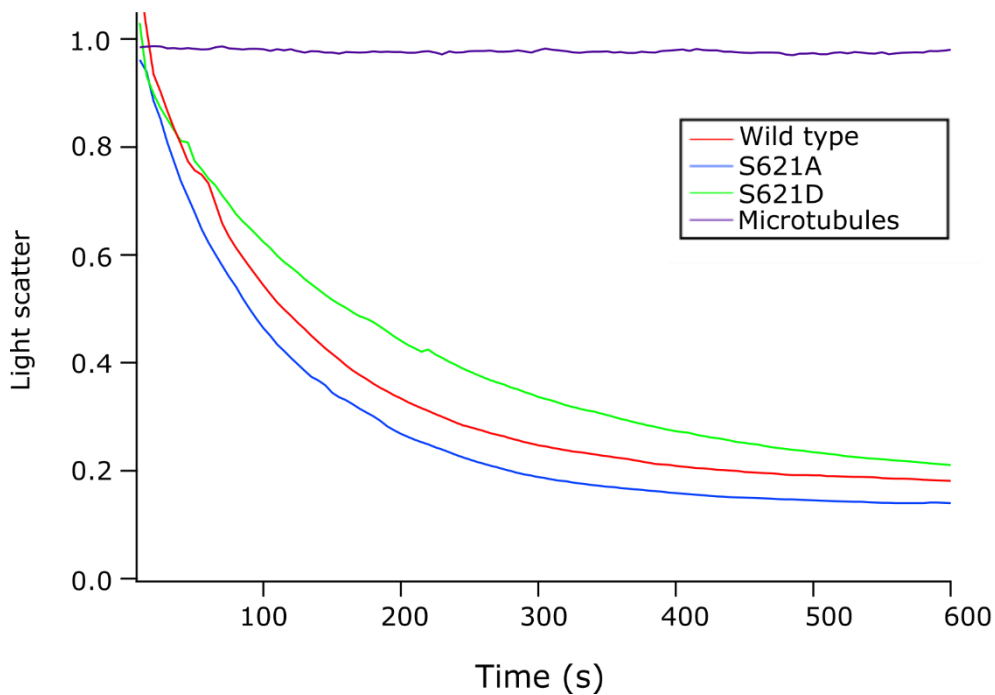


Figure 4.3. Wild type MCAK and the mutants S621A and S621D show similar rates of depolymerisation when measured using a light scattering assay. The depolymerisation of microtubules was measured using the light scattering assay and normalised to the average reading of microtubules over 150

seconds prior to the addition of MCAK. The curves on the graph represent the average values from 5 experiments.

The turbidity assay showed similar rates of depolymerisation for wild type MCAK and S621A and S621D. To measure the rate of depolymerisation of individual microtubules fluorescence microscopy was used to image them over time after the addition of MCAK (2.11). The rate of depolymerisation by S621A and S621D was found to be not significantly different from wild type, as shown in **Figure 4.4**.

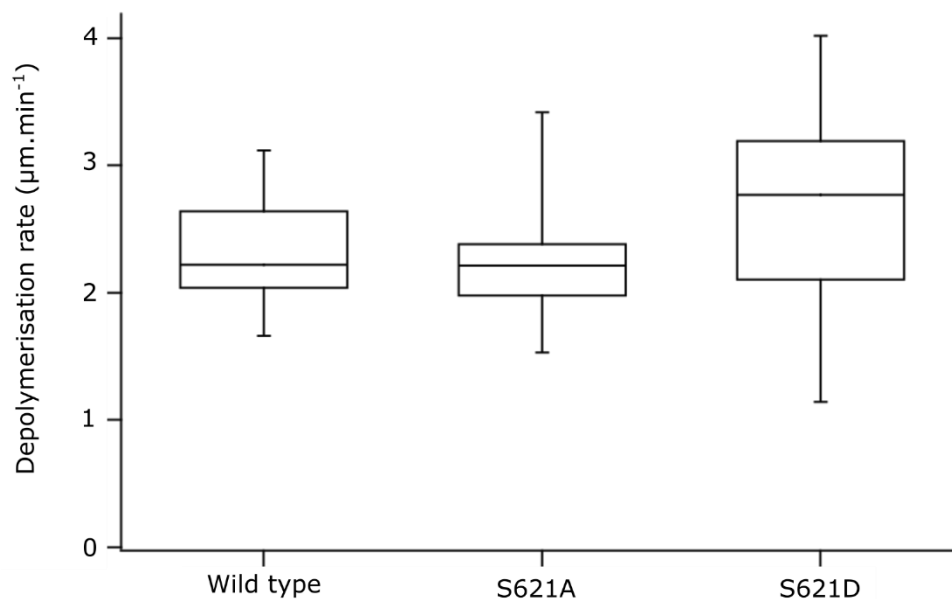


Figure 4.4. The rate of depolymerisation by wild type MCAK and the mutants S621A and S621D are not significantly different.

The ATPase and depolymerisation rates of wild type MCAK and the mutants S621A and S621D are summarised in **Table 3**.

Table 3. The ATPase and depolymerisation rates of S621A and S621D are not significantly different from wild type.

	WT	S621A	S621D
ATPase rate (s ⁻¹ , mean ± s.d., n=3)	0.0021 ± 0.0007	0.0030 ± 0.0006	0.0033 ± 0.0008
Depolymerisation rate (µm.min ⁻¹ , mean ± s.d., n=20)	2.30 ± 0.38	2.31 ± 0.51	2.62 ± 0.79

4.5 Summary

S621 has been identified as the prominent phosphorylation site of MCAK by Plk1 (Sanhaji, Ritter et al. 2014). The MCAK variants S621A and S621D, as phosphomimetic and phosphonull mutants respectively, were expressed and purified (**Figure 4.1**). There was no significant difference between wild type MCAK and the mutants in terms of ATPase activity (**Figure 4.2**). Further, the microtubule depolymerisation activity of MCAK was not significantly altered by either the S621A or S621D mutations (**Figure 4.3** and **Figure 4.4**).

This shows that the alterations in spindle length, inter-kinetochore distance and polymerised tubulin content found in cells expressing S621A and S621D are not caused by a change in MCAK activity but suggests that the primary role of phosphorylation at S621 by Plk1 is to regulate MCAK's stability. Plk1 phosphorylation at S621 may cause a conformational change in MCAK, which exposes the D-box to ubiquitination. This then targets the molecule for degradation by the 26S proteasome through the APC/C^{Cdc20} pathway, reducing the level of MCAK in the cell and consequently reducing depolymerisation activity.

4.6 The role of phosphorylation by Plk1 at other residues

The Yuan lab then went on to propose the S632/S633 site as the phosphorylation site by Plk1 which regulates its depolymerisation activity (Ritter, Sanhaji et al. 2015). Preliminary data we had collected showed no difference in depolymerisation activity between the wild type and SS632/3AA and SS632/3DD (data not shown). However, Ritter et al incubated MCAK and microtubules together for 15 minutes and found a significant decrease in the length and number of microtubules in the presence of the SS632/3DD mutant and a significant increase in the length and number of microtubules in the presence of the SS632/3AA mutant compared to wild type protein. A possible explanation for this difference is that the Yuan lab used MCAK at 500 nM, whereas in our experiments we used 40 nM MCAK, and as shown in chapter 3 MCAK variants can respond differently to changes in concentration. Also, looking at the microtubules at only the start and the end of the incubation doesn't allow the rate of depolymerisation to be calculated or compared. In HeLa cells, with endogenous MCAK knocked down by siRNA, the Yuan lab found 22 % more polymerised tubulin in cells transfected with the SS/AA mutant than wild type, while those transfected with the SS/DD mutant had 34 % less polymerised tubulin. SS/AA cells had longer, denser spindles, and SS/DD had shorter, thinner spindles with fewer microtubules compared with wild type. After cold treatment, and microtubule regrowth, more

microtubules were present in the cells transfected with the SS/AA protein and fewer microtubules were present with SS/DD. The cells transfected with the SS/DD mutant also had shorter k-fibres than cells with wild type MCAK. Transfection with the mutants also led to problems with chromosome alignment. Cells transfected with SS/AA often exhibited metaphase arrest as a result of chromosome congression failure. The cells that did manage to align the chromosomes showed decreased inter-centromeric distance and were unable to properly segregate. This suggests that phosphorylation is required to correct improper kinetochore-microtubule attachments. Cells transfected with the SS/DD plasmid displayed fewer chromosome misalignments than SS/AA but more than wild type. An increased inter-centromeric distance was also seen in cells transfected with SS/DD. In short, in cells the SS/AA protein appears to be less active in depolymerising microtubules than wild type MCAK, while the SS/DD protein appears to be more active. However, since the activity of the SS/DD mutant protein *in vitro* is in dispute, it is unclear whether this is directly as a result of its catalytic activity being changed or whether, like the S621 mutants, other processes are affecting its ability to depolymerise microtubules.

4.7 *The use of phosphomimic residues*

In this work, aspartate has been used as a phosphomimic residue. Although conventionally serine has been replaced with aspartate and threonine with glutamate there are several reasons why glutamate is more accurate mimic of

phosphorylation at serine residues as well. The pKa of the glutamate side chain is ~4.2, compared to ~3.8 for aspartate and ~5.8 for the formation of phosphoserine. The structures are also more similar (as shown in **Figure 4.5**). However, for this work we used the S621D mutant as this allowed direct comparison with the cell biology experiments performed by the Yuan lab. Generating an SS/EE mutant and analysing its activity *in vitro* and in cells might help clarify the effect of phosphorylation at SS632/3 on MCAK's activity. While phosphomimic constructs can be useful for understanding more about the effects of phosphorylation, especially when using proteins in *in vitro* assays, they cannot mimic the effect of phosphorylation exactly.

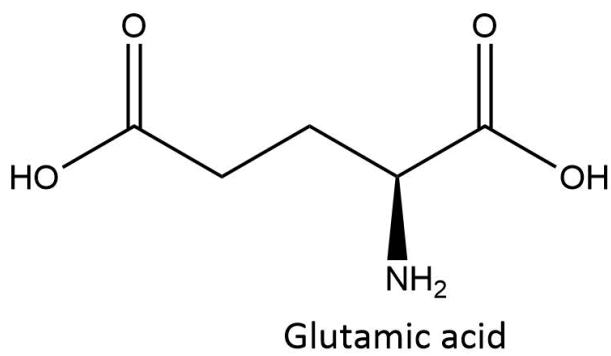
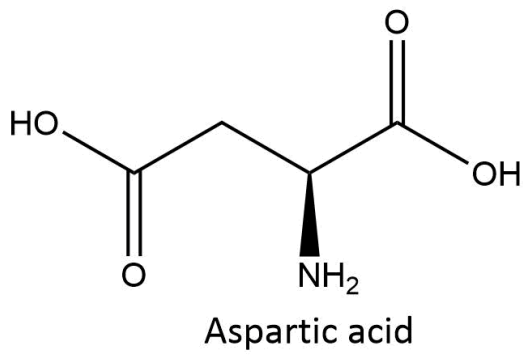
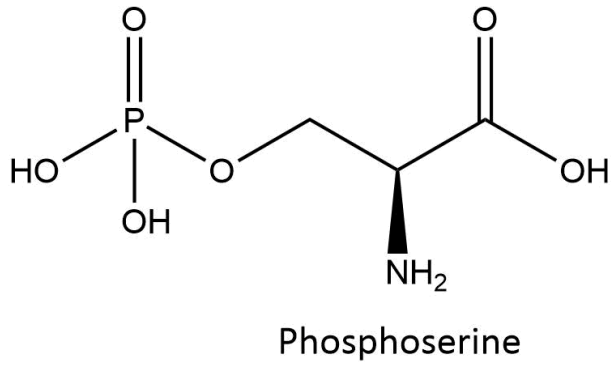
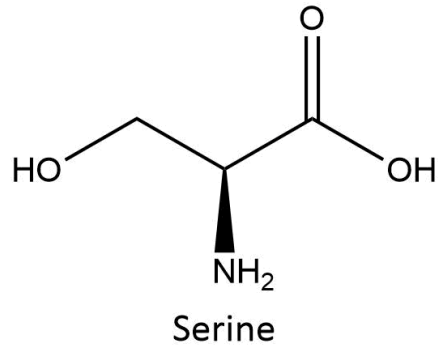


Figure 4.5. Structure of phosphoserine compared with aspartic and glutamic acids.

Chapter 5 The effect of substituting Kinesin-13 residues, crucial to microtubule end recognition, in the Kinesin-1 motor domain

5.1 Microtubule end recognition is an important feature of microtubule regulating kinesins

Microtubule end recognition is an important feature of kinesins which regulate microtubule dynamics, as discussed in chapter 1.9, whereas kinesins which are purely translocators do not need to know where the end of the microtubule is. Recognition of the microtubule end leads to long residence times at microtubule ends. For example, Eg5 is a microtubule polymerase in the Kinesin-5 family which resides at microtubule ends for 7 seconds (Chen and Hancock 2015) and the depolymerase Kip-3, a Kinesin-8, walks along the microtubule lattice before pausing at the microtubule end for tens of seconds (Varga, Leduc et al. 2009). It was recently shown that insertion of the Loop 11- α 4 region of Eg5 into a Kinesin-1, is sufficient to lead to accumulation of the kinesin at the microtubule plus ends (Chen, Cleary et al. 2019).

Previous work from this lab looking at how MCAK recognises microtubule ends has identified K524, E525 and R528 in the α 4 helix as key residues (Patel, Belsham et al. 2016). They were initially investigated because of their high degree of conservation in Kinesin-13s, while not being present in other kinesin families such as Kinesin-1 (see sequence consensus and alignment in Appendix 1). A screen was conducted assessing the depolymerisation activity

of MCAK mutants where residues that were highly conserved within, but only in, the Kinesin-13 family were mutated to alanine. The K524A, E525A and R528A mutants all showed only very slow depolymerisation activity. Next the ATPase activity of these proteins was studied and it was found that the rates of microtubule-stimulated ATPase and microtubule-stimulated mADP dissociation were decreased. The mutant proteins also show a reduced residence time at the microtubule end (0.59 ± 0.02 s, 0.59 ± 0.02 s and 0.65 ± 0.02 s for K524A, E525A and R528A respectively, compared to 2.03 ± 0.13 s for wild type), while demonstrating a comparable level of microtubule binding (k_{off} values for the microtubule lattice 2.90 ± 0.16 s⁻¹, 2.54 ± 0.22 s⁻¹, 2.81 ± 0.24 s⁻¹, 2.29 ± 0.18 s⁻¹ for wild type MCAK, K524A, E525A and R528A respectively) (Patel, Belsham et al. 2016). This suggests that modification at these sites affects the ability of MCAK to recognise microtubule ends and consequently the ends do not stimulate ADP dissociation (the rate limiting step of ATP turnover in the presence of microtubules for wild type protein (Friel and Howard 2011)). In turn, this means that ATP does not bind, preventing tight binding of MCAK at the microtubule end, which would lead to increased residency time and microtubule depolymerisation. Additionally, recent structural studies have observed K524, E525 and R528 being important for stabilising the curved conformation of tubulin at the microtubule end (Wang, Cantos-Fernandes et al. 2017).

5.2 *Identifying end binding residues*

To test whether the residues K524, E525 and R528 could induce microtubule end recognition in a kinesin that does not normally respond to the microtubule end, the equivalent amino acid substitutions have been introduced into a Kinesin-1. The modified rat KIF5C rkin430-GFP was used, which has been extensively studied (Rogers, Weiss et al. 2001, Leduc, Ruhnow et al. 2007, Walter, Beranek et al. 2012, Scharrel, Ma et al. 2014, Grover, Fischer et al. 2016, Ruhnow, Klobeta et al. 2017). Kinesin-1 is a dimeric translocating kinesin (Vale, Reese et al. 1985) unlike Kinesin-13, which is a depolymerase (Hunter, Caplow et al. 2003). Initially the residues corresponding to the MCAK residues K524, E525 and R528 had to be identified. This was achieved by two methods; the first was by sequence alignment, using the Huang and Miller algorithm (Huang and Miller 1991) shown in **Figure 5.1A**, and the second was comparison of the two structures, which are shown in **Figure 5.1B**. Residues G262, N263 and S266 in the Kinesin-1 were identified, by both methods, as corresponding to the residues K524, E525 and R528 respectively. Consequently the decision was made to make the substitutions G262K, N263E and S266R as well as a triple substitution replacing all three residues.

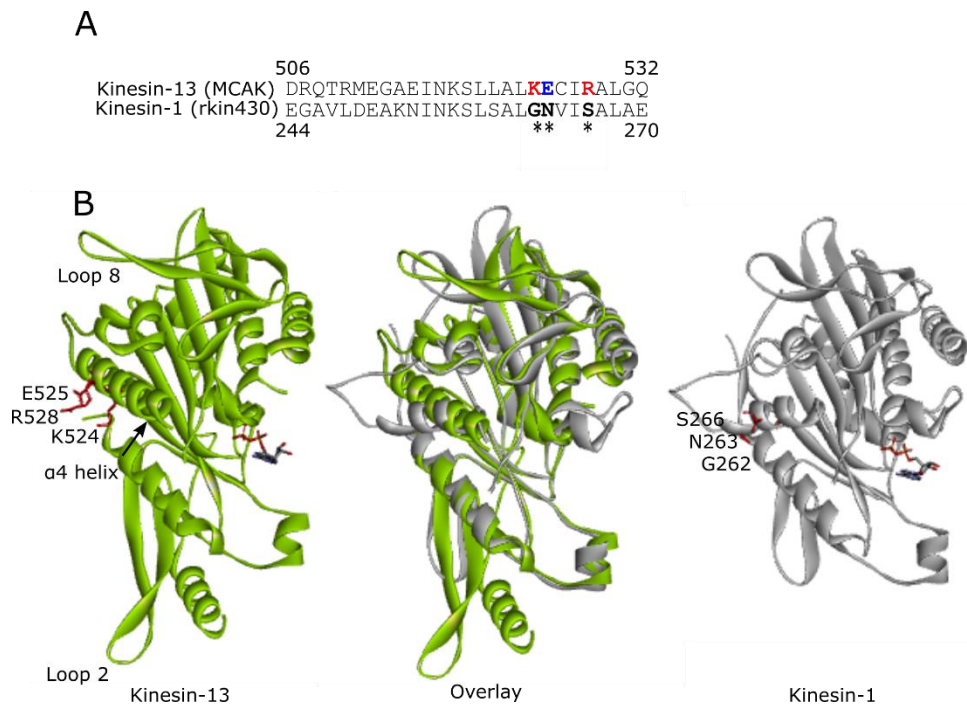


Figure 5.1. Sequence and structural alignment of Kinesin-13 and Kinesin-1.

A) Alignment of α 4 helix of Kinesin-13 (MCAK residues 506 - 532) and Kinesin-1 (rKin430 residues 244 - 270). K524, E525 and R528 in Kinesin-13 and G262, N263 and S266 in Kinesin-1 are shown in bold and coloured red for positively charged, blue for negatively charged and black for neutral. B) The structures of MCAK (*Homo sapiens*, PDB ID: 2HEH) and KIF5C (*Mus musculus*, PDB ID: 3X2T, (Morikawa, Yajima et al. 2015)) are shown separately and then the two structures were overlaid. The residues K524, E525 and R528 in MCAK and the corresponding residues G262, N263 and S266 in KIF5C are represented as sticks and highlighted in red.

5.3 Expression and purification of Kinesin-1

The rkin430-GFP construct was kindly provided by Stefan Diez, Max Plank Institute of Molecular Cell Biology and Genetics, Dresden (Leduc, Ruhnnow et al. 2007). The Kinesin-1 protein was expressed in *E.coli* BL21 cells (2.13) and

then purified by nickel affinity and anion exchange chromatography (2.14). Bacterial protein expression is faster, cheaper and simpler than expression in insect cells, but relies on the proteins being able to fold correctly without the more complex protein folding machinery available in eukaryotic cells. Attempts to express MCAK in bacteria led to the formation of insoluble inclusion bodies, and so the insect cell system was adopted instead. The results from the purification of Kinesin-1 are shown in **Figure 5.2**.

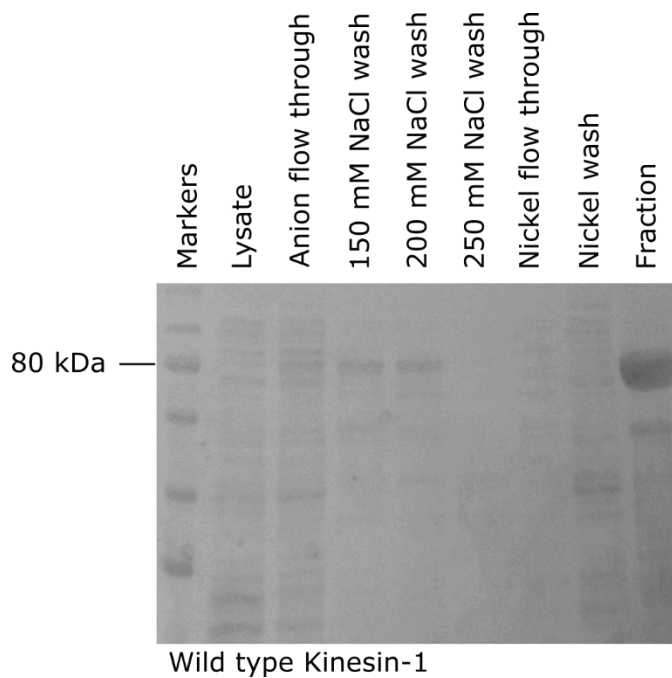


Figure 5.2. Purification of Kinesin-1. SDS-PAGE gel stained with Instant Blue of progression through purification. Lysate: Cleared cell lysate. Anion flow through: Flow through from cleared lysate applied to anion exchange column. 150-250 mM NaCl wash: Wash with 150, 200 and 250 mM NaCl. Nickel flow through: Flow through from combined 150 mM and 200 mM NaCl washes applied to Nickel affinity column. Nickel wash: 75 mM imidazole wash.

Fraction: Eluate from Nickel affinity column in 300 mM imidazole.

rKin430GFP molecular weight 75 kDa.

5.4 Kinesin-1 has a shorter end residence time than Kinesin-13

To study the effect of the mutations on Kinesin-1's interaction with the microtubule, and particularly the microtubule end, TIRF microscopy was used as described (2.15). This allowed the observation of the kinesin's translocating activity and yielded measurements of its velocity, run length and microtubule end and lattice residence times. Firstly, the velocity and run length of the kinesin-1 were measured, these were found to be 810 ± 227 nm/s and 3.06 ± 1.16 μ m respectively, which are comparable to other literature values (540 ± 140 nm/s (Korten and Diez 2008), 670 ± 140 nm/s (Grover, Fischer et al. 2016), 1089 ± 155 nm/s (Walter, Beranek et al. 2012)). The end residence time of wild type Kinesin-1 was then measured and compared to wild type Kinesin-13 (data from Chapter 3). As shown in **Figure 5.3**, Kinesin-1 has a much shorter end residence time (0.46 ± 0.01 s) compared to Kinesin-13 (2.03 ± 0.13 s). This value of end residence is consistent with that measured previously by Varga et al of 0.38 ± 0.23 s (Varga, Leduc et al. 2009). Furthermore, Kinesin-1 lacks the long end residence events that are seen with Kinesin-13; 32 % of Kinesin-13 end residence events lasted longer than 2 seconds, compared to only 3 % of Kinesin-1 events. This makes sense, as unlike microtubule regulating kinesins, which require end recognition to exert their effect on microtubule dynamics, purely translocating kinesins do not

require this function. The end residence time of Kinesin-1 is approximately 4.4-fold shorter than for Kinesin-13. It was then investigated whether the introduction of Kinesin-13 residues, shown to be important for microtubule end residence, into Kinesin-1 could increase microtubule end residence times.

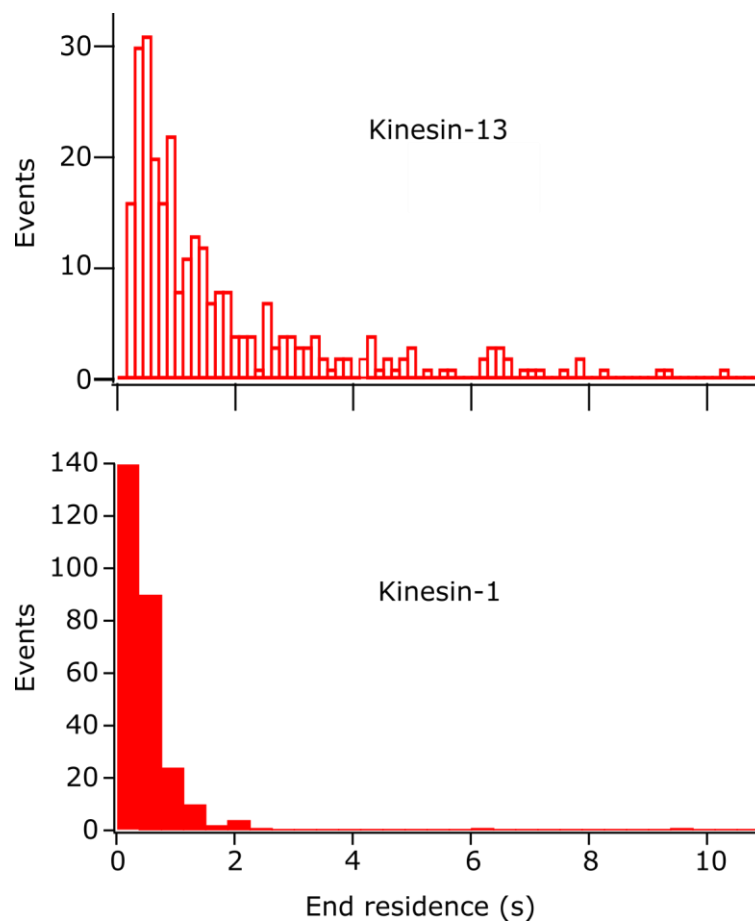


Figure 5.3. Kinesin-1 has a shorter end residence time than Kinesin-13. Histograms showing the number of events with a specific duration of end residence (Kinesin-1 $n = 273$, Kinesin-13 $n=289$) (Belsham and Friel 2019).

5.5 Expression and purification of Kinesin-1 mutants

Having established that Kinesin-1 was an appropriate candidate to use as a model for a kinesin with a short microtubule end residence, site directed

mutagenesis was used to introduce the substitutions G262K, N263E, S266R and a GNS triple mutant (as described in Section 2.1). The mutant proteins were then expressed and purified using the same method as for the wild type Kinesin-1 (2.13-2.14). The results of the purifications are shown in **Figure 5.4**.

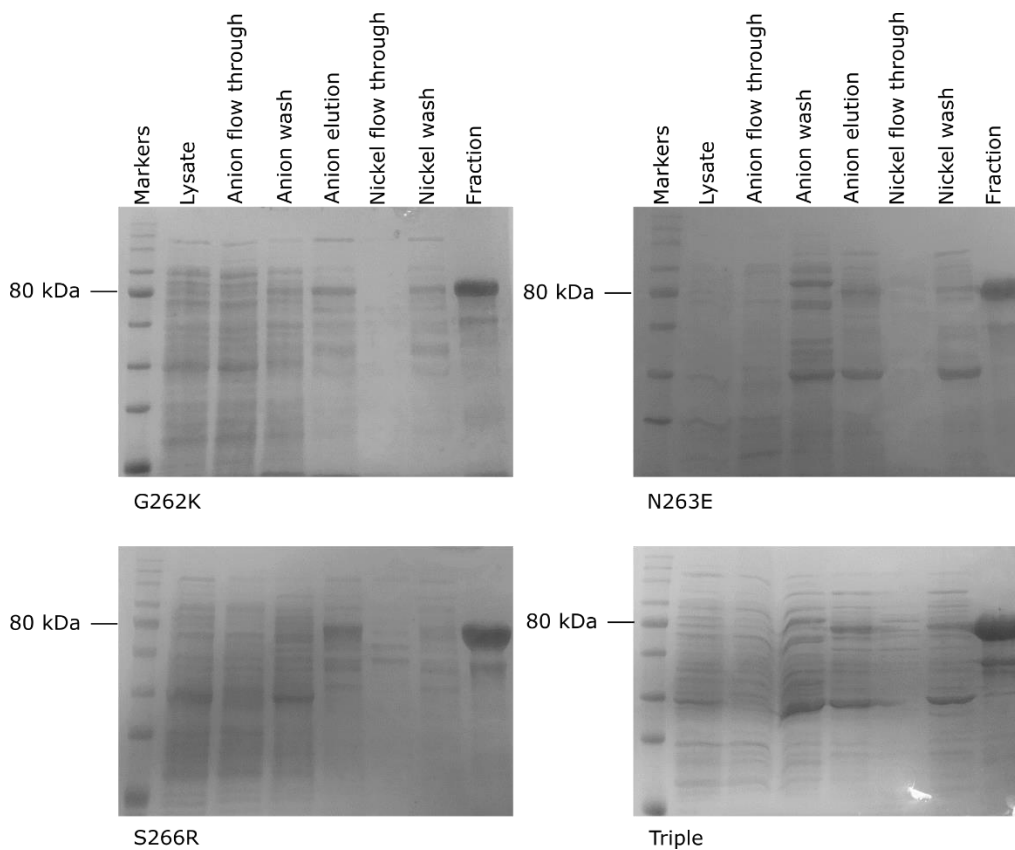


Figure 5.4 The mutant proteins G262K, N263E, S266R and a triple mutant were expressed and purified. SDS-PAGE gel stained with Instant Blue of progression through purification. Lysate: Cleared *E. coli* cell lysate. Anion flow through: Flow through from cleared lysate applied to anion exchange column. Anion wash: 100 mM NaCl wash. Anion elution: Eluate from the anion column in 200mM NaCl. Ni flow through: Flow through from anion exchange eluate applied to Nickel affinity column. Ni wash: 75 mM imidazole wash. Fraction: Eluate from Nickel affinity column in 300 mM imidazole. rKin430GFP molecular weight 75 kDa.

5.6 Introducing residues into Kinesin-1 that are important for Kinesin-13s end recognition ability, leads to increased end residence times

The end residence times of the mutant Kinesin-1 proteins were measured using TIRF microscopy (2.15) as described for the wild type protein. The distributions of end residence time are shown in **Figure 5.5B**. Cumulative distributions of this data were constructed and fitted to an exponential function (Appendix 3, A3.1) to calculate an end residence time and k_{off} for each mutant; these are shown in **Table 4**.

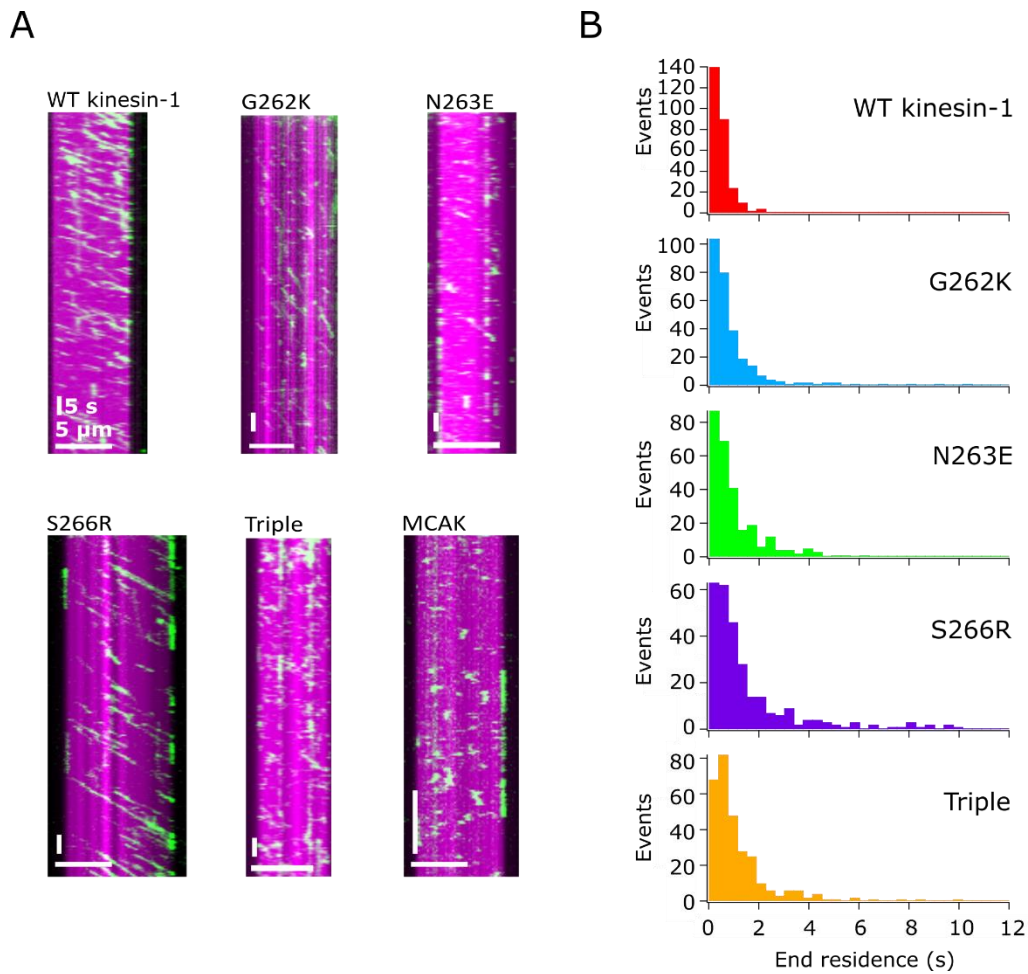


Figure 5.5. Mutant kinesin-1 proteins have a longer end residence time than wild type Kinesin-1. A) Representative kymographs showing the interaction of GFP-tagged rkin430 (green), with GMPCPP-stabilised, rhodamine labelled microtubules (magenta). B) Histograms showing the number of events with a specific duration of end residence (Kinesin-1 wild type $n = 273$, G262K $n = 285$, N263 $n = 272$, S266R $n = 284$, Triple $n = 296$) (Belsham and Friel 2019).

Table 4. The end residence time, microtubule interaction rate constants, velocities and run lengths of wild type Kinesin-1 and the mutants.

* indicates statistically significant difference from wild type

	WT	G262K	N263E	S266R	Triple
End residence (s)	0.46 ± 0.01 (n=273)	0.78 ± 0.03 (n=285)*	0.95 ± 0.03 (n=272)*	1.41 ± 0.06 (n=284)*	1.09 ± 0.03 (n=296)*
k_{off} end (s^{-1})	2.18 ± 0.03 (n=273)	1.28 ± 0.02 (n=285)*	1.05 ± 0.01 (n=272)*	0.71 ± 0.01 (n=284)*	0.92 ± 0.01 (n=296)*
k_{off} lattice (s^{-1})	0.44 ± 0.01 (n=194)	0.54 ± 0.01 (n=207)*	0.80 ± 0.02 (n=232)*	0.44 ± 0.01 (n=203)*	0.61 ± 0.02 (n=239)*
k_{on} ($\mu m^{-1} nM^{-1} s^{-1}$)	0.05 ± 0.40 (n=5)	0.11 ± 0.17 (n=4)	0.18 ± 0.16 (n=4)	0.08 ± 0.22 (n=5)	0.14 ± 0.24 (n=5)
% events translocating	48	38	25	55	23
% events diffusive	20	34	38	14	51
Velocity (nm/s)	810 ± 227 (n=382)	522 ± 237 (n=363)*	686 ± 276 (n=342)*	676 ± 179 (n=375)*	646 ± 341 (n=363)*
Run length (μm)	3.06 ± 1.16 (n=382)	1.29 ± 0.49 (n=363)*	1.05 ± 0.39 (n=342)*	1.54 ± 0.89 (n=375)*	0.92 ± 0.38 (n=363)*

The Kinesin-1 mutants all have longer end residence times than wild type and correspondingly, a decrease in the value of the dissociation rate constant k_{off} .

The distributions of end residence were assessed as being significantly different from wild type using a Kolmogorov-Smirnov test ($p < 0.0001$ for all mutants). The G262K, N263E and S266R mutants have increasingly long end residence times (1.7, 2.1 and 3.1-fold longer respectively than wild type Kinesin-1). To highlight the difference in behaviour at the microtubule end of

wild type Kinesin-1 and the S266R mutant cartoons of the kymographs are shown in **Figure 5.6**. When the S266R mutant reaches the microtubule end it stays at the microtubule end for an average of 5 frames before dissociating compared to a single frame for wild type. For all the mutants the increase in end residence time is due to an increase in the proportion of long end residence events (>2 s), rather than an increase in duration of all events, as shown in **Figure 5.5B**. These longer end residence events are characteristic of Kinesin-13 (see **Figure 5.3**). Surprisingly the triple mutant protein does not accumulate the effect of all three substitutions, but instead behaves similarly to the N263E mutant.

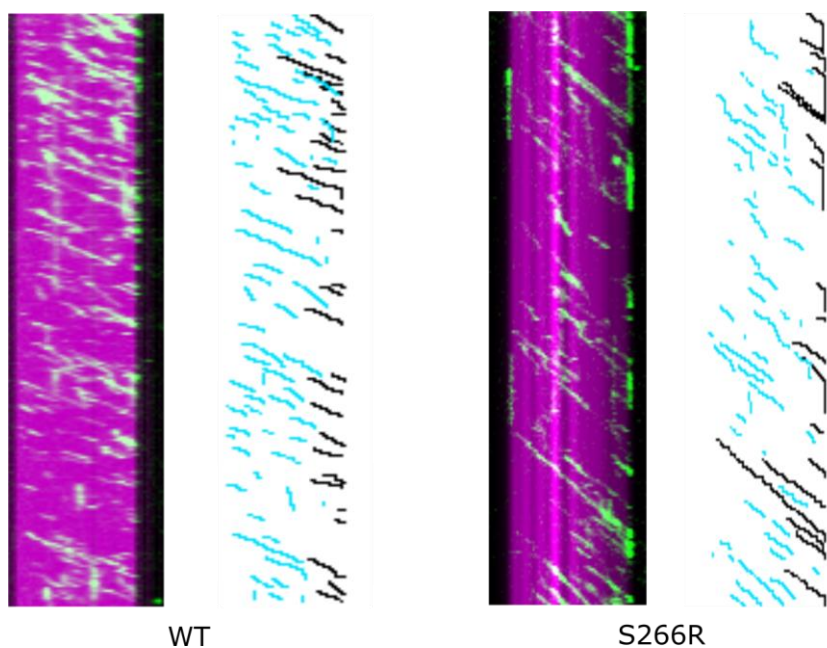


Figure 5.6. S266R stays at the microtubule end much longer than wild type Kinesin-1. Cartoon versions of kymographs of WT Kinesin-1 and S266R. Kymographs show microtubules in magenta and kinesin in green. In the cartoons events on the lattice are shown in blue and events which reach the microtubule end are shown in black (Belsham and Friel 2019).

5.7 *The increase in residence time is specific to the microtubule end*

The lattice residence times of the mutant proteins was also measured to test whether the increase in end residence time was specific to the microtubule end. As can be seen in **Figure 5.7**, the mutants actually have a decreased lattice residence time compared to wild type Kinesin-1, which shows that the increase in microtubule end residence time is specific to the microtubule end. Cumulative distributions of this data were constructed and fitted to an exponential function (Appendix 2, A2.1) to calculate k_{off} . No significant differences between the values of k_{on} were observed for the mutants and wild type Kinesin-1.

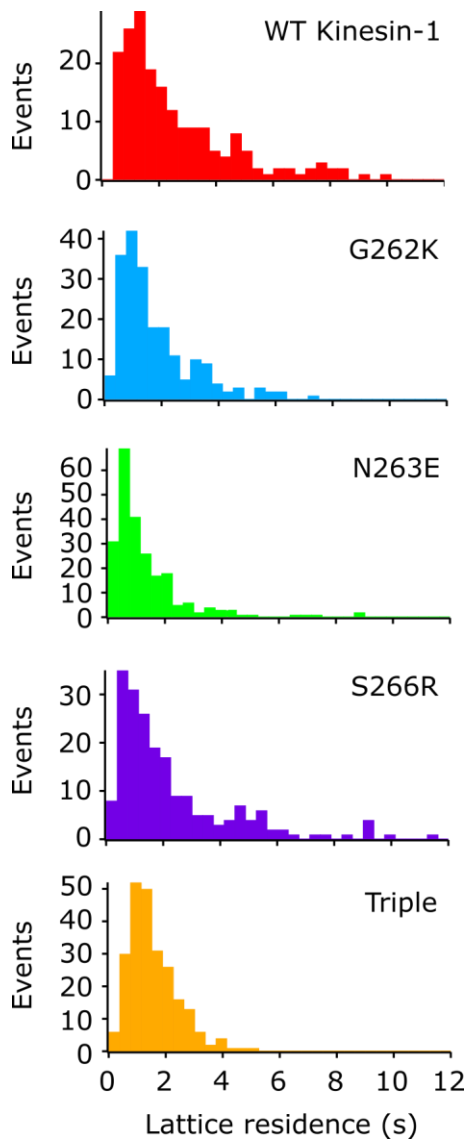


Figure 5.7. The lattice residence time for the mutant proteins is decreased compared to wild type Kinesin-1. Histograms showing the number of events with a specific duration of lattice residence (Kinesin-1 wild type $n = 194$, G262K $n = 207$, N263 $n = 232$, S266R $n = 203$, Triple $n = 239$) (Belsham and Friel 2019).

5.8 Amino acid substitutions affect translocation activity, but these changes do not correlate with the effect on end residence time

In addition to affecting the end residence time of Kinesin-1, the substitutions studied also affect other properties of the kinesin (**Figure 5.5A and Table 4**). All four mutants show decreased velocities and run lengths compared with wild type Kinesin-1. The magnitude of the observed increases in end residence time do not correlate with the magnitude of changes in velocity (**Figure 5.8**). The G262K mutant displayed the slowest velocity but the shortest end residence time of the mutants, while S266R showed the longest end residence times but one of the fastest velocities.

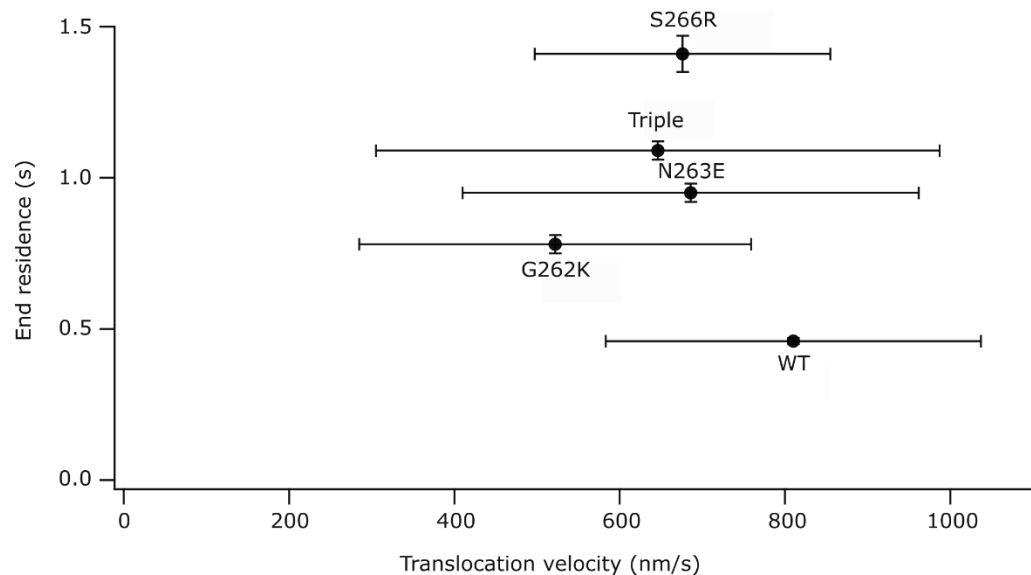


Figure 5.8. Translocation velocity does not correlate with end residence.

The end residence times of wild type Kinesin-1 and the mutants \pm s.e.m. plotted against their translocation velocity \pm s.d. (modified from (Belsham and Friel 2019)).

Of all the wild-type Kinesin-1 microtubule interaction events observed, 48 % displayed unidirectional translocating activity, 32 % of the events were too short (< 750 ms) to observe directional translocation, while the remaining 20 % showed no consistent directional movement. A smaller proportion of the G262K, N263E and triple mutant protein molecules (38, 25 and 23 % respectively) displayed translocating behaviour than for wild type Kinesin-1. Instead they have a more diffusive behaviour on the microtubule, more similar to wild type Kinesin-13 (**Figure 5.5A**). For the G262K, N263E and triple Kinesin-1 variants 34, 38 and 51% of events respectively were diffusive in nature (non-directed). However, the S266R mutant has a similar proportion of molecules displaying translocating behaviour to wild type (55 %) and only 14 % events were diffusive, despite having the greatest increase in microtubule end residence time.

5.9 An alanine mutant displays an increased end residence time compared to wild type Kinesin-1, but not as long as substitution to the equivalent Kinesin-13 residue

To test whether the effects on end residence time were a result of the gain of the Kinesin-13 residues or the loss of the Kinesin-1 residues, an S266A mutant was made, through site directed mutagenesis. The S266 residue was chosen because the S266R mutant had the largest impact on end residence time, while also retaining the most Kinesin-1-like translocation activity. The S266A

mutant was expressed and purified as with the other mutants (2.13-2.14) (Figure 5.9).

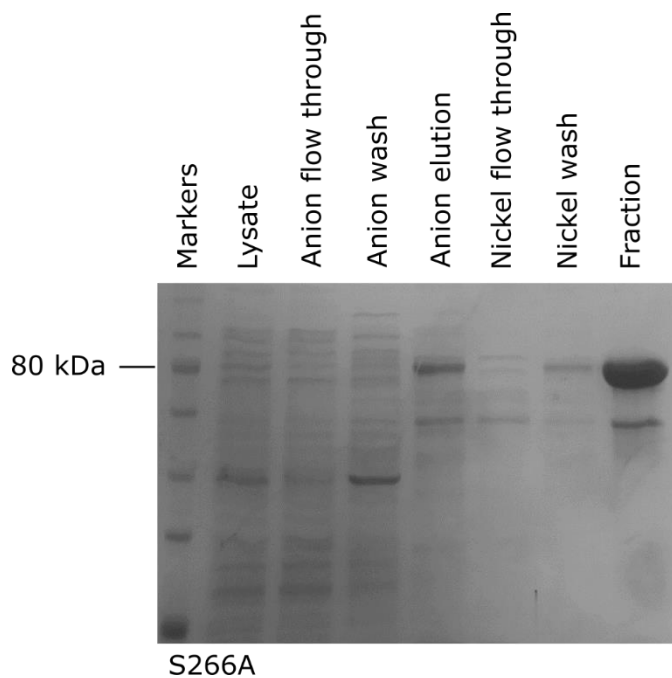


Figure 5.9. The purification of S266A. SDS-PAGE gel stained with Instant Blue of progression through purification. Lysate: Cleared cell lysate. Anion flow through: Flow through from cleared lysate applied to anion exchange column. Anion wash: 100 mM NaCl wash. Anion elution: Eluate from the anion column in 200mM NaCl. Ni flow through: Flow through from anion exchange eluate applied to Nickel affinity column; Ni wash: 75 mM imidazole wash. Fraction: Eluate from Nickel affinity column in 300 mM imidazole. rKin430GFP molecular weight 75 kDa.

The S266A mutant's interaction with microtubules was analysed by TIRF microscopy. It had a longer microtubule end residence time than wild type Kinesin-1 (0.92 ± 0.02 s, compared with 0.46 ± 0.01 s), but shorter than the S266R mutant (1.41 ± 0.06 s) (Figure 5.10). This suggests that not only are

Kinesin-13s adapted to have long end residence times, to facilitate their depolymerisation activity, but Kinesin-1s are adapted to have short end residence times. This could be advantageous as it prevents the Kinesin-1 staying unproductively at the microtubule end, and can instead dissociate and resume its translocation activity more rapidly. The Kinesin-1 residues also help the kinesin to translocate rapidly and processively along the lattice, which is advantageous for a transporter.

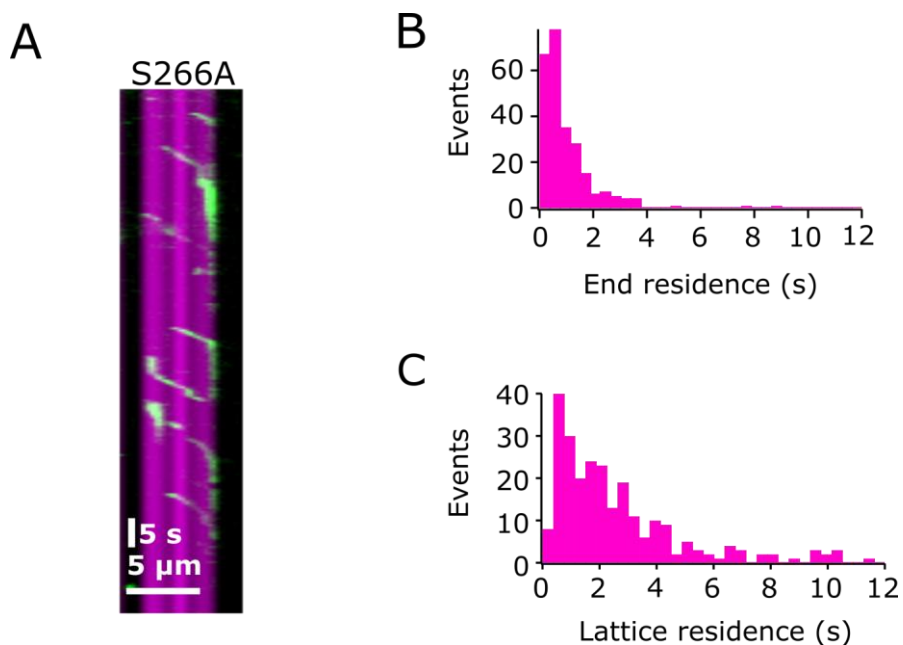


Figure 5.10. S266A has a longer end residence time than wild type Kinesin-1, but shorter than S266R. A) Representative kymographs showing the interaction of GFP-tagged rkin430S266A (green), with GMPCPP-stabilised, rhodamine labelled microtubules (magenta). B) Histograms showing the number of events with a specific duration of end residence (n = 252) C) Histograms showing the number of events with a specific duration of lattice residence (n = 249) (Belsham and Friel 2019).

Table 5. The end residence time, microtubule interaction rate constants, velocities and run lengths of S266A.

	End residence (s)	$k_{off\ end}$ (s^{-1})	$k_{off\ lattice}$ (s^{-1})	k_{on} ($\mu m^{-1} nM^{-1} s^{-1}$)	% events walking	% events diffusive	Velocity (nm/s)	Run length (μm)
S266A	0.92 \pm 0.02 (n=252)	1.09 \pm 0.01 (n=252)	0.38 \pm 0.02 (n=249)	0.06 \pm 0.28 (n=7)	30	33	548 \pm 223 (n=382)	1.48 \pm 0.99 (n=367)

5.10 Differences in mutant kinesin behaviour are not due to deficiencies in protein function

To confirm that all the different protein constructs were functional and that the differences observed in their behaviour were not, for example because of protein misfolding, ATPase assays were carried out. As shown in **Figure 5.11** no significant difference was observed in the ATPase rate of all the Kinesin-1 constructs compared to wild type (G262K p=0.6124, N263E p=0.6709, S266R p=0.6585, Triple p=0.5385, S266A p=0.1569).

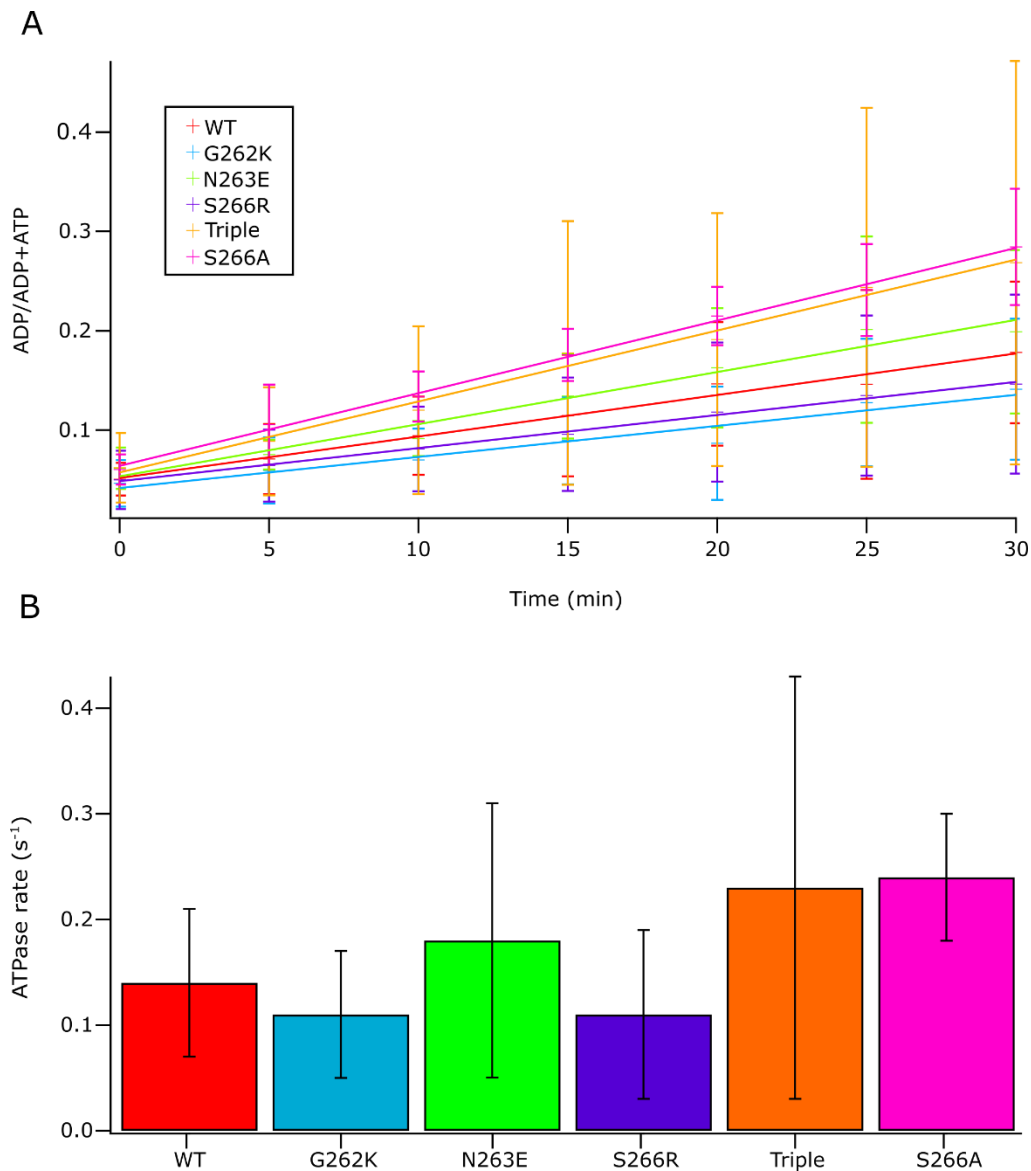


Figure 5.11. Kinesin-1 mutants show no significant difference in ATPase rate from wild type. A) The change in the fraction of ADP of total nucleotides at five minute intervals was measured using HPLC. Points are mean \pm standard deviation, $n=3$ for each protein, and a line of best fit is shown. B) The mean ATPase rate, from the gradient of the fit for each experiment \pm standard deviation is shown for each protein (Belsham and Friel 2019).

5.11 An increase in end residence time is not sufficient to promote microtubule depolymerisation

For Kinesin-13, the long microtubule end residence time, when the kinesin binds tightly to tubulin subunits near the end of the microtubule, is thought to lead to deformation of the bound tubulin, destabilising the protofilament and leading to depolymerisation. To test whether increased end residence time is sufficient to allow a Kinesin-1 to depolymerise microtubules, the wild type and mutant kinesins were incubated with GMPCPP-stabilised, rhodamine-labelled microtubules for 20 minutes in the presence of ATP. The outcome of this assay was examined using fluorescence microscopy (**Figure 5.12**).

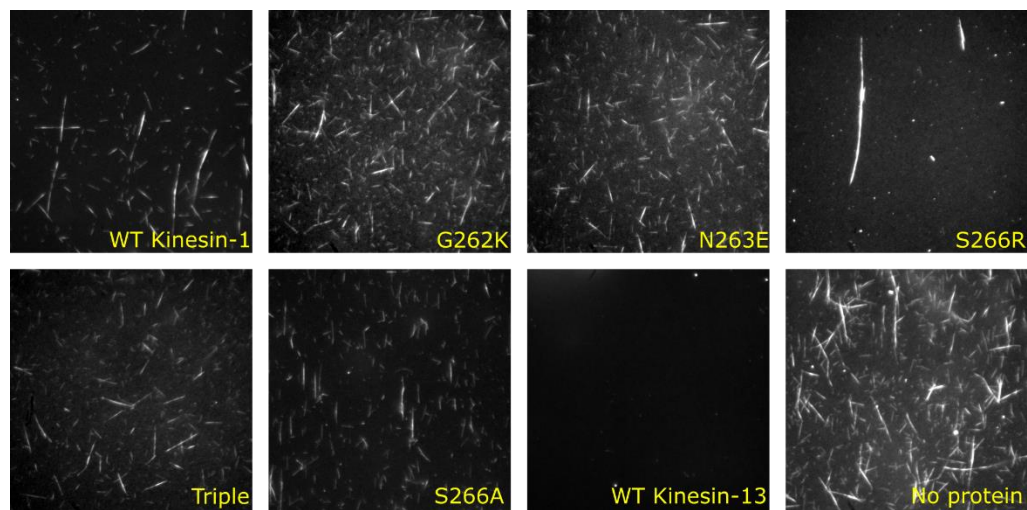


Figure 5.12 Kinesin-1 mutants cannot depolymerise microtubules. 40 nM kinesin was mixed with 0.4 μ M microtubules and 5 mM ATP and incubated for 20 minutes. The resulting microtubules were placed on poly-L-lysine coated coverslips and imaged (Belsham and Friel 2019).

None of the Kinesin-1 mutants appeared to be depolymerisation competent. However the S266R mutant did show increased microtubule bundling, which suggests it is more able to make stable contacts with multiple microtubules.

The lack of depolymerisation activity of the Kinesin-1 variants was confirmed using a light scattering assay (**Figure 5.13**). This showed that the mutant proteins, like wild type Kinesin-1, had no depolymerisation activity. This is in contrast to wild type Kinesin-13 where the amount of light scatter decreases over time as the microtubules are depolymerised.

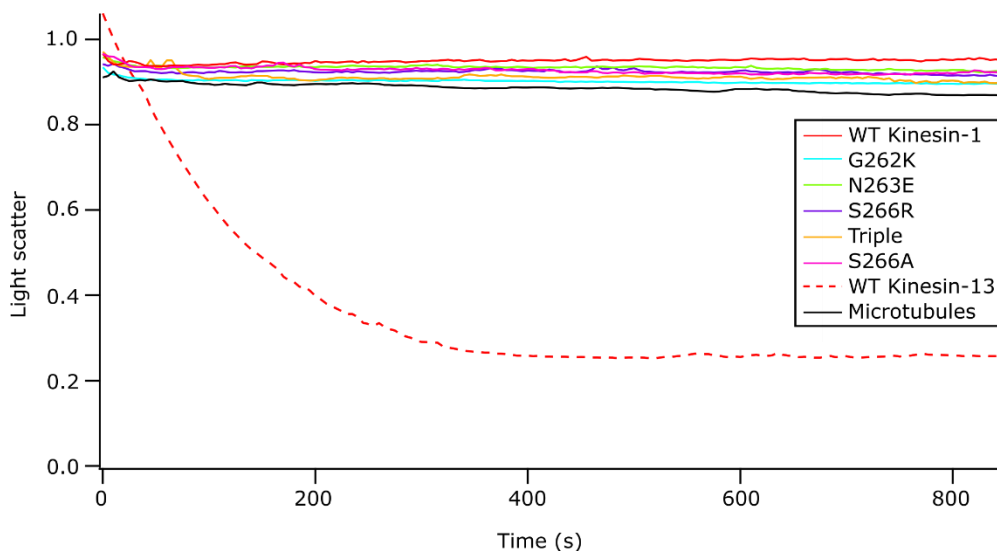


Figure 5.13. Light scattering assay shows no depolymerisation by Kinesin-1 mutants. The depolymerisation of microtubules was measured using light scattering and normalised to the average reading of microtubules over 150 seconds prior to the addition of kinesin. The curves on the graph represent the average values for 3 experiments for each protein (Belsham and Friel 2019).

5.12 Summary

The residues K524, E525 and R528 in MCAK had been identified as being important for depolymerisation, and in particular for their role in allowing MCAK to recognise the end of the microtubule. Substitution of any of these residues in MCAK to alanine leads to the loss of long end residence events - <1 % of end events lasted longer than 2 s for the mutants compared with 34 % for wild type.

Unlike Kinesin-13, when Kinesin-1 reaches the microtubule end it does not make a significant pause. However, when the Kinesin-13 residues were introduced at the positions G262, N263 and S266, identified by sequence and structural alignment to correspond to these key residues, longer end residence times, similar to those displayed by Kinesin-13, were observed. All the Kinesin-1 mutants showed microtubule end residence times that were increased between 1.7 and 3.1-fold. The side chains of lysine, glutamate and arginine found in Kinesin-13 are larger and charged compared to the side chains of glycine, asparagine and serine found in Kinesin-1. As the $\alpha 4$ helix binds at the intra-dimer groove of tubulin, the large, bulky side chains found in Kinesin-13 may help in the sensing of microtubule curvature at the end of the microtubule, triggering ADP dissociation, tight binding to the microtubule and depolymerisation.

With the G262K, N263E and triple Kinesin-1 mutants, the substitutions also affected the kinesin's interaction with the microtubule lattice. Their ability to translocate along the microtubule seemed to be increasingly impaired, and

instead they showed a more diffusive behaviour, more like MCAK. Although this was not the intended effect of introducing the mutations, it is not surprising that introducing MCAK residues at the kinesin-microtubule interface makes the kinesin's behaviour on the microtubule more like MCAK. In contrast S266R retained the ability to translocate along the microtubule, while having the largest increase in microtubule end residence time. From studying the structure of kinesin-1 on tubulin, the side chain of S266 appears orientated parallel to tubulin (see **Figure 5.14**), which may explain why when the tubulin is straight, along the microtubule lattice, the S266R mutation has little effect, but when the microtubule filaments curl at the microtubule end, the substitution has an effect.

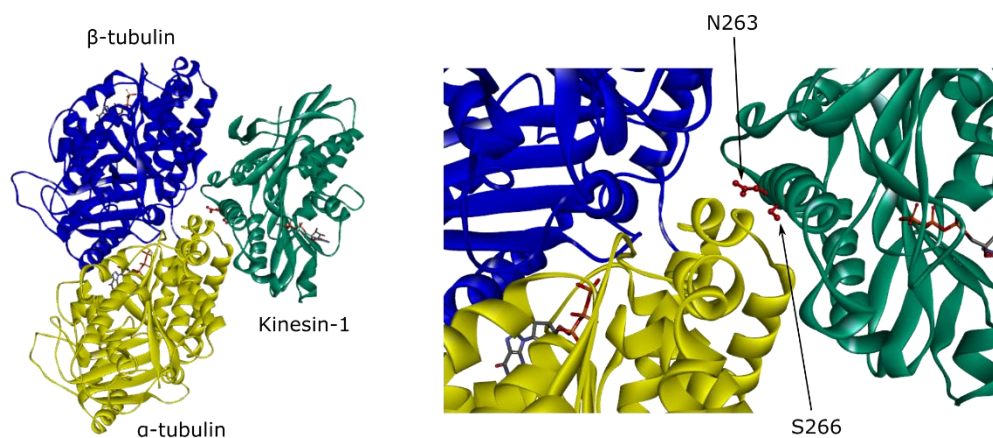


Figure 5.14. The structure of Kinesin-1 in complex with tubulin. A) Human KIF5B on a microtubule PDB ID: 3J8Y. (Shang, Zhou et al. 2014) B) Close up of the α 4 helix-tubulin interaction site.

Another interesting observation from studying the structures is that N263 points directly towards the tubulin. This may explain why N263E seems to be

the dominant mutant – the triple mutant, rather than showing an additive effect from all three changes, closely resembled the N263E mutant.

Comparing k_{off} at the microtubule end and on the microtubule lattice showed that the effects of the substitutions on microtubule end residence time are specific to the microtubule end. The mutants have larger values of k_{off} on the microtubule lattice than wild type, in contrast to at the microtubule end, where k_{off} is smaller for the mutants than wild type. The larger k_{off} lattice values for the mutants reflect that they are all poorer motors – they are slower than wild type and have shorter run lengths, in addition to a lower proportion actually translocating. We found no significant difference in k_{on} values.

The differences in velocity do not appear coupled to the difference in end residence times (**Figure 5.8**). From the velocities measured, it is possible to determine the dwell times of each mutant on a tubulin dimer given that each dimer is 8 nm in length. These range from 0.01 – 0.015 s. Even considering that each pixel is 20 dimers in length, this gives a predicted end residence time of 300 ms for the slowest mutant and all the mutants spend longer than this at the microtubule end, indeed even the wild type protein spends slightly longer on the terminal dimer than on internal dimers. This could be because it spends some time searching for the next dimer before it dissociates. The end residence time of wild type may be an over estimate as it is at the limit of our time resolution, so the difference between the wild type and the mutants may be greater than we can measure. The increase in end residence times

displayed by the Kinesin -1 mutants is insufficient for them to be able to depolymerise microtubules. This suggests that other regions of Kinesin-13s are required for their depolymerisation activity. In particular, loop 2 has been suggested to be important for the depolymerisation activity of Kinesin-13s and it would be interesting to look at whether modification of a Kinesin-1 loop 2, with or without the modification of the α 4 helix, results in the creation of a Kinesin-1 which is depolymerisation competent. A Kinesin-1 construct containing the neck, Loop 2 and Loop 11 regions of Kinesin-8 has been found to be an active microtubule depolymerase (Arellano-Santoyo, Geyer et al. 2017).

Other papers have also looked at replacing specific regions of Kinesin-1 with those of other kinesins. A recent study showed that inserting the Loop 11 – α 4 region of a microtubule polymerising Kinesin-5 into Kinesin-1 leads to accumulation at the microtubule plus ends and a decrease in velocity just as I have shown with the insertion of α 4 MCAK residues. They also found their insertion promoted microtubule nucleation, stabilisation and polymerisation (Chen, Cleary et al. 2019). The authors propose that Eg5 is involved in recognising the straight, rather than curved, form of tubulin and/or straightening the tubulin conformation. This increases the lateral bond energy, enhancing the growth rate and stabilising the microtubule against depolymerisation. This is consistent with the α 4 helix being important for sensing the tubulin curvature and shows that this can be used either to sense the curved form of tubulin, whether the tubulin is free in solution or at the

microtubule ends, or for sensing the straight form of tubulin in the microtubule lattice. The importance of the Loop 11 – α 4 region in sensing tubulin conformation was also shown by (Shima, Morikawa et al. 2018), who found that replacing the Kinesin-1 Loop 11 – α 4 region with that of a Kinesin-3 prevented the Kinesin-1 from recognising an extended form of the microtubule lattice. While these papers have been able to identify the Loop-11 – α 4 helix region as important for sensing the tubulin conformation, here we have been able to narrow this down to specific residues in Kinesin-13s.

Chapter 6 Discussion

6.1 Phosphorylation of MCAK regulates its activity through multiple distinct pathways

The activity of MCAK is determined by external regulation and by its innate structural features. While phosphorylation allows MCAK's depolymerisation activity to be adjusted on a rapid timescale, the evolution of the structural adaptations of MCAK that allow it to function as a depolymerase has taken much longer.

Phosphorylation of MCAK is known to affect MCAK's depolymerisation activity through a range of different mechanisms. At residue T537, phosphorylation by Cdk1 has been shown previously to reduce MCAK's ability to depolymerise microtubules (Sanhaji, Friel et al. 2010), and has been confirmed here (**Figure 3.3** and **Figure 3.4**). Using the phosphomimic mutant T537E it has now been demonstrated here that this effect is due to an inability to recognise the microtubule end as being distinct from the microtubule lattice. The microtubule end does not stimulate ADP dissociation by T537E and consequently the ATPase rate of T537E, in the presence of microtubules, is comparable to that in the presence of free tubulin (**Figure 3.15** and **Table 2**). The loss of long microtubule end residence events was demonstrated using TIRF microscopy, while it was apparent that lattice residence was not affected (**Figure 3.11** and **Figure 3.12**).

The phosphomimic S621D, which mimics the effect of phosphorylation of S621 by Plk1, also shows decreased depolymerisation activity in cells (Sanhaji, Ritter et al. 2014). However, this effect was not observed *in vitro* (**Figure 4.4**).

This is because phosphorylation at S621 affects MCAK's depolymerisation activity in cells by promoting MCAK's degradation (Sanhaji, Ritter et al. 2014).

It has been demonstrated elsewhere that phosphorylation at S192 decreases MCAK's depolymerisation activity by promoting the formation of the closed conformation and reducing its affinity for the microtubule (Ems-McClung, Hainline et al. 2013).

I have shown that different kinases phosphorylating different MCAK residues lead to different mechanisms of regulating MCAK's activity. These different methods of influencing MCAK's activity have differing degrees of reversibility – replacing degraded protein is more time-consuming than redistributing MCAK's localisation along a microtubule. The differences in the method of regulation may be related to the point in the cell cycle when the phosphorylation event occurs. Phosphorylation by Plk1, which can affect MCAK's degradation, occurs towards the end of mitosis, whereas the phosphorylation events at S192 and T537 occur earlier. Hence, it is useful for regulation at these sites to be highly reversible as this allows MCAK's activity to change as mitosis proceeds.

Although studies using phosphomimic mutants tell us something about how phosphorylation events at these residues might affect MCAK's activity in cells, there are limitations to these experiments. The phosphomimic mutants may

not precisely replicate the effect of phosphorylation and, in cells, the effect of phosphorylation may be modulated by other factors. The phosphomimic proteins used here only mimic phosphorylation at a single site, whereas in cells all the known kinases phosphorylate multiple residues and the phosphorylation states are dynamic through the cell cycle – there may be stages where MCAK is phosphorylated at multiple sites from the activities of multiple kinases.

6.2 The microtubule residence time of Kinesin-1 and Kinesin-13 can be modified through altering residues in the α 4 helix

MCAK's bias towards binding to the microtubule end is a key feature required for its microtubule regulating activity, that is shared by other microtubule regulating kinesins (Cui, Sproul et al. 2005, Varga, Leduc et al. 2009, Sardar, Luczak et al. 2010, Subramanian, Ti et al. 2013, Chen and Hancock 2015). Key residues in the α 4 helix of MCAK have been shown to be important for MCAK's microtubule end residence (Patel, Belsham et al. 2016) and it has now been shown that these residues are sufficient to increase the microtubule end residence time of a translocating kinesin (**Figure 5.5**). Specifically the substitutions G262K, N263E, S266R and a triple mutant (containing all 3 substitutions), all increased microtubule end residence time, by 1.7, 2.1 and 3.1-fold, respectively. The substitution S266A also led to an increase in microtubule end residence time (**Figure 5.10**), which suggests that Kinesin-1s

are specifically adapted to have a short microtubule end residence time. The increase in end residence time was not sufficient to lead to depolymerisation (**Figure 5.12** and **Figure 5.13**).

Recent work has shown that translocating movement and the diffusive movement observed with kinesins like MCAK may not be as far apart as first imagined. Kinesins have been shown to switch between processive and diffusive modes, for example for KIF18B and KIF15 (Drechsler, McHugh et al. 2014, Shin, Du et al. 2015). Additionally, it has been suggested that the 'lagging' head of Kinesin-1 does not simply detach from the microtubule and rebind at the next free dimer, but rather diffuses along the microtubule surface (Ramaiya, Roy et al. 2017). This could mean that in both translocating and regulating kinesins, the motor domains are diffusing along the microtubule in an ADP bound state. While in translocating kinesins the next available tubulin dimer is sufficient to promote nucleotide exchange and tight binding to the microtubule, in kinesins like MCAK only the conformation of tubulin at the microtubule end is able to do that.

In the context of the microtubule mutants, this suggests that with G262K, N263E and the triple mutant which show a more diffusive, rather than directional, behaviour on the microtubule lattice (**Figure 5.5**) the adjacent tubulin dimer is no longer able to promote the nucleotide exchange that allows tight binding on the lattice, characteristic of translocating kinesins. Instead, the Kinesin-13 residues allow the kinesin to interact with the tubulin in the curved conformation found at the microtubule end, leading to tight

binding and an increased end residence time. In the case of the S266R substitution, the kinesin seems to bind tightly on the lattice, allowing it to translocate processively, and also to the microtubule end, leading to long end residence times. Compared to the S266A mutant, S266R is better at binding at both locations – this may be due to electrostatic interactions between the positively charged arginine and negatively charged E-hook of tubulin. The importance of the K524, E525 and R528 residues in the $\alpha 4$ helix of MCAK for recognising the curved conformation of tubulin at the microtubule end fits with other studies. These have shown the importance of the Loop 11- $\alpha 4$ region for sensing tubulin conformation in other kinesin families, specifically Kinesin-1 (Shima, Morikawa et al. 2018), Kinesin-5 (Chen, Cleary et al. 2019) and Kinesin-8 (Arellano-Santoyo, Geyer et al. 2017). This work extends previous results by being able to identify specific residues in Kinesin-13s important for recognising the tubulin conformation.

The Kinesin-1 mutants also show something interesting about directionality of the kinesin. When the kinesin is interacting diffusively the probability of it moving towards either the plus or minus end is equal. For wild type kinesin-1 optical trapping experiments have shown that the load required for the probability of forward and backward steps to be equal is 7 pN (Nishiyama, Higuchi et al. 2002). However, the Kinesin-1 mutants here are exhibiting this behaviour under no load.

6.3 Further areas for exploration

It would be useful to look more at the ATP turnover cycles of the Kinesin-1 mutants, particularly in the presence of microtubules, as this would give more information about the nature of the interactions between the kinesin molecules and the microtubule and whether there are any changes in when nucleotide exchange is being stimulated.

Determining the minimal components of a kinesin for depolymerisation activity would also be interesting to investigate. Having established that increased end residence time alone is not sufficient to allow depolymerisation activity, it would be intriguing to look at the role of residues in loop 2 which are thought to be involved in severing the inter- and intra- protofilament bonds. This could be analysed either by introducing these residues alone, or in combination with those that give MCAK its increased microtubule end residence time, to determine whether it is possible to induce depolymerisation activity in a translocating kinesin through substituting only a small number of amino acids.

It would also be interesting to be able to modify other kinesin properties such as processivity. This might be achieved through a similar approach to that which we have used for end residence time – by comparison of the sequences of kinesins with low and high processivity, the production of a variety of mutants and then the screening of them.

6.4 Implications for cancer

High levels of MCAK have been shown to be present in several different cancer types and been linked to increased invasiveness and metastasis of tumours (Nakamura, Tanaka et al. 2007, Ishikawa, Kamohara et al. 2008, Shimo, Tanikawa et al. 2008, Gnjatic, Cao et al. 2010, Wang, Xiang et al. 2014). However, low levels of MCAK can lead to chromosomal instability – a stage of tumourigenesis (Carter, Eklund et al. 2006). In healthy cells, the amount of protein and its localisation and activity are all regulated by phosphorylation. The variety of strategies employed by the cell to do this – from proteasomal targeting to reducing end residence time – include both reversible and irreversible strategies. It may well be the case that to counteract the MCAK properties that are contributing to the development and/or progression of tumours its activity must be targeted in a reversible, location or cell cycle stage specific manner. Affecting the kinases involved would naturally produce such effects, however the kinases known to phosphorylate MCAK are involved in a large number of other cellular processes. Additionally, phosphorylation of MCAK has been shown to increase the invasiveness of tumour cells (Ritter, Sanhaji et al. 2015) which should be considered if altering MCAK's phosphorylation state.

6.5 Manipulating kinesin function for nanotechnology

Molecular motors and tracks, such as kinesins and microtubules offer exciting potential for nanotechnology. They allow the precise movement of cargo in a single, predefined direction and at a known velocity. Molecular shuttles are particularly useful for components involving transport across distances of between 100 nm and 10 μm , where fluid flow is not feasible and diffusion is not dominant. Kinesins have been shown to be able to transport nanoparticles (Muthukrishnan, Hutchins et al. 2006). However the requirement for close to physiological conditions, particularly in terms of salt and ATP concentration, temperature and pH puts fairly stringent conditions on the application of molecular motors. Molecular motors have the ability to produce order, unlike processes such as diffusion, which may allow the transport of particles in a predetermined order, which would be useful for assembly lines. The efficiency of molecular motors means that energy requirements are low. Microtubules can be aligned using reflector junctions and concentrated using a spiral (Clemmens, Hess et al. 2004) and guided along channels a few micrometres wide, due to the relative rigidity of microtubules. The microtubules can be guided using electric fields because of their negative net charge (Stracke, Bohm et al. 2002). Motor proteins can also be used to transport nanoparticles inside cells, for example for delivering gene therapy (Suh, Wirtz et al. 2003). The nanoparticles can be transported between cells and across intracellular barriers (Dalmou-Mena, del Pino et al. 2018). The ability to manipulate the properties of such motors increases their

versatility. We have shown that single amino acid modifications that can affect the microtubule end residence time and translocation efficiency of transport.

6.6 Closing remarks

In summary, this work has shown that MCAK's activity can be regulated by phosphorylation through a variety of mechanisms, with a variety of outcomes including affecting protein degradation and microtubule end binding. Additionally, residues K524, E525 and R528 in the α 4 helix, which are important for MCAK's recognition of the microtubule end, can be introduced into a different kinesin to allow it to recognise the microtubule end. To extend this work it would be interesting to look more at the ATPase cycle of the Kinesin-1 mutants, and to use similar strategies to try to find the minimal requirements for a depolymerisation competent kinesin motor domain. In the future, this work could prove useful for designing targeted cancer treatments or producing nanodevices.

Bibliography

- Andersen, S. S. (1999). "Balanced regulation of microtubule dynamics during the cell cycle: a contemporary view." Bioessays **21**(1): 53-60.
- Andrews, P. D., Y. Ovechkina, N. Morrice, M. Wagenbach, K. Duncan, L. Wordeman and J. R. Swedlow (2004). "Aurora B regulates MCAK at the mitotic centromere." Dev Cell **6**(2): 253-268.
- Appleton, P. (2011). CIL:39052, Homo sapiens, osteosarcoma. B. H. o. c. C. m. 2009., Wellcome Images. CIL.
- Arellano-Santoyo, H., E. A. Geyer, E. Stokasimov, G. Y. Chen, X. Su, W. Hancock, L. M. Rice and D. Pellman (2017). "A Tubulin Binding Switch Underlies Kip3/Kinesin-8 Depolymerase Activity." Dev Cell **42**(1): 37-51 e38.
- Asbury, C. L., A. N. Fehr and S. M. Block (2003). "Kinesin moves by an asymmetric hand-over-hand mechanism." Science **302**(5653): 2130-2134.
- Asenjo, A. B., C. Chatterjee, D. Tan, V. DePaoli, W. J. Rice, R. Diaz-Avalos, M. Silvestry and H. Sosa (2013). "Structural model for tubulin recognition and deformation by kinesin-13 microtubule depolymerases." Cell Rep **3**(3): 759-768.
- Bakhom, S. F., G. Genovese and D. A. Compton (2009). "Deviant kinetochore microtubule dynamics underlie chromosomal instability." Curr Biol **19**(22): 1937-1942.
- Bakhom, S. F., S. L. Thompson, A. L. Manning and D. A. Compton (2009). "Genome stability is ensured by temporal control of kinetochore-microtubule dynamics." Nat Cell Biol **11**(1): 27-35.
- Barnes, C. J., R. K. Vadlamudi, S. K. Mishra, R. H. Jacobson, F. Li and R. Kumar (2003). "Functional inactivation of a transcriptional corepressor by a signaling kinase." Nat Struct Biol **10**(8): 622-628.
- Belsham, H. R. and C. T. Friel (2017). "A Cdk1 phosphomimic mutant of MCAK impairs microtubule end recognition." PeerJ **5**: e4034.
- Belsham, H. R. and C. T. Friel (2019). "Identification of key residues that regulate the interaction of kinesins with microtubule ends." Cytoskeleton (Hoboken) **76**(7-8): 440-446.
- Benoit, M., A. B. Asenjo and H. Sosa (2018). "Cryo-EM reveals the structural basis of microtubule depolymerization by kinesin-13s." Nat Commun **9**(1): 1662.
- Blangy, A., H. A. Lane, P. d'Herin, M. Harper, M. Kress and E. A. Nigg (1995). "Phosphorylation by p34cdc2 regulates spindle association of human Eg5, a kinesin-related motor essential for bipolar spindle formation in vivo." Cell **83**(7): 1159-1169.
- Blocker, A., F. F. Severin, J. K. Burkhardt, J. B. Bingham, H. Yu, J. C. Olivo, T. A. Schroer, A. A. Hyman and G. Griffiths (1997). "Molecular requirements for bi-

directional movement of phagosomes along microtubules." J Cell Biol **137**(1): 113-129.

Bloom, G. S., M. C. Wagner, K. K. Pfister and S. T. Brady (1988). "Native structure and physical properties of bovine brain kinesin and identification of the ATP-binding subunit polypeptide." Biochemistry **27**(9): 3409-3416.

Bowman, A. B., A. Kamal, B. W. Ritchings, A. V. Philp, M. McGrail, J. G. Gindhart and L. S. Goldstein (2000). "Kinesin-dependent axonal transport is mediated by the sunday driver (SYD) protein." Cell **103**(4): 583-594.

Braun, A., K. Dang, F. Buslig, M. A. Baird, M. W. Davidson, C. M. Waterman and K. A. Myers (2014). "Rac1 and Aurora A regulate MCAK to polarize microtubule growth in migrating endothelial cells." J Cell Biol **206**(1): 97-112.

Bringmann, H., G. Skiniotis, A. Spilker, S. Kandels-Lewis, I. Vernos and T. Surrey (2004). "A kinesin-like motor inhibits microtubule dynamic instability." Science **303**(5663): 1519-1522.

Brouhard, G. J., J. H. Stear, T. L. Noetzel, J. Al-Bassam, K. Kinoshita, S. C. Harrison, J. Howard and A. A. Hyman (2008). "XMAP215 is a processive microtubule polymerase." Cell **132**(1): 79-88.

Burgess, S. A., M. L. Walker, H. Sakakibara, P. J. Knight and K. Oiwa (2003). "Dynein structure and power stroke." Nature **421**(6924): 715-718.

Burns, K. M., M. Wagenbach, L. Wordeman and D. C. Schriemer (2014). "Nucleotide exchange in dimeric MCAK induces longitudinal and lateral stress at microtubule ends to support depolymerization." Structure **22**(8): 1173-1183.

Busson, S., D. Dujardin, A. Moreau, J. Dompierre and J. R. De Mey (1998). "Dynein and dynactin are localized to astral microtubules and at cortical sites in mitotic epithelial cells." Curr Biol **8**(9): 541-544.

Byrd, D. T., M. Kawasaki, M. Walcoff, N. Hisamoto, K. Matsumoto and Y. Jin (2001). "UNC-16, a JNK-signaling scaffold protein, regulates vesicle transport in *C. elegans*." Neuron **32**(5): 787-800.

Carlsson, L., L. E. Nystrom, I. Sundkvist, F. Markey and U. Lindberg (1977). "Actin polymerizability is influenced by profilin, a low molecular weight protein in non-muscle cells." J Mol Biol **115**(3): 465-483.

Carmena, M., M. G. Riparbelli, G. Minestrini, A. M. Tavares, R. Adams, G. Callaini and D. M. Glover (1998). "Drosophila polo kinase is required for cytokinesis." J Cell Biol **143**(3): 659-671.

Carter, S. L., A. C. Eklund, I. S. Kohane, L. N. Harris and Z. Szallasi (2006). "A signature of chromosomal instability inferred from gene expression profiles predicts clinical outcome in multiple human cancers." Nat Genet **38**(9): 1043-1048.

Castoldi, M. and A. V. Popov (2003). "Purification of brain tubulin through two cycles of polymerization-depolymerization in a high-molarity buffer." Protein Expr Purif **32**(1): 83-88.

Chen, G. Y., J. M. Cleary, A. B. Asenjo, Y. Chen, J. A. Mascaro, D. F. J. Arginteanu, H. Sosa and W. O. Hancock (2019). "Kinesin-5 Promotes Microtubule Nucleation and Assembly by Stabilizing a Lattice-Competent Conformation of Tubulin." Curr Biol.
Chen, Y. and W. O. Hancock (2015). "Kinesin-5 is a microtubule polymerase." Nat Commun **6**: 8160.

Chretien, D. and R. H. Wade (1991). "New data on the microtubule surface lattice." Biol Cell **71**(1-2): 161-174.

Clemmens, J., H. Hess, R. Doot, C. M. Matzke, G. D. Bachand and V. Vogel (2004). "Motor-protein "roundabouts": Microtubules moving on kinesin-coated tracks through engineered networks." Lab on a Chip **4**(2): 83-86.

Connolly, A. A., K. Sugioka, C. H. Chuang, J. B. Lowry and B. Bowerman (2015). "KLP-7 acts through the Ndc80 complex to limit pole number in *C. elegans* oocyte meiotic spindle assembly." J Cell Biol **210**(6): 917-932.

Cooper, J. R., M. Wagenbach, C. L. Asbury and L. Wordeman (2010). "Catalysis of the microtubule on-rate is the major parameter regulating the depolymerase activity of MCAK." Nat Struct Mol Biol **17**(1): 77-82.

Cowley, D. O., J. A. Rivera-Perez, M. Schliekelman, Y. J. He, T. G. Oliver, L. Lu, R. O'Quinn, E. D. Salmon, T. Magnuson and T. Van Dyke (2009). "Aurora-A kinase is essential for bipolar spindle formation and early development." Mol Cell Biol **29**(4): 1059-1071.

Cui, W., L. R. Sproul, S. M. Gustafson, H. J. Matthies, S. P. Gilbert and R. S. Hawley (2005). "Drosophila Nod protein binds preferentially to the plus ends of microtubules and promotes microtubule polymerization in vitro." Mol Biol Cell **16**(11): 5400-5409.

Dalmáu-Mena, I., P. del Pino, B. Pelaz, M. A. Cuesta-Geijo, I. Galindo, M. Moros, J. M. de la Fuente and C. Alonso (2018). "Nanoparticles engineered to bind cellular motors for efficient delivery." Journal of Nanobiotechnology **16**: 33.

Decarreau, J., M. Wagenbach, E. Lynch, A. R. Halpern, J. C. Vaughan, J. Kollman and L. Wordeman (2017). "The tetrameric kinesin Kif25 suppresses pre-mitotic centrosome separation to establish proper spindle orientation." Nat Cell Biol **19**(4): 384-390.

Desai, A. and T. J. Mitchison (1998). "Preparation and characterization of caged fluorescein tubulin." Methods Enzymol **298**: 125-132.

Desai, A., S. Verma, T. J. Mitchison and C. E. Walczak (1999). "Kin I kinesins are microtubule-destabilizing enzymes." Cell **96**(1): 69-78.

Drechsler, H. and A. D. McAinsh (2016). "Kinesin-12 motors cooperate to suppress microtubule catastrophes and drive the formation of parallel microtubule bundles." Proc Natl Acad Sci U S A **113**(12): E1635-1644.

Drechsler, H., T. McHugh, M. R. Singleton, N. J. Carter and A. D. McAinsh (2014). "The Kinesin-12 Kif15 is a processive track-switching tetramer." Elife **3**: e01724.

Driskell, O. J., A. Mironov, V. J. Allan and P. G. Woodman (2007). "Dynein is required for receptor sorting and the morphogenesis of early endosomes." Nat Cell Biol **9**(1): 113-120.

Du, Y., C. A. English and R. Ohi (2010). "The kinesin-8 Kif18A dampens microtubule plus-end dynamics." Curr Biol **20**(4): 374-380.

Dujardin, D. L., L. E. Barnhart, S. A. Stehman, E. R. Gomes, G. G. Gundersen and R. B. Vallee (2003). "A role for cytoplasmic dynein and LIS1 in directed cell movement." J Cell Biol **163**(6): 1205-1211.

Ems-McClung, S. C., S. G. Hainline, J. Devare, H. Zong, S. Cai, S. K. Carnes, S. L. Shaw and C. E. Walczak (2013). "Aurora B Inhibits MCAK Activity through a Phosphoconformational Switch that Reduces Microtubule Association." Curr Biol **23**(24): 2491-2499.

Ems-McClung, S. C., K. M. Hertzler, X. Zhang, M. W. Miller and C. E. Walczak (2007). "The interplay of the N- and C-terminal domains of MCAK control microtubule depolymerization activity and spindle assembly." Mol Biol Cell **18**(1): 282-294.

Ems-McClung, S. C. and C. E. Walczak (2010). "Kinesin-13s in mitosis: Key players in the spatial and temporal organization of spindle microtubules." Semin Cell Dev Biol **21**(3): 276-282.

Evans, K. J., E. R. Gomes, S. M. Reisenweber, G. G. Gundersen and B. P. Lauring (2005). "Linking axonal degeneration to microtubule remodeling by Spastin-mediated microtubule severing." J Cell Biol **168**(4): 599-606.

Faulkner, N. E., D. L. Dujardin, C. Y. Tai, K. T. Vaughan, C. B. O'Connell, Y. Wang and R. B. Vallee (2000). "A role for the lissencephaly gene LIS1 in mitosis and cytoplasmic dynein function." Nat Cell Biol **2**(11): 784-791.

Feldman, M. E., B. Apsel, A. Uotila, R. Loewith, Z. A. Knight, D. Ruggero and K. M. Shokat (2009). "Active-site inhibitors of mTOR target rapamycin-resistant outputs of mTORC1 and mTORC2." PLoS Biol **7**(2): e38.

Friel, C. T. and J. Howard (2011). "The kinesin-13 MCAK has an unconventional ATPase cycle adapted for microtubule depolymerization." EMBO J **30**(19): 3928-3939.

Galisteo, M. L., J. Chernoff, Y. C. Su, E. Y. Skolnik and J. Schlessinger (1996). "The adaptor protein Nck links receptor tyrosine kinases with the serine-threonine kinase Pak1." J Biol Chem **271**(35): 20997-21000.

Ganem, N. J. and D. A. Compton (2004). "The KinI kinesin Kif2a is required for bipolar spindle assembly through a functional relationship with MCAK." J Cell Biol **166**(4): 473-478.

- Ganem, N. J., K. Upton and D. A. Compton (2005). "Efficient mitosis in human cells lacking poleward microtubule flux." Curr Biol **15**(20): 1827-1832.
- Ganguly, A., H. Yang and F. Cabral (2011). "Overexpression of mitotic centromere-associated Kinesin stimulates microtubule detachment and confers resistance to paclitaxel." Mol Cancer Ther **10**(6): 929-937.
- Gard, D. L. and M. W. Kirschner (1987). "A microtubule-associated protein from *Xenopus* eggs that specifically promotes assembly at the plus-end." J Cell Biol **105**(5): 2203-2215.
- Gardner, M. K., M. Zanic, C. Gell, V. Bormuth and J. Howard (2011). "Depolymerizing kinesins Kip3 and MCAK shape cellular microtubule architecture by differential control of catastrophe." Cell **147**(5): 1092-1103.
- Gibbons, I. R. and A. J. Rowe (1965). "Dynein: A Protein with Adenosine Triphosphatase Activity from Cilia." Science **149**(3682): 424-426.
- Gnjatic, S., Y. Cao, U. Reichelt, E. F. Yekebas, C. Nolker, A. H. Marx, A. Erbersdobler, H. Nishikawa, Y. Hildebrandt, K. Bartels, C. Horn, T. Stahl, I. Gout, V. Filonenko, K. L. Ling, V. Cerundolo, T. Luetkens, G. Ritter, K. Friedrichs, R. Leuwer, S. Hegewisch-Becker, J. R. Izbicki, C. Bokemeyer, L. J. Old and D. Atanackovic (2010). "NY-CO-58/KIF2C is overexpressed in a variety of solid tumors and induces frequent T cell responses in patients with colorectal cancer." Int J Cancer **127**(2): 381-393.
- Grover, R., J. Fischer, F. W. Schwarz, W. J. Walter, P. Schwille and S. Diez (2016). "Transport efficiency of membrane-anchored kinesin-1 motors depends on motor density and diffusivity." Proc Natl Acad Sci U S A **113**(46): E7185-E7193.
- Gwon, M. R., J. H. Cho and J. R. Kim (2012). "Mitotic centromere-associated kinase (MCAK/Kif2C) regulates cellular senescence in human primary cells through a p53-dependent pathway." FEBS Lett **586**(23): 4148-4156.
- Hackney, D. D. (1988). "Kinesin ATPase: rate-limiting ADP release." Proc Natl Acad Sci U S A **85**(17): 6314-6318.
- Hackney, D. D. (1994). "Evidence for alternating head catalysis by kinesin during microtubule-stimulated ATP hydrolysis." Proc Natl Acad Sci U S A **91**(15): 6865-6869.
- Hancock, W. O. and J. Howard (1999). "Kinesin's processivity results from mechanical and chemical coordination between the ATP hydrolysis cycles of the two motor domains." Proc Natl Acad Sci U S A **96**(23): 13147-13152.
- Hannak, E., M. Kirkham, A. A. Hyman and K. Oegema (2001). "Aurora-A kinase is required for centrosome maturation in *Caenorhabditis elegans*." J Cell Biol **155**(7): 1109-1116.
- Hartman, J. J., J. Mahr, K. McNally, K. Okawa, A. Iwamatsu, S. Thomas, S. Cheesman, J. Heuser, R. D. Vale and F. J. McNally (1998). "Katanin, a microtubule-severing protein, is a novel AAA ATPase that targets to the centrosome using a WD40-containing subunit." Cell **93**(2): 277-287.

Hauf, S., R. W. Cole, S. LaTerra, C. Zimmer, G. Schnapp, R. Walter, A. Heckel, J. van Meel, C. L. Rieder and J. M. Peters (2003). "The small molecule Hesperadin reveals a role for Aurora B in correcting kinetochore-microtubule attachment and in maintaining the spindle assembly checkpoint." J Cell Biol **161**(2): 281-294.

Helenius, J., G. Brouhard, Y. Kalaidzidis, S. Diez and J. Howard (2006). "The depolymerizing kinesin MCAK uses lattice diffusion to rapidly target microtubule ends." Nature **441**(7089): 115-119.

Hertzer, K. M., S. C. Ems-McClung, S. L. Kline-Smith, T. G. Lipkin, S. P. Gilbert and C. E. Walczak (2006). "Full-length dimeric MCAK is a more efficient microtubule depolymerase than minimal domain monomeric MCAK." Mol Biol Cell **17**(2): 700-710.

Hibbel, A., A. Bogdanova, M. Mahamdeh, A. Jannasch, M. Storch, E. Schaffer, D. Liakopoulos and J. Howard (2015). "Kinesin Kip2 enhances microtubule growth in vitro through length-dependent feedback on polymerization and catastrophe." Elife **4**: e10542.

Hirota, T., N. Kunitoku, T. Sasayama, T. Marumoto, D. Zhang, M. Nitta, K. Hatakeyama and H. Saya (2003). "Aurora-A and an interacting activator, the LIM protein Ajuba, are required for mitotic commitment in human cells." Cell **114**(5): 585-598.

Honnappa, S., S. M. Gouveia, A. Weisbrich, F. F. Damberger, N. S. Bhavesh, H. Jawhari, I. Grigoriev, F. J. van Rijssel, R. M. Buey, A. Lawera, I. Jelesarov, F. K. Winkler, K. Wuthrich, A. Akhmanova and M. O. Steinmetz (2009). "An EB1-binding motif acts as a microtubule tip localization signal." Cell **138**(2): 366-376.

Hood, E. A., A. N. Kettenbach, S. A. Gerber and D. A. Compton (2012). "Plk1 regulates the kinesin-13 protein Kif2b to promote faithful chromosome segregation." Mol Biol Cell **23**(12): 2264-2274.

Howell, B. J., B. F. McEwen, J. C. Canman, D. B. Hoffman, E. M. Farrar, C. L. Rieder and E. D. Salmon (2001). "Cytoplasmic dynein/dynactin drives kinetochore protein transport to the spindle poles and has a role in mitotic spindle checkpoint inactivation." J Cell Biol **155**(7): 1159-1172.

Hu, C. K., M. Coughlin, C. M. Field and T. J. Mitchison (2011). "KIF4 regulates midzone length during cytokinesis." Curr Biol **21**(10): 815-824.

Huang, X. Q. and W. Miller (1991). "A Time-Efficient, Linear-Space Local Similarity Algorithm." Advances in Applied Mathematics **12**(3): 337-357.

Hunter, A. W., M. Caplow, D. L. Coy, W. O. Hancock, S. Diez, L. Wordeman and J. Howard (2003). "The kinesin-related protein MCAK is a microtubule depolymerase that forms an ATP-hydrolyzing complex at microtubule ends." Mol Cell **11**(2): 445-457.

Hyman, A. A., D. Chretien, I. Arnal and R. H. Wade (1995). "Structural changes accompanying GTP hydrolysis in microtubules: information from a slowly

hydrolyzable analogue guanylyl-(alpha,beta)-methylene-diphosphonate." J Cell Biol **128**(1-2): 117-125.

Hyman, A. A., S. Salser, D. N. Drechsel, N. Unwin and T. J. Mitchison (1992). "Role of GTP hydrolysis in microtubule dynamics: information from a slowly hydrolyzable analogue, GMPCPP." Mol Biol Cell **3**(10): 1155-1167.

Inoue, H., H. Nojima and H. Okayama (1990). "High efficiency transformation of Escherichia coli with plasmids." Gene **96**(1): 23-28.

Ishikawa, K., Y. Kamohara, F. Tanaka, N. Haraguchi, K. Mimori, H. Inoue and M. Mori (2008). "Mitotic centromere-associated kinesin is a novel marker for prognosis and lymph node metastasis in colorectal cancer." Br J Cancer **98**(11): 1824-1829.

Jaqaman, K., E. M. King, A. C. Amaro, J. R. Winter, J. F. Dorn, H. L. Elliott, N. McHedlishvili, S. E. McClelland, I. M. Porter, M. Posch, A. Toso, G. Danuser, A. D. McAinsh, P. Meraldi and J. R. Swedlow (2010). "Kinetochore alignment within the metaphase plate is regulated by centromere stiffness and microtubule depolymerases." J Cell Biol **188**(5): 665-679.

Jeppesen, G. M. and J. K. Hoerber (2012). "The mechanical properties of kinesin-1: a holistic approach." Biochem Soc Trans **40**(2): 438-443.

Jordens, I., M. Fernandez-Borja, M. Marsman, S. Dusseljee, L. Janssen, J. Calafat, H. Janssen, R. Wubbolts and J. Neefjes (2001). "The Rab7 effector protein RILP controls lysosomal transport by inducing the recruitment of dynein-dynactin motors." Curr Biol **11**(21): 1680-1685.

Jun, D. Y., J. Y. Lee, H. S. Park, Y. H. Lee and Y. H. Kim (2017). "Tumor suppressor protein p53-mediated repression of human mitotic centromere-associated kinesin gene expression is exerted via down-regulation of Sp1 level." PLoS One **12**(12): e0189698.

Kaitna, S., M. Mendoza, V. Jantsch-Plunger and M. Glotzer (2000). "Incenp and an aurora-like kinase form a complex essential for chromosome segregation and efficient completion of cytokinesis." Curr Biol **10**(19): 1172-1181.

Kanai, Y., N. Dohmae and N. Hirokawa (2004). "Kinesin transports RNA: isolation and characterization of an RNA-transporting granule." Neuron **43**(4): 513-525.

Kanai, Y., Y. Okada, Y. Tanaka, A. Harada, S. Terada and N. Hirokawa (2000). "KIF5C, a novel neuronal kinesin enriched in motor neurons." J Neurosci **20**(17): 6374-6384.

Kim, S., K. Lee, J. H. Choi, N. Ringstad and B. D. Dynlacht (2015). "Nek2 activation of Kif24 ensures cilium disassembly during the cell cycle." Nat Commun **6**: 8087.

Kimura, K., M. Hirano, R. Kobayashi and T. Hirano (1998). "Phosphorylation and activation of 13S condensin by Cdc2 in vitro." Science **282**(5388): 487-490.

King, S. M. (2000). "AAA domains and organization of the dynein motor unit." J Cell Sci **113** (Pt 14): 2521-2526.

Kline-Smith, S. L., A. Khodjakov, P. Hergert and C. E. Walczak (2004). "Depletion of centromeric MCAK leads to chromosome congression and segregation defects due to improper kinetochore attachments." Mol Biol Cell **15**(3): 1146-1159.

Kobayashi, T., W. Y. Tsang, J. Li, W. Lane and B. D. Dynlacht (2011). "Centriolar kinesin Kif24 interacts with CP110 to remodel microtubules and regulate ciliogenesis." Cell **145**(6): 914-925.

Komarova, Y. A., A. S. Akhmanova, S. Kojima, N. Galjart and G. G. Borisy (2002). "Cytoplasmic linker proteins promote microtubule rescue in vivo." J Cell Biol **159**(4): 589-599.

Korten, T. and S. Diez (2008). "Setting up roadblocks for kinesin-1: mechanism for the selective speed control of cargo carrying microtubules." Lab Chip **8**(9): 1441-1447.

Kotani, S., S. Tugendreich, M. Fujii, P. M. Jorgensen, N. Watanabe, C. Hoog, P. Hieter and K. Todokoro (1998). "PKA and MPF-activated polo-like kinase regulate anaphase-promoting complex activity and mitosis progression." Mol Cell **1**(3): 371-380.

Kull, F. J., E. P. Sablin, R. Lau, R. J. Fletterick and R. D. Vale (1996). "Crystal structure of the kinesin motor domain reveals a structural similarity to myosin." Nature **380**(6574): 550-555.

Kumagai, A. and W. G. Dunphy (1996). "Purification and molecular cloning of Plx1, a Cdc25-regulatory kinase from *Xenopus* egg extracts." Science **273**(5280): 1377-1380.

Kumar, A., V. Rajendran, R. Sethumadhavan and R. Purohit (2013). "Evidence of colorectal cancer-associated mutation in MCAK: a computational report." Cell Biochem Biophys **67**(3): 837-851.

Kunitoku, N., T. Sasayama, T. Marumoto, D. Zhang, S. Honda, O. Kobayashi, K. Hatakeyama, Y. Ushio, H. Saya and T. Hirota (2003). "CENP-A phosphorylation by Aurora-A in prophase is required for enrichment of Aurora-B at inner centromeres and for kinetochore function." Dev Cell **5**(6): 853-864.

Kural, C., H. Kim, S. Syed, G. Goshima, V. I. Gelfand and P. R. Selvin (2005). "Kinesin and dynein move a peroxisome in vivo: a tug-of-war or coordinated movement?" Science **308**(5727): 1469-1472.

Lan, W., X. Zhang, S. L. Kline-Smith, S. E. Rosasco, G. A. Barrett-Wilt, J. Shabanowitz, D. F. Hunt, C. E. Walczak and P. T. Stukenberg (2004). "Aurora B phosphorylates centromeric MCAK and regulates its localization and microtubule depolymerization activity." Curr Biol **14**(4): 273-286.

Lane, H. A. and E. A. Nigg (1996). "Antibody microinjection reveals an essential role for human polo-like kinase 1 (Plk1) in the functional maturation of mitotic centrosomes." J Cell Biol **135**(6 Pt 2): 1701-1713.

Lawrence, C. J., R. K. Dawe, K. R. Christie, D. W. Cleveland, S. C. Dawson, S. A. Endow, L. S. Goldstein, H. V. Goodson, N. Hirokawa, J. Howard, R. L. Malmberg, J. R.

- McIntosh, H. Miki, T. J. Mitchison, Y. Okada, A. S. Reddy, W. M. Saxton, M. Schliwa, J. M. Scholey, R. D. Vale, C. E. Walczak and L. Wordeman (2004). "A standardized kinesin nomenclature." J Cell Biol **167**(1): 19-22.
- Leduc, C., F. Ruhnow, J. Howard and S. Diez (2007). "Detection of fractional steps in cargo movement by the collective operation of kinesin-1 motors." Proc Natl Acad Sci U S A **104**(26): 10847-10852.
- Lipp, J. J., T. Hirota, I. Poser and J. M. Peters (2007). "Aurora B controls the association of condensin I but not condensin II with mitotic chromosomes." J Cell Sci **120**(Pt 7): 1245-1255.
- Lowe, J., H. Li, K. H. Downing and E. Nogales (2001). "Refined structure of alpha beta-tubulin at 3.5 Å resolution." J Mol Biol **313**(5): 1045-1057.
- Lowe, M., C. Rabouille, N. Nakamura, R. Watson, M. Jackman, E. Jamsa, D. Rahman, D. J. Pappin and G. Warren (1998). "Cdc2 kinase directly phosphorylates the cis-Golgi matrix protein GM130 and is required for Golgi fragmentation in mitosis." Cell **94**(6): 783-793.
- Lu, H., C. Wang, L. Xue, Q. Zhang, F. Luh, J. Wang, T. G. Lin, Y. Yen and X. Liu (2019). "Human Mitotic Centromere-Associated Kinesin Is Targeted by MicroRNA 485-5p/181c and Prognosticates Poor Survivability of Breast Cancer." J Oncol **2019**: 2316237.
- Ma, Y. Z. and E. W. Taylor (1997). "Interacting head mechanism of microtubule-kinesin ATPase." J Biol Chem **272**(2): 724-730.
- Maney, T., A. W. Hunter, M. Wagenbach and L. Wordeman (1998). "Mitotic centromere-associated kinesin is important for anaphase chromosome segregation." J Cell Biol **142**(3): 787-801.
- Maney, T., M. Wagenbach and L. Wordeman (2001). "Molecular dissection of the microtubule depolymerizing activity of mitotic centromere-associated kinesin." J Biol Chem **276**(37): 34753-34758.
- Manka, S. W. and C. A. Moores (2018). "The role of tubulin-tubulin lattice contacts in the mechanism of microtubule dynamic instability." Nat Struct Mol Biol **25**(7): 607-615.
- Manning, A. L., N. J. Ganem, S. F. Bakhoun, M. Wagenbach, L. Wordeman and D. A. Compton (2007). "The kinesin-13 proteins Kif2a, Kif2b, and Kif2c/MCAK have distinct roles during mitosis in human cells." Mol Biol Cell **18**(8): 2970-2979.
- Manser, E., T. Leung, H. Salihuddin, Z. S. Zhao and L. Lim (1994). "A brain serine/threonine protein kinase activated by Cdc42 and Rac1." Nature **367**(6458): 40-46.
- Marumoto, T., S. Honda, T. Hara, M. Nitta, T. Hirota, E. Kohmura and H. Saya (2003). "Aurora-A kinase maintains the fidelity of early and late mitotic events in HeLa cells." J Biol Chem **278**(51): 51786-51795.

McHugh, T., J. Zou, V. A. Volkov, A. Bertin, S. K. Talapatra, J. Rappsilber, M. Dogterom and J. P. I. Welburn (2019). "The depolymerase activity of MCAK shows a graded response to Aurora B kinase phosphorylation through allosteric regulation." J Cell Sci **132**(4).

Mickolajczyk, K. J., E. A. Geyer, T. Kim, L. M. Rice and W. O. Hancock (2019). "Direct observation of individual tubulin dimers binding to growing microtubules." Proc Natl Acad Sci U S A **116**(15): 7314-7322.

Mitchison, T. and M. Kirschner (1984). "Dynamic instability of microtubule growth." Nature **312**(5991): 237-242.

Moore, A. and L. Wordeman (2004). "C-terminus of mitotic centromere-associated kinesin (MCAK) inhibits its lattice-stimulated ATPase activity." Biochem J **383**(Pt 2): 227-235.

Moore, A. T., K. E. Rankin, G. von Dassow, L. Peris, M. Wagenbach, Y. Ovechkina, A. Andrieux, D. Job and L. Wordeman (2005). "MCAK associates with the tips of polymerizing microtubules." J Cell Biol **169**(3): 391-397.

Moores, C. A., M. Perderiset, C. Kappeler, S. Kain, D. Drummond, S. J. Perkins, J. Chelly, R. Cross, A. Houdusse and F. Francis (2006). "Distinct roles of doublecortin modulating the microtubule cytoskeleton." EMBO J **25**(19): 4448-4457.

Morikawa, M., H. Yajima, R. Nitta, S. Inoue, T. Ogura, C. Sato and N. Hirokawa (2015). "X-ray and Cryo-EM structures reveal mutual conformational changes of Kinesin and GTP-state microtubules upon binding." EMBO J **34**(9): 1270-1286.

Mountain, V., C. Simerly, L. Howard, A. Ando, G. Schatten and D. A. Compton (1999). "The kinesin-related protein, HSET, opposes the activity of Eg5 and cross-links microtubules in the mammalian mitotic spindle." J Cell Biol **147**(2): 351-366.

Mulder, A. M., A. Glavis-Bloom, C. A. Moores, M. Wagenbach, B. Carragher, L. Wordeman and R. A. Milligan (2009). "A new model for binding of kinesin 13 to curved microtubule protofilaments." J Cell Biol **185**(1): 51-57.

Muthukrishnan, G., B. M. Hutchins, M. E. Williams and W. O. Hancock (2006). "Transport of semiconductor nanocrystals by kinesin molecular motors." Small **2**(5): 626-630.

Nakamura, Y., F. Tanaka, N. Haraguchi, K. Mimori, T. Matsumoto, H. Inoue, K. Yanaga and M. Mori (2007). "Clinicopathological and biological significance of mitotic centromere-associated kinesin overexpression in human gastric cancer." Br J Cancer **97**(4): 543-549.

Niclas, J., F. Navone, N. Hom-Booher and R. D. Vale (1994). "Cloning and localization of a conventional kinesin motor expressed exclusively in neurons." Neuron **12**(5): 1059-1072.

- Nishiyama, M., H. Higuchi and T. Yanagida (2002). "Chemomechanical coupling of the forward and backward steps of single kinesin molecules." Nat Cell Biol **4**(10): 790-797.
- Niwa, S., K. Nakajima, H. Miki, Y. Minato, D. Wang and N. Hirokawa (2012). "KIF19A is a microtubule-depolymerizing kinesin for ciliary length control." Dev Cell **23**(6): 1167-1175.
- Noetzel, T. L., D. N. Drechsel, A. A. Hyman and K. Kinoshita (2005). "A comparison of the ability of XMAP215 and tau to inhibit the microtubule destabilizing activity of XKCM1." Philos Trans R Soc Lond B Biol Sci **360**(1455): 591-594.
- Nogales, E., K. H. Downing, L. A. Amos and J. Lowe (1998). "Tubulin and FtsZ form a distinct family of GTPases." Nat Struct Biol **5**(6): 451-458.
- Nogales, E., S. G. Wolf and K. H. Downing (1998). "Structure of the alpha beta tubulin dimer by electron crystallography." Nature **391**(6663): 199-203.
- Ogawa, T., R. Nitta, Y. Okada and N. Hirokawa (2004). "A common mechanism for microtubule destabilizers-M type kinesins stabilize curling of the protofilament using the class-specific neck and loops." Cell **116**(4): 591-602.
- Ohi, R., M. L. Coughlin, W. S. Lane and T. J. Mitchison (2003). "An inner centromere protein that stimulates the microtubule depolymerizing activity of a KinI kinesin." Dev Cell **5**(2): 309-321.
- Ohi, R., T. Sapra, J. Howard and T. J. Mitchison (2004). "Differentiation of cytoplasmic and meiotic spindle assembly MCAK functions by Aurora B-dependent phosphorylation." Mol Biol Cell **15**(6): 2895-2906.
- Osterweil, E., D. G. Wells and M. S. Mooseker (2005). "A role for myosin VI in postsynaptic structure and glutamate receptor endocytosis." J Cell Biol **168**(2): 329-338.
- Ovechkina, Y., M. Wagenbach and L. Wordeman (2002). "K-loop insertion restores microtubule depolymerizing activity of a "neckless" MCAK mutant." J Cell Biol **159**(4): 557-562.
- Pakala, S. B., V. S. Nair, S. D. Reddy and R. Kumar (2012). "Signaling-dependent phosphorylation of Mitotic Centromere Associated Kinesin regulates microtubule depolymerization and its centrosomal localization." J Biol Chem **287**(48): 40560-40569.
- Parke, C. L., E. J. Wojcik, S. Kim and D. K. Worthylake (2010). "ATP hydrolysis in Eg5 kinesin involves a catalytic two-water mechanism." J Biol Chem **285**(8): 5859-5867.
- Paschal, B. M., H. S. Shpetner and R. B. Vallee (1987). "MAP 1C is a microtubule-activated ATPase which translocates microtubules in vitro and has dynein-like properties." J Cell Biol **105**(3): 1273-1282.

Paschal, B. M. and R. B. Vallee (1987). "Retrograde transport by the microtubule-associated protein MAP 1C." Nature **330**(6144): 181-183.

Patel, J. T., H. R. Belsham, A. J. Rathbone and C. T. Friel (2014). "Use of stopped-flow fluorescence and labeled nucleotides to analyze the ATP turnover cycle of kinesins." J Vis Exp(92): e52142.

Patel, J. T., H. R. Belsham, A. J. Rathbone, B. Wickstead, C. Gell and C. T. Friel (2016). "The family-specific alpha4-helix of the kinesin-13, MCAK, is critical to microtubule end recognition." Open Biol **6**(10): 160223.

Peet, D. R., N. J. Burroughs and R. A. Cross (2018). "Kinesin expands and stabilizes the GDP-microtubule lattice." Nat Nanotechnol **13**(5): 386-391.

Peter, M., J. Nakagawa, M. Doree, J. C. Labbe and E. A. Nigg (1990). "In vitro disassembly of the nuclear lamina and M phase-specific phosphorylation of lamins by cdc2 kinase." Cell **61**(4): 591-602.

Pilling, A. D., D. Horiuchi, C. M. Lively and W. M. Saxton (2006). "Kinesin-1 and Dynein are the primary motors for fast transport of mitochondria in Drosophila motor axons." Mol Biol Cell **17**(4): 2057-2068.

Ramaiya, A., B. Roy, M. Bugiel and E. Schaffer (2017). "Kinesin rotates unidirectionally and generates torque while walking on microtubules." Proc Natl Acad Sci U S A **114**(41): 10894-10899.

Ritter, A., M. Sanhaji, A. Friemel, S. Roth, U. Rolle, F. Louwen and J. Yuan (2015). "Functional analysis of phosphorylation of the mitotic centromere-associated kinesin by Aurora B kinase in human tumor cells." Cell Cycle **14**(23): 3755-3767.

Ritter, A., M. Sanhaji, K. Steinhauser, S. Roth, F. Louwen and J. Yuan (2015). "The activity regulation of the mitotic centromere-associated kinesin by Polo-like kinase 1." Oncotarget **6**(9): 6641-6655.

Rogers, K. R., S. Weiss, I. Crevel, P. J. Brophy, M. Geeves and R. Cross (2001). "KIF1D is a fast non-processive kinesin that demonstrates novel K-loop-dependent mechanochemistry." EMBO J **20**(18): 5101-5113.

Rogers, S. L., G. C. Rogers, D. J. Sharp and R. D. Vale (2002). "Drosophila EB1 is important for proper assembly, dynamics, and positioning of the mitotic spindle." J Cell Biol **158**(5): 873-884.

Ruhnow, F., L. Klobeta and S. Diez (2017). "Challenges in Estimating the Motility Parameters of Single Processive Motor Proteins." Biophys J **113**(11): 2433-2443.

Samsó, M., M. Radermacher, J. Frank and M. P. Koonce (1998). "Structural characterization of a dynein motor domain." J Mol Biol **276**(5): 927-937.

Sanhaji, M., C. T. Friel, N. N. Kreis, A. Kramer, C. Martin, J. Howard, K. Strebhardt and J. Yuan (2010). "Functional and spatial regulation of mitotic centromere-associated kinesin by cyclin-dependent kinase 1." Mol Cell Biol **30**(11): 2594-2607.

- Sanhaji, M., A. Ritter, H. R. Belsham, C. T. Friel, S. Roth, F. Louwen and J. Yuan (2014). "Polo-like kinase 1 regulates the stability of the mitotic centromere-associated kinesin in mitosis." *Oncotarget* **5**(10): 3130-3144.
- Sardar, H. S., V. G. Luczak, M. M. Lopez, B. C. Lister and S. P. Gilbert (2010). "Mitotic kinesin CENP-E promotes microtubule plus-end elongation." *Curr Biol* **20**(18): 1648-1653.
- Scharrel, L., R. Ma, R. Schneider, F. Julicher and S. Diez (2014). "Multimotor transport in a system of active and inactive kinesin-1 motors." *Biophys J* **107**(2): 365-372.
- Schindelin, J., I. Arganda-Carreras, E. Frise, V. Kaynig, M. Longair, T. Pietzsch, S. Preibisch, C. Rueden, S. Saalfeld, B. Schmid, J. Y. Tinevez, D. J. White, V. Hartenstein, K. Eliceiri, P. Tomancak and A. Cardona (2012). "Fiji: an open-source platform for biological-image analysis." *Nat Methods* **9**(7): 676-682.
- Schnapp, B. J. and T. S. Reese (1989). "Dynein is the motor for retrograde axonal transport of organelles." *Proc Natl Acad Sci U S A* **86**(5): 1548-1552.
- Schurmann, A., A. F. Mooney, L. C. Sanders, M. A. Sells, H. G. Wang, J. C. Reed and G. M. Bokoch (2000). "p21-activated kinase 1 phosphorylates the death agonist bad and protects cells from apoptosis." *Mol Cell Biol* **20**(2): 453-461.
- Sells, M. A., U. G. Knaus, S. Bagrodia, D. M. Ambrose, G. M. Bokoch and J. Chernoff (1997). "Human p21-activated kinase (Pak1) regulates actin organization in mammalian cells." *Curr Biol* **7**(3): 202-210.
- Shang, Z., K. Zhou, C. Xu, R. Csencsits, J. C. Cochran and C. V. Sindelar (2014). "High-resolution structures of kinesin on microtubules provide a basis for nucleotide-gated force-generation." *Elife* **3**: e04686.
- Shima, T., M. Morikawa, J. Kaneshiro, T. Kambara, S. Kamimura, T. Yagi, H. Iwamoto, S. Uemura, H. Shigematsu, M. Shirouzu, T. Ichimura, T. M. Watanabe, R. Nitta, Y. Okada and N. Hirokawa (2018). "Kinesin-binding-triggered conformation switching of microtubules contributes to polarized transport." *J Cell Biol* **217**(12): 4164-4183.
- Shimo, A., C. Tanikawa, T. Nishidate, M. L. Lin, K. Matsuda, J. H. Park, T. Ueki, T. Ohta, K. Hirata, M. Fukuda, Y. Nakamura and T. Katagiri (2008). "Involvement of kinesin family member 2C/mitotic centromere-associated kinesin overexpression in mammary carcinogenesis." *Cancer Sci* **99**(1): 62-70.
- Shin, Y., Y. Du, S. E. Collier, M. D. Ohi, M. J. Lang and R. Ohi (2015). "Biased Brownian motion as a mechanism to facilitate nanometer-scale exploration of the microtubule plus end by a kinesin-8." *Proc Natl Acad Sci U S A* **112**(29): E3826-3835.
- Shiple, K., M. Hekmat-Nejad, J. Turner, C. Moores, R. Anderson, R. Milligan, R. Sakowicz and R. Fletterick (2004). "Structure of a kinesin microtubule depolymerization machine." *EMBO J* **23**(7): 1422-1432.

Shirasu-Hiza, M., P. Coughlin and T. Mitchison (2003). "Identification of XMAP215 as a microtubule-destabilizing factor in *Xenopus* egg extract by biochemical purification." J Cell Biol **161**(2): 349-358.

Song, Y. H. and E. Mandelkow (1993). "Recombinant kinesin motor domain binds to beta-tubulin and decorates microtubules with a B surface lattice." Proc Natl Acad Sci U S A **90**(5): 1671-1675.

Sproul, L. R., D. J. Anderson, A. T. Mackey, W. S. Saunders and S. P. Gilbert (2005). "Cik1 targets the minus-end kinesin depolymerase kar3 to microtubule plus ends." Curr Biol **15**(15): 1420-1427.

Stracke, R., K. J. Bohm, L. Wollweber, J. A. Tuszyński and E. Unger (2002). "Analysis of the migration behaviour of single microtubules in electric fields." Biochemical and Biophysical Research Communications **293**(1): 602-609.

Stumpff, J., G. von Dassow, M. Wagenbach, C. Asbury and L. Wordeman (2008). "The kinesin-8 motor Kif18A suppresses kinetochore movements to control mitotic chromosome alignment." Dev Cell **14**(2): 252-262.

Stumpff, J., M. Wagenbach, A. Franck, C. L. Asbury and L. Wordeman (2012). "Kif18A and chromokinesins confine centromere movements via microtubule growth suppression and spatial control of kinetochore tension." Dev Cell **22**(5): 1017-1029.

Subramanian, R., S. C. Ti, L. Tan, S. A. Darst and T. M. Kapoor (2013). "Marking and measuring single microtubules by PRC1 and kinesin-4." Cell **154**(2): 377-390.

Suh, J., D. Wirtz and J. Hanes (2003). "Efficient active transport of gene nanocarriers to the cell nucleus." Proc Natl Acad Sci U S A **100**(7): 3878-3882.

Summers, K. E. and I. R. Gibbons (1971). "Adenosine triphosphate-induced sliding of tubules in trypsin-treated flagella of sea-urchin sperm." Proc Natl Acad Sci U S A **68**(12): 3092-3096.

Svoboda, K., C. F. Schmidt, B. J. Schnapp and S. M. Block (1993). "Direct observation of kinesin stepping by optical trapping interferometry." Nature **365**(6448): 721-727.

Talapatra, S. K., B. Harker and J. P. Welburn (2015). "The C-terminal region of the motor protein MCAK controls its structure and activity through a conformational switch." Elife **4**: e06421.

Tanaka, Y., Y. Kanai, Y. Okada, S. Nonaka, S. Takeda, A. Harada and N. Hirokawa (1998). "Targeted disruption of mouse conventional kinesin heavy chain, kif5B, results in abnormal perinuclear clustering of mitochondria." Cell **93**(7): 1147-1158.

Tanenbaum, M. E., L. Macurek, B. van der Vaart, M. Galli, A. Akhmanova and R. H. Medema (2011). "A complex of Kif18b and MCAK promotes microtubule depolymerization and is negatively regulated by Aurora kinases." Curr Biol **21**(16): 1356-1365.

- Tanno, Y., T. S. Kitajima, T. Honda, Y. Ando, K. Ishiguro and Y. Watanabe (2010). "Phosphorylation of mammalian Sgo2 by Aurora B recruits PP2A and MCAK to centromeres." Genes Dev **24**(19): 2169-2179.
- Tirnauer, J. S., E. O'Toole, L. Berrueta, B. E. Bierer and D. Pellman (1999). "Yeast Bim1p promotes the G1-specific dynamics of microtubules." J Cell Biol **145**(5): 993-1007.
- Trofimova, D., M. Paydar, A. Zara, L. Talje, B. H. Kwok and J. S. Allingham (2018). "Ternary complex of Kif2A-bound tandem tubulin heterodimers represents a kinesin-13-mediated microtubule depolymerization reaction intermediate." Nat Commun **9**(1): 2628.
- Uehara, R., Y. Tsukada, T. Kamasaki, I. Poser, K. Yoda, D. W. Gerlich and G. Goshima (2013). "Aurora B and Kif2A control microtubule length for assembly of a functional central spindle during anaphase." J Cell Biol **202**(4): 623-636.
- Uhlen, M., P. Oksvold, L. Fagerberg, E. Lundberg, K. Jonasson, M. Forsberg, M. Zwahlen, C. Kampf, K. Wester, S. Hober, H. Wernerus, L. Bjorling and F. Ponten (2010). "Towards a knowledge-based Human Protein Atlas." Nat Biotechnol **28**(12): 1248-1250.
- Vale, R. D. and L. S. Goldstein (1990). "One motor, many tails: an expanding repertoire of force-generating enzymes." Cell **60**(6): 883-885.
- Vale, R. D., T. S. Reese and M. P. Sheetz (1985). "Identification of a novel force-generating protein, kinesin, involved in microtubule-based motility." Cell **42**(1): 39-50.
- Vallee, R. B., J. S. Wall, B. M. Paschal and H. S. Shpetner (1988). "Microtubule-associated protein 1C from brain is a two-headed cytosolic dynein." Nature **332**(6164): 561-563.
- VanDelinder, V., P. G. Adams and G. D. Bachand (2016). "Mechanical splitting of microtubules into protofilament bundles by surface-bound kinesin-1." Sci Rep **6**: 39408.
- Varga, V., J. Helenius, K. Tanaka, A. A. Hyman, T. U. Tanaka and J. Howard (2006). "Yeast kinesin-8 depolymerizes microtubules in a length-dependent manner." Nat Cell Biol **8**(9): 957-962.
- Varga, V., C. Leduc, V. Bormuth, S. Diez and J. Howard (2009). "Kinesin-8 motors act cooperatively to mediate length-dependent microtubule depolymerization." Cell **138**(6): 1174-1183.
- Verhey, K. J., D. Meyer, R. Deehan, J. Blenis, B. J. Schnapp, T. A. Rapoport and B. Margolis (2001). "Cargo of kinesin identified as JIP scaffolding proteins and associated signaling molecules." J Cell Biol **152**(5): 959-970.
- Vogt, E., M. Sanhaji, W. Klein, T. Seidel, L. Wordeman and U. Eichenlaub-Ritter (2010). "MCAK is present at centromeres, midspindle and chiasmata and involved in

silencing of the spindle assembly checkpoint in mammalian oocytes." Mol Hum Reprod **16**(9): 665-684.

Walczak, C. E., E. C. Gan, A. Desai, T. J. Mitchison and S. L. Kline-Smith (2002). "The microtubule-destabilizing kinesin XKCM1 is required for chromosome positioning during spindle assembly." Curr Biol **12**(21): 1885-1889.

Walter, W. J., V. Beranek, E. Fischermeier and S. Diez (2012). "Tubulin acetylation alone does not affect kinesin-1 velocity and run length in vitro." PLoS One **7**(8): e42218.

Wang, C. Q., F. G. Xiang, Y. J. Li, X. M. Xing, N. Wang, J. H. Chi and W. J. Yu (2014). "Relation between the expression of mitotic centromere-associated kinesin and the progression of squamous cell carcinoma of the tongue." Oral Surg Oral Med Oral Pathol Oral Radiol **117**(3): 353-360.

Wang, K. and S. J. Singer (1977). "Interaction of filamin with f-actin in solution." Proc Natl Acad Sci U S A **74**(5): 2021-2025.

Wang, W., S. Cantos-Fernandes, Y. Lv, H. Kuerban, S. Ahmad, C. Wang and B. Gigant (2017). "Insight into microtubule disassembly by kinesin-13s from the structure of Kif2C bound to tubulin." Nat Commun **8**(1): 70.

Welburn, J. P. and I. M. Cheeseman (2012). "The microtubule-binding protein Cep170 promotes the targeting of the kinesin-13 depolymerase Kif2b to the mitotic spindle." Mol Biol Cell **23**(24): 4786-4795.

Wickstead, B. and K. Gull (2006). "A "holistic" kinesin phylogeny reveals new kinesin families and predicts protein functions." Mol Biol Cell **17**(4): 1734-1743.

Wickstead, B., K. Gull and T. A. Richards (2010). "Patterns of kinesin evolution reveal a complex ancestral eukaryote with a multifunctional cytoskeleton." BMC Evol Biol **10**: 110.

Wordeman, L., J. Decarreau, J. J. Vicente and M. Wagenbach (2016). "Divergent microtubule assembly rates after short- versus long-term loss of end-modulating kinesins." Mol Biol Cell **27**(8): 1300-1309.

Wordeman, L. and T. J. Mitchison (1995). "Identification and partial characterization of mitotic centromere-associated kinesin, a kinesin-related protein that associates with centromeres during mitosis." J Cell Biol **128**(1-2): 95-104.

Wordeman, L., M. Wagenbach and G. von Dassow (2007). "MCAK facilitates chromosome movement by promoting kinetochore microtubule turnover." J Cell Biol **179**(5): 869-879.

Xu, Y., S. Takeda, T. Nakata, Y. Noda, Y. Tanaka and N. Hirokawa (2002). "Role of KIFC3 motor protein in Golgi positioning and integration." J Cell Biol **158**(2): 293-303.

Yin, H. L., J. H. Hartwig, K. Maruyama and T. P. Stossel (1981). "Ca²⁺ control of actin filament length. Effects of macrophage gelsolin on actin polymerization." J Biol Chem **256**(18): 9693-9697.

Zhang, L., H. Shao, Y. Huang, F. Yan, Y. Chu, H. Hou, M. Zhu, C. Fu, F. Aikhionbare, G. Fang, X. Ding and X. Yao (2011). "PLK1 phosphorylates mitotic centromere-associated kinesin and promotes its depolymerase activity." J Biol Chem **286**(4): 3033-3046.

Zhang, X., S. C. Ems-McClung and C. E. Walczak (2008). "Aurora A phosphorylates MCAK to control ran-dependent spindle bipolarity." Mol Biol Cell **19**(7): 2752-2765.

Zhang, X., W. Lan, S. C. Ems-McClung, P. T. Stukenberg and C. E. Walczak (2007). "Aurora B phosphorylates multiple sites on mitotic centromere-associated kinesin to spatially and temporally regulate its function." Mol Biol Cell **18**(9): 3264-3276.

Appendices

Appendix 1

A1.1 Alignment of the motor domains of Kinesin-1 and Kinesin-13

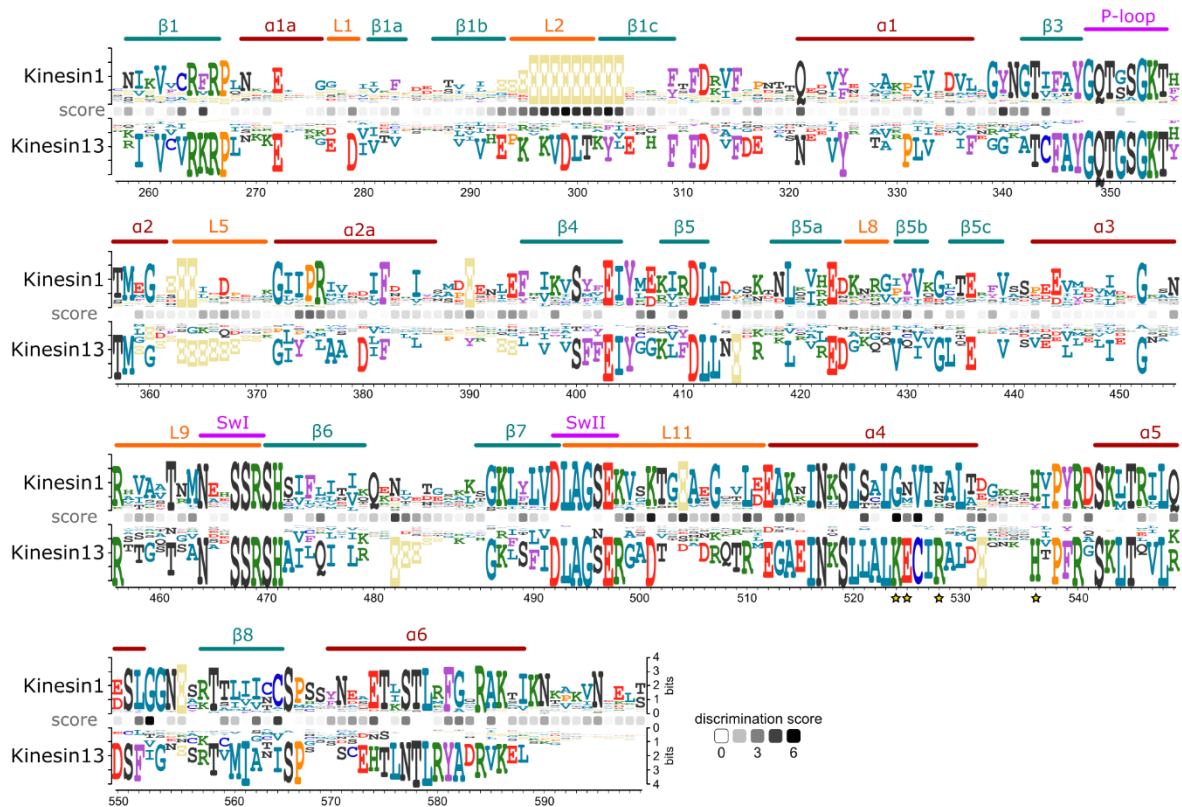


Figure A1.1 A comparison of sequence alignments of the motor domains of **Kinesin-1 and Kinesin-13**. Alignments of Kinesin-1s and Kinesin-13s from 45 diverse eukaryotes (Wickstead, Gull et al. 2010). The size of the residues indicates the degree of conservation within the family, while the discrimination score shows the difference between the mean of the BLOSUM62 substitution matrix scores for each family at each residue. Positions are numbered according to the human MCAK sequence. (Figure modified from (Patel, Belsham et al. 2016))

Appendix 2

A2.1 T537A and T537E microtubule end and lattice residence fits

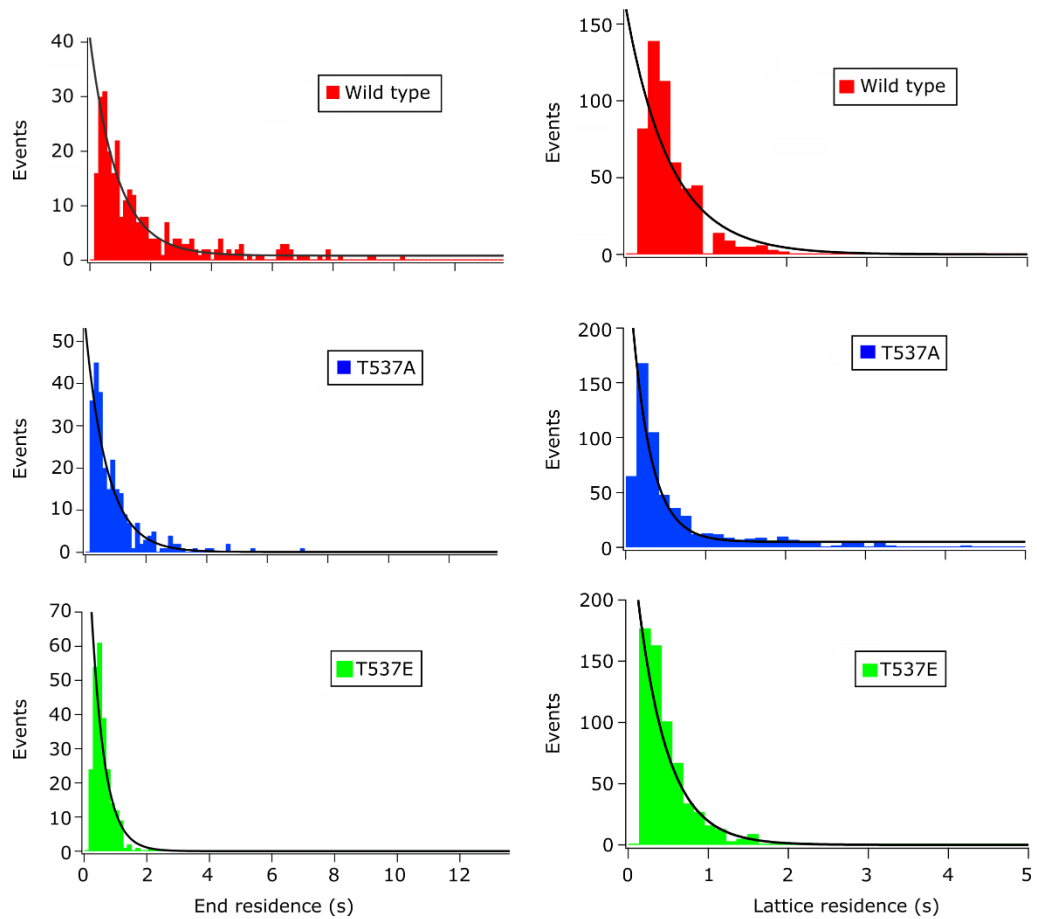


Figure A2.1 MCAK's microtubule end and lattice residence times for wild type, T537A and T537E were fit to an exponential function. Histograms show the number of events with a specific duration of end residence (WT n=289, T537A n=261, T537E n=242) or lattice residence (WT n=526, T537A n=582, T537E n=622). The data were fitted to a single exponential to calculate the k_{off} values given in **Table 1**.

A2.2 T537A and T537E deviation and fits of mADP dissociation data

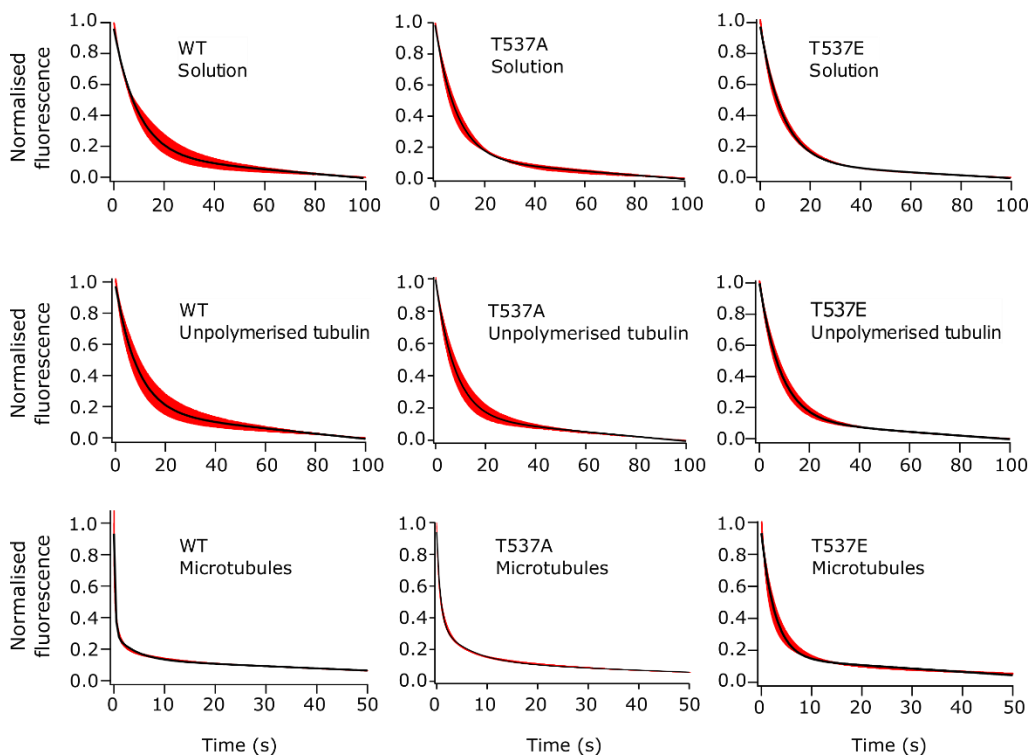


Figure A2.2 The dissociation of mADP from wild type MCAK, T537A and T537E in solution, in the presence of unpolymerised tubulin and in the presence of microtubules were fit to exponential functions. Graphs show average \pm standard deviation in red, with fits in black. The fits are single exponential equations plus a line of constant negative slope to account for photobleaching of mant, with the exceptions of WT with microtubules and T537A with microtubules which were fitted to a double exponential plus a line of constant negative slope.

Appendix 3

A3.1 End and lattice residence fits wild type Kinesin-1, G262K, N263E, S266R,

Triple and S266A

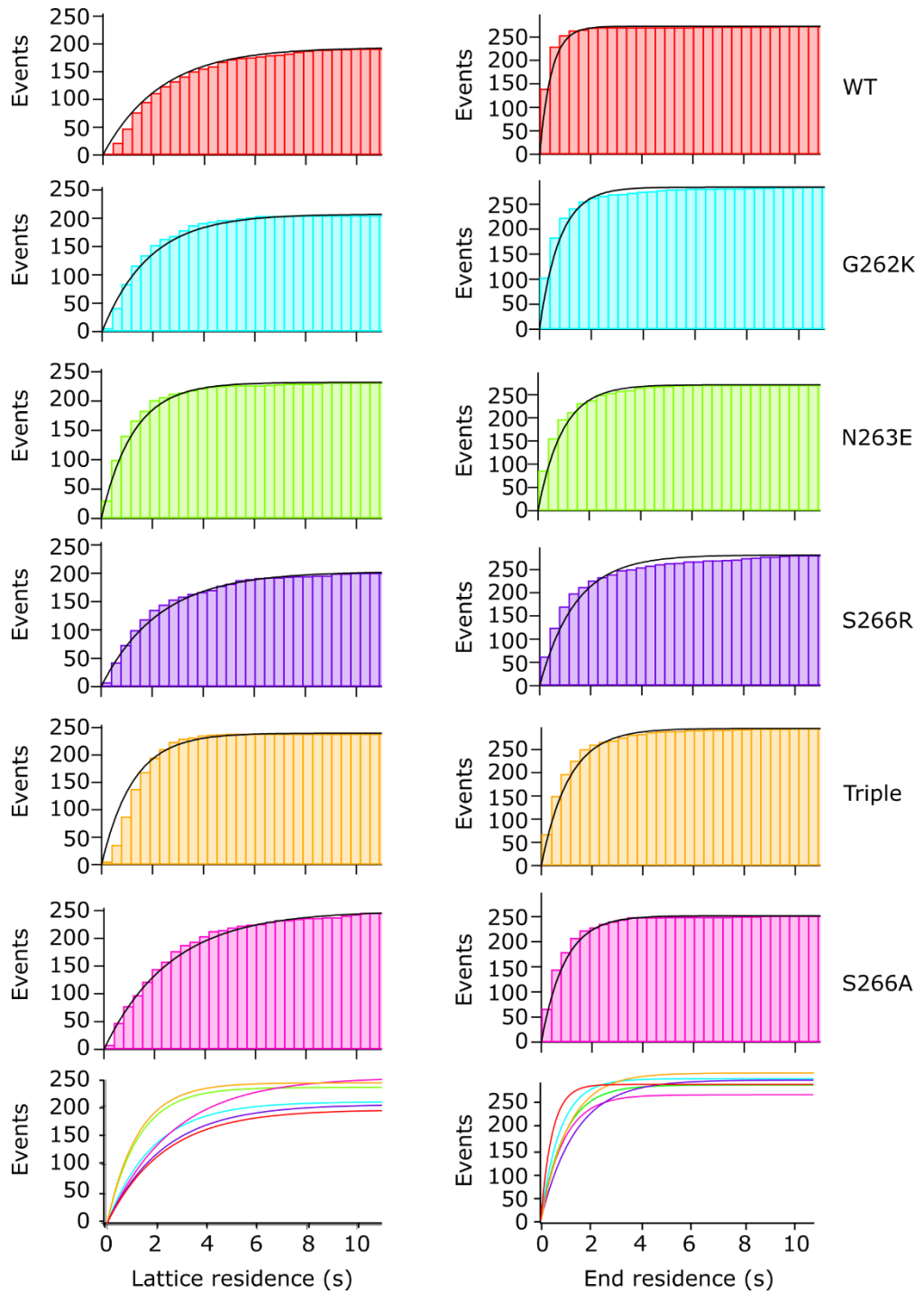


Figure A3.1 Microtubule end and lattice residence times for wild type Kinesin-1, G262K, N263E, S266R, Triple and S266A were fit to an exponential function. Histograms show the number of events with a specific duration of end residence (WT n = 273, G262K n = 285, N263E n = 272, S266R n = 284, Triple n = 296, S266A n = 252) or lattice residence (WT n = 194, G262K n = 207, N263E n = 232, S266R n = 203, Triple n = 239, S266A n = 249). The data were fitted to a single exponential to calculate the k_{off} values given in **Table 4** and **Table 5**.